



COMMONWEALTH OF KENTUCKY  
DEPARTMENT OF TRANSPORTATION

ELIJAH M. HOGGE  
SECRETARY

FRANKFORT, KENTUCKY 40601

WENDELL H. FORD  
GOVERNOR

BUREAU OF HIGHWAYS  
JAMES E. GRAY  
COMMISSIONER

February 15, 1974

MEMO TO: J. R. Harbison  
State Highway Engineer  
Chairman, Research Committee

SUBJECT: Research Report No. 382; "The Creep Response of Cohesive Soils: A Method of Design Using Rheological Strength Parameters;" Final Report; KYHPR-65-38; HPR-1(9), Part II

The design of earth structures (foundations and embankments) on the basis of peak strengths involves risks and uncertainties which are judiciously weighted into the factor of safety. Factors as high as 2.0 would be necessary in some instances to prevent failure. More often, 1.35 has proven to be adequate. When creep or other movement occurs in plastic or cohesive soils, shear resistance decreases. Movement may arise from creep or earth tremors; afterwards, the structure may fail. Consequently, it has become increasingly necessary to distinguish between "initial" and "residual" strength parameters and to compute the true factor of safety from residual values. The residual value is defined in some shear tests on plastic materials as the more-or-less steady-state shear value following the peak value.

The case history analysis pertaining to MP 96 on the West Kentucky Parkway supplements a more detailed site history submitted to the Director of Maintenance and other principals on July 5, 1973. The site at MP 44 on I 64 has not been reported previously. Histories of both sites will be included in a forthcoming report on Research Project KYHPR-68-48. The Division of Materials will finalize the investigation at MP 96 (WKP) and submit the action plan. Implementation of findings from this study will come as a matter of course in the design of earth embankments and landslide corrections plans.

Respectfully submitted

A handwritten signature in black ink, appearing to read "Jas. H. Havens".

Jas. H. Havens  
Director of Research

JHH:gd  
Attachment  
CC's: Research Committee



1. Report No.		2. Government Accession No.		3. Recipient's Catalog No.	
4. Title and Subtitle The Creep Response of Cohesive Soils: A Method of Design Using Rheological Strength Parameters			5. Report Date December 1973		
			6. Performing Organization Code		
7. Author(s) David L. Allen			8. Performing Organization Report No. 382		
9. Performing Organization Name and Address Division of Research Kentucky Bureau of Highways 533 South Limestone Lexington, Kentucky 40508			10. Work Unit No.		
			11. Contract or Grant No. KYHPR- 65-38		
12. Sponsoring Agency Name and Address			13. Type of Report and Period Covered Final		
			14. Sponsoring Agency Code		
15. Supplementary Notes Prepared in cooperation with the US Department of Transportation, Federal Highway Administration  Study Title: RHEOLOGICAL STUDY OF COHESIVE SOILS					
16. Abstract  The creep response of four remolded soils and undisturbed soils from two landslide sites is presented. A method for obtaining the yield stress of soil from creep test data is presented and discussed. "Viscosity diagrams", showing the location of the yield stress is approximately 50 percent of peak stress, were obtained from conventional triaxial tests. There is more scatter in data from undisturbed soils than in data from remolded soils. Mohr's failure envelopes, constructed from yield stress data, give internal friction angles having values from approximately five to ten degrees. Strength data, calculated indirectly from peak relaxation modulus, are also presented. Stability analyses are presented on two selected landslides. Analyses are made and compared using peak, "Residual", and yield stresses. Results indicate yield stress should be considered when designing earth structures.					
17. Key Words Peak Stress      Yield Stress Relaxation Modulus      Creep Tests Slope Stability Soil Creep Viscosity Diagram			18. Distribution Statement		
19. Security Classif. (of this report) Unclassified		20. Security Classif. (of this page) Unclassified		21. No. of Pages	22. Price



Research Report  
382

**THE CREEP RESPONSE OF COHESIVE SOILS:  
A METHOD OF DESIGN USING RHEOLOGICAL STRENGTH PARAMETERS**

KYHPR 65-38, HPR-1(9), Part II  
Final Report

by

David L. Allen  
Research Engineer

Division of Research  
Bureau of Highways  
DEPARTMENT OF TRANSPORTATION  
Commonwealth of Kentucky

in cooperation with the  
U. S. Department of Transportation  
Federal Highway Administration

The contents of this report reflect the views of  
the authors who are responsible for the facts and  
the accuracy of the data presented herein. The  
contents do not necessarily reflect the official  
views or policies of the Bureau of Highways.  
This report does not constitute a standard,  
specification, or regulation.

December 1973



## INTRODUCTION

The process of slow, continuous deformation or yielding of a soil mass under constant stress is defined as soil creep. The point or magnitude of stress that causes this process to accelerate with time is defined as the yield limit or yield stress. It is known that nearly all soil structures undergo a certain amount of creep, and in many cases, masses have failed completely as a result of creeping.

Schultze and Krause (1), Murayama and Shibata (2) and Suklje (3) have indicated there are at least two yield limits: (1) the upper yield limit already defined and (2) a lower yield limit below which no slippage or deformation occurs. However, Bishop and Lovenbury (4), in performing long-term creep tests (for approximately 4 years), indicated there appeared to be no value of stress that did not produce time-dependent deformation.

Singh and Mitchell (5); Mitchell, Campanella, and Singh (6); and Mitchell and Campanella (7) have shown in three separate reports the rate-of-creep function is time dependent and decreasing according to an inverse power law. General agreement with this data was published by Casagrande and Wilson (8). Their data indicated shear strength of undisturbed soils generally decreased in proportion to the logarithm of elapsed time to failure. Vislov and Skibitsky (9) stated there is a decrease in both the cohesive ( $c$ ) and frictional ( $\phi$ ) components of shear strength;  $c$  generally decreases more than  $\phi$ .

Roscoe and Schofield (10), Walker (11), and Arulanandan, et al (12) indicate pore pressures play a very important role in an earth structure undergoing creep deformation. Walker concludes: ". . . undrained creep may result in significant pore pressure build-up, with a consequent tendency towards foundation instability."

Murayama and Shibata (13) state the upper yield stress of clay is always smaller than peak failure strength. Therefore, any stability analysis based on peak strength (obtained from conventional triaxial tests) would always lie on the dangerous side when compared to the "true critical strength" based on the upper yield stress. The same authors have recommended for design of permanent earth structures the minimum factor of safety should be increased by a factor of  $(\sigma_p/\sigma_y)$ , where  $\sigma_p$  is the peak stress and  $\sigma_y$  is the yield stress.

## OBJECTIVES

The objectives of this phase of study were:

1. to determine the creep characteristics of four remolded soils and also undisturbed soils from two landslide sites,
2. to determine the relationship between peak stress from conventional triaxial tests and yield stress from creep tests,
3. to develop a criterion for design of earth structures which will more accurately account for the time dependency of soil behavior than do present methods, and
4. to further verify the methods proposed by Scott (14) in the first phase of this study, using peak relaxation modulus in determining shear strength.

## PROCEDURES

Disturbed samples were obtained from Adair County (Baxter Series), Clark County (Eden series), Fayette County (Maury series), and Fulton County (Calloway series). The four soils ranged from a clay to a silty loam. A kaolin clay was purchased from the Edgar Plastic Kaolin Company, Edgar, Florida. Classification data for the four soils and the kaolinite are shown in Table 1.

The Kentucky soils were air dried, pulverized, and passed through a No. 10 sieve; the plus 10 material was discarded. Distilled water was added to achieve the necessary moisture content. The soil was covered with plastic and allowed to cure overnight to assure an even distribution of moisture. The prepared soil was run through a "Vac-Aire" extrusion machine, cut to the necessary length, and waxed. The wax prevented moisture loss until testing.

The kaolinite was obtained in dry, powdered form. Water was added and samples were prepared in the same manner as for the other four soils.

A complete and detailed description of samples, sample preparation, testing equipment, and procedures for relaxation and triaxial testing was reported by Scott (14). A complete description of the mechanical procedures of performing creep tests was reported by Allen (15).

**Table 1. Summary of Classification Test Results – Kentucky Soils.**

County	Liquid Limit (%)	Plastic Limit (%)	Specific Gravity	Standard Proctor Density (lbs/ft <sup>3</sup> )	Optimum Moisture (%)	Kentucky CBR	Classifications			
							Unified	AASHO	Agricultural	Textural
Adair	61	27	2.768	96	24	5.0	MH	A-7.5(19)	Baxter Cherty Silt Loam	Clay
Clark	37	25	2.705	96	22	6.5	CL	A-6(13)	Eden Silty Clay Loam	Silty Caly
Fayette	35	21	2.685	101	20	9.5	CL	A-6(12)	Maury Silt Loam	Clay Loam
Fulton	26	NP	2.657	106	16	10.0	ML	A-4( 8)	Calloway Silt Loam	Silty Loam

County	Percent Finer Than													
	1"	3/4"	3/8"	4	10	20	40	60	140	200	.05 mm	.02 mm	.005 mm	.002 mm
Adair	100	95	93	92	91	90	89	89	88	88	82	74	58	50
Clark	100	100	100	100	99	98	98	97	94	91	88	75	44	31
Fayette	100	100	100	100	99	96	94	92	85	79	76	61	30	20
Fulton	100	100	100	100	99	98	98	97	87	78	79	40	17	13

In this phase of the study, samples were placed in a triaxial chamber and allowed to consolidate overnight. Four consolidation pressures (confining pressure) were used -- 10, 30, 50, and 70 psi. The samples were loaded hydraulically to stresses of 10, 25, 40, 55, 70 and 85 percent of peak stress (obtained from Scott's data (14)). Each stress level was allowed to remain 24 hours before the next higher stress was applied.

Strain readings were taken periodically throughout the 24-hour test. A plot was made of deflection versus time in an attempt to determine the rate of strain at 24 hours. This attempt was unsuccessful since the rate of strain was not linear any time during the 24-hour period, indicating the soil had not reached the condition of steady-state creeping. Singh, et al (5) and Mitchell, et al (6) have indicated, however, that true steady-state creep does not exist in soils for any significant period of time.

The same authors in addition to Murayama and Shibata (13) have demonstrated a procedure for comparing rates of strain for different stress levels which avoids the problem of non-steady-state flow. This is accomplished by plotting deflection against the logarithm of time and calculating the rate of strain,  $\epsilon$ , with respect to the logarithm of time according to Equation 1:

$$\epsilon = \Delta\epsilon / \Delta \log t \tag{1}$$

where  $\epsilon$  = strain rate,  
 $\Delta\epsilon$  =  $\epsilon_2 - \epsilon_1$ , and  
 $\Delta \log t$  =  $\log t_2 - \log t_1$ .

This method was used to analyze data from this study, and an example is shown in Figures 1 and 2. To find the yield stress, the strain rate calculated from Equation 1 was plotted against effective, applied, deviator stress. The first major "break point" in the curve was

considered the yield stress. Murayama and Shibata (13) refer to these plots as the "viscosity diagrams".

In many of the 24-hour tests, problems were encountered in the hydraulic system. There appeared to be minor pressure drops in the system overnight which caused decreases in effective stress. In addition, the rubber o-ring in the top cap of the triaxial chamber, which served as a pressure seal, produced drag on the loading piston at very slow rates of strain and caused erroneous results. Consequently, some load increments in the 24-hour tests were considered invalid. Maintaining each stress level on the sample for 24 hours made it necessary to keep a sample under a confining pressure for over a week. This was undesirable since possible diffusion of air through the membrane might lead to unreliable pore pressure measurements.

Murayama and Shibata (13, 16) proposed and documented a method by which yield stress can be located from tests of much shorter duration than 24 hours. In their procedure, a deviator stress is applied in equal increments at a uniform interval and in a stepwise fashion. The strain is measured at an equal time lapse from each beginning of the step of stress. Their results indicated the location of yield stress obtained was independent of time at which the strain readings were taken. An example of their viscosity diagrams showing this relationship is given in Figure 3. This procedure was used in later testing in this study. The strain rate was calculated using the logarithmic slope of the deflection-time curve from four to eight minutes. Using this procedure allows one to avoid most of the problems associated with the 24-hour test. Also, the entire creep test can be run in less than one day. Viscosity diagrams, presented under the section titled RESULTS AND ANALYSES, having only three or four points are from tests lasting 24 hours.



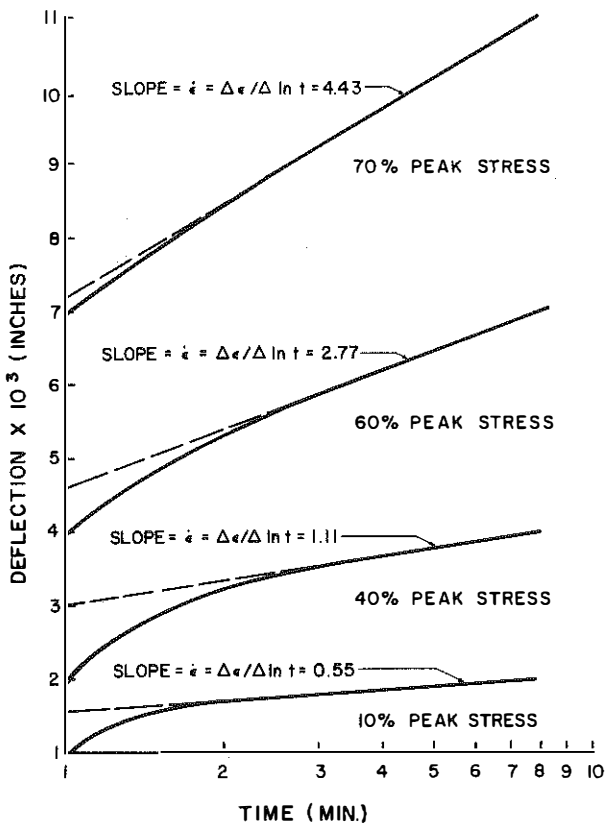


Figure 1. Example Creep Curves.

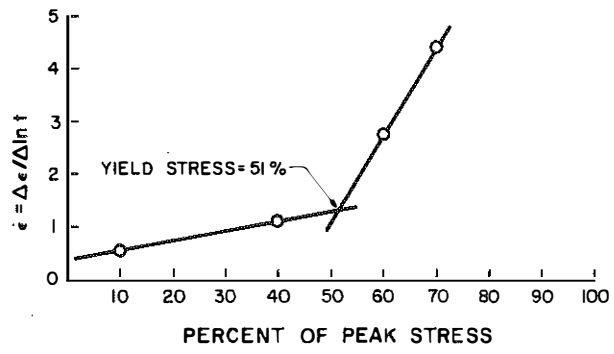
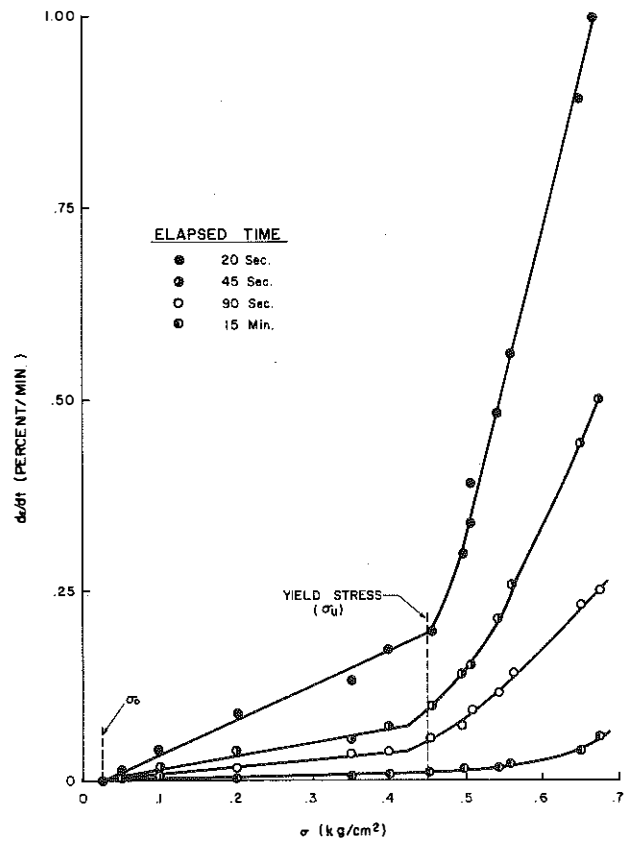


Figure 2. Example Viscosity Diagram.

Figure 3. Relationship between Yield Stress and Time (Reference 1).



## RESULTS AND ANALYSES

Viscosity diagrams for the remolded soils are presented in Figures 4 through 8. Strain rates were calculated from Equation 1, and the times for figuring  $\epsilon$  were either 24 hours or 8 minutes. Two methods were used randomly to insure the compensation of systematic errors. The magnitudes of  $\epsilon$  cannot be compared from test to test because they were calculated for different times.

Many of the diagrams exhibit more than one break point. Kawakami and Ogawa (17), in reporting data from repeated loading tests on triaxial and uniaxial compression samples, presented viscosity diagrams containing several break points. They were using a rheological model consisting of Maxwell, Voigt, and Bingham bodies. The break points were considered beginning points of slip occurring in the specimen. This would be equivalent to slippage of the Bingham body of the rheological model. The lower yield limit mentioned by Murayama and Shibata (13) and Schultze and Krause (1) below which no slippage in the sample occurs was undefinable in most viscosity diagrams reported herein.

Two of the viscosity diagrams for the Calloway soil series exhibited an unusual property. At stress levels approaching or exceeding the peak stress, the slope of the viscosity diagram began to decrease. In one case (Calloway Series -- confining pressure = 10 psi) the magnitude of  $\epsilon$  itself actually decreased (deviator stress = 14.4 psi). It was suspected that application of a stress approaching the peak stress to a sandy-silty soil could initiate dilation in the sample as a shear plane was formed. This process of dilation could possibly offset the effects of creep. To test this hypothesis, a creep test was performed on an Ottawa sand sample under a confining pressure of 10 psi. Results in Figure 9 seem to substantiate the idea that dilation does become a behavioral factor for sandy soils near the level of peak stress.

The first major break point in the viscosity diagram was considered the yield stress. All of the yield stresses for the remolded soils occurred in the vicinity of 50 percent of the peak stress. The highest was 58 percent and the lowest was 40 percent. The average value of yield stress occurred at 49.7 percent of peak stress. This relationship is displayed graphically in Figure 10.

A multiple regression analysis was performed on the data in Figure 10. The resulting relationship between yield stress and peak stress is given by

$$\sigma_y = 0.497 \sigma_u \quad (2)$$

where  $\sigma_y$  = yield stress and  
 $\sigma_u$  = peak stress.

In this analysis, the regression line was constrained through the point (0, 0). The  $\sigma_u$  versus  $\sigma_y$  correlation coefficient was 0.996 and  $R^2$  equaled 0.991. To determine the range over which the average could vary without contradicting the data, a two-tailed test of hypothesis was performed using the student's t distribution (18):

$$r = y \pm 2.11 \sqrt{s^2/n} \quad (3)$$

where  $r$  = range,  
 $y$  = average of the observations,  
 $s^2$  = estimate of the variance, and  
 2.11 = constant that leaves 2.5 percent area in each tail of the distribution curve.

From Equation 3, the 95-percent confidence limits are  $\pm 2.5$ .

To show the effects of confining pressure and the percent of clay on location of the yield stress, Figures 11 and 12 were plotted. It is evident neither confining pressure nor percent of clay appeared to have any effect on the location (within the range of values tested). This, apparently, is further confirmation of data presented in Figure 10.

The magnitude of yield stress did not increase linearly with confining pressure; the functions were slightly concave downward (Figures 13 and 14). This was not exactly in agreement with Scott's data (14) which indicated a linear relationship existed between peak stress and confining pressure (Figure 19). However, there is excellent agreement between these data and Scott's at the intercept of the functions with zero confining pressure. In the present data, the zero intercept varied between 4.5 and 5.5 psi while Scott's data varied between 8.0 and 12.0 psi (twice the yield stress). This would indicate the yield stress of an unconfined creep test would be about 5 psi. This was not confirmed experimentally.

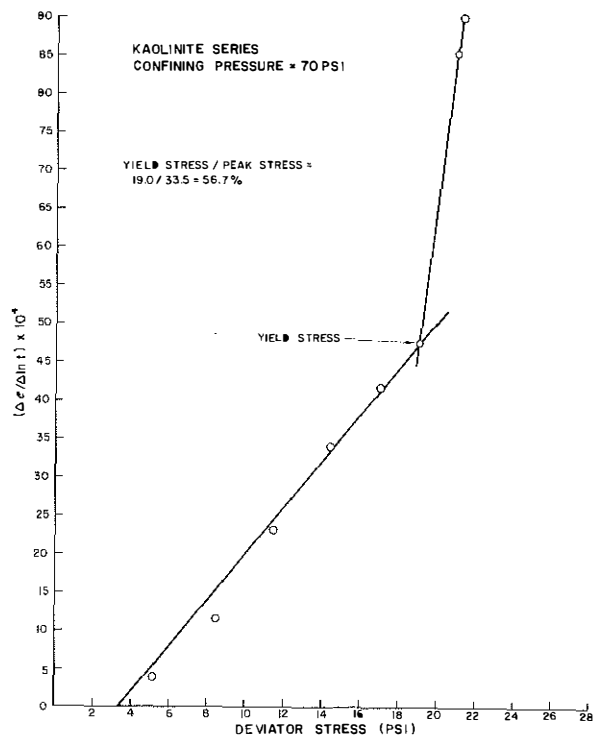
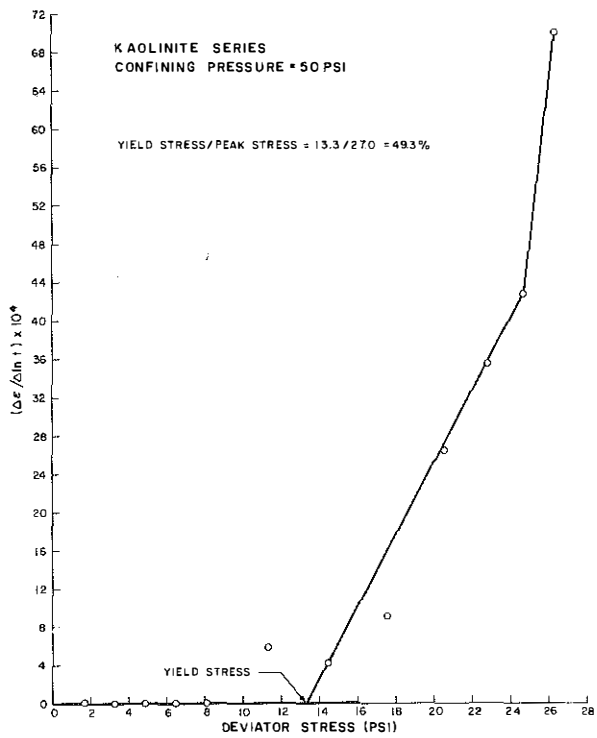
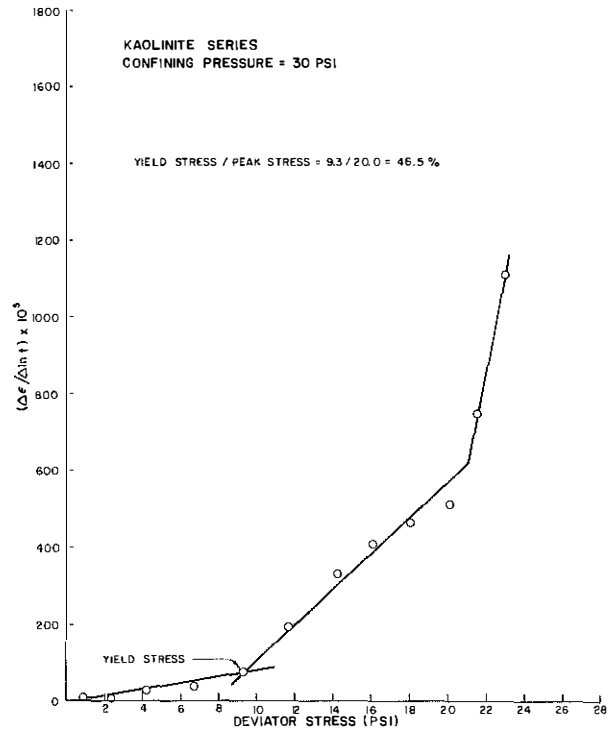
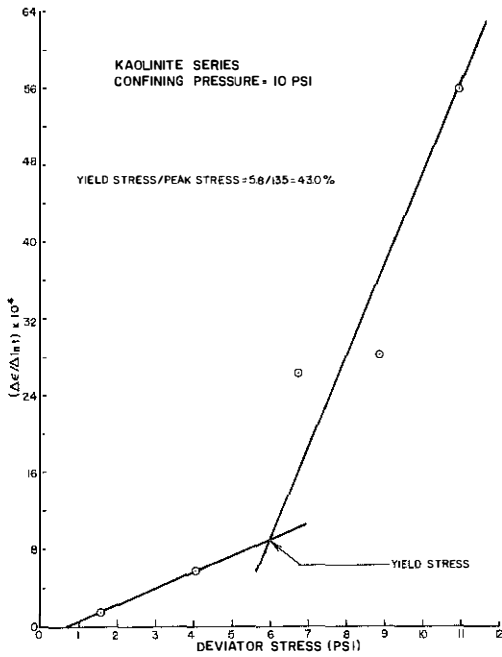
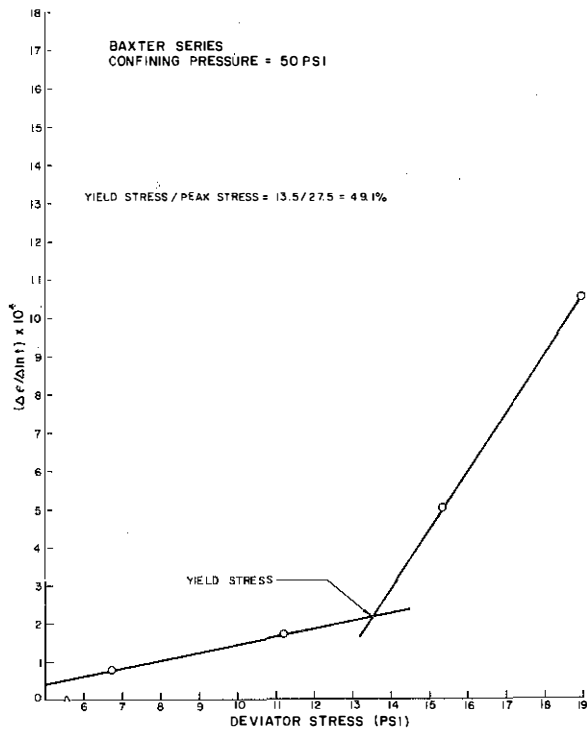
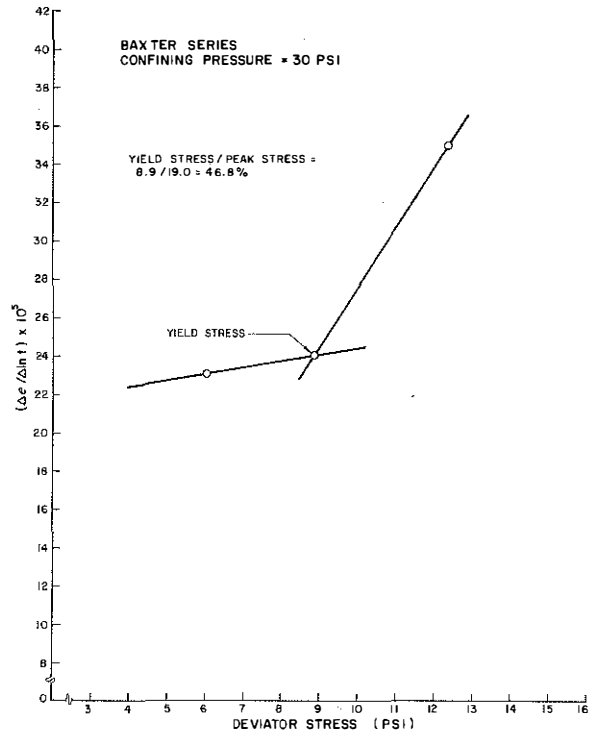
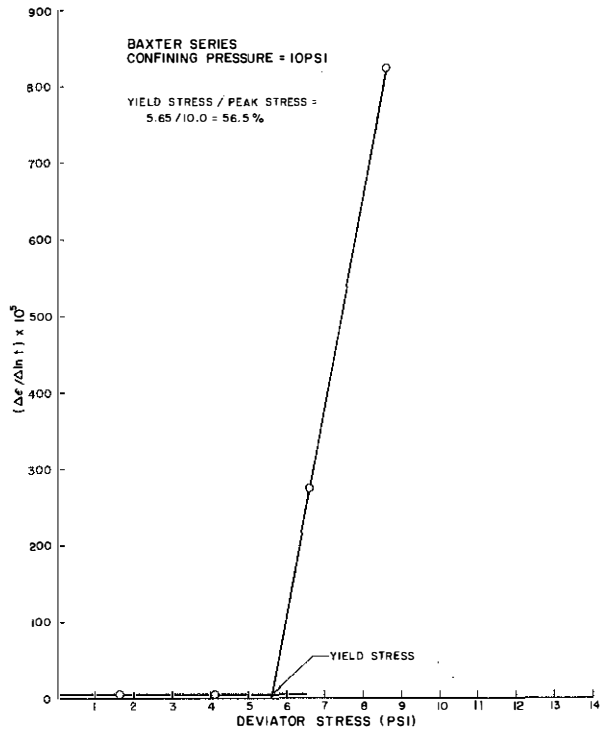


Figure 4. Viscosity Diagrams - Kaolinite Series.



**Figure 5. Viscosity Diagrams - Baxter Series.**

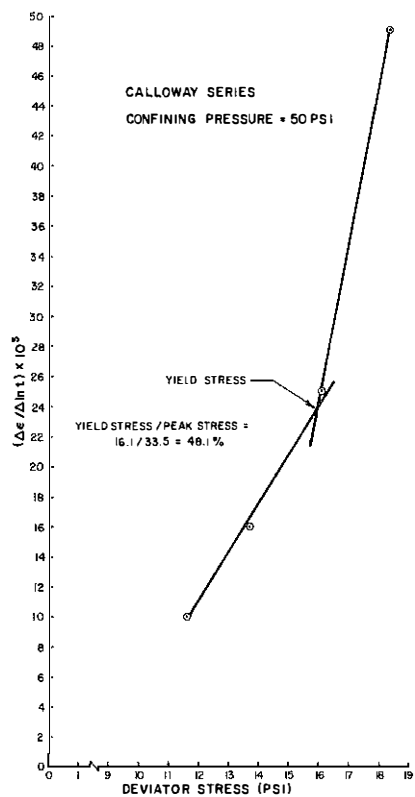
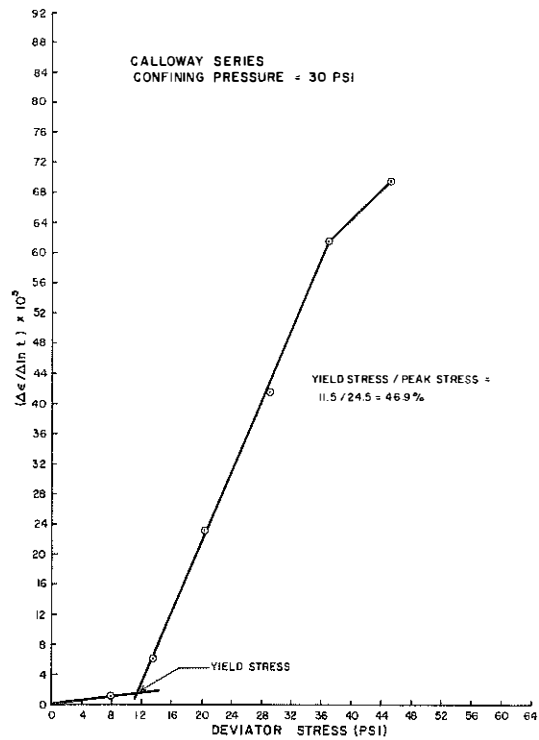
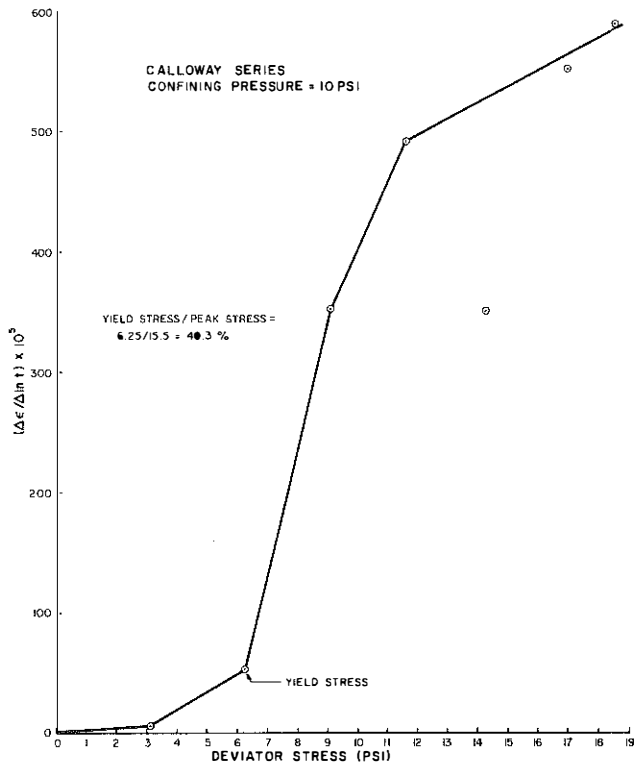


Figure 6. Viscosity Diagrams - Calloway Series.

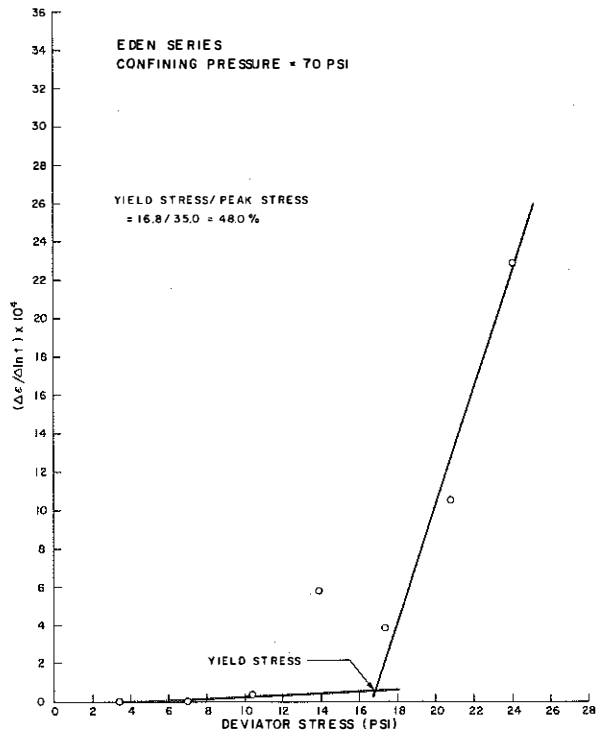
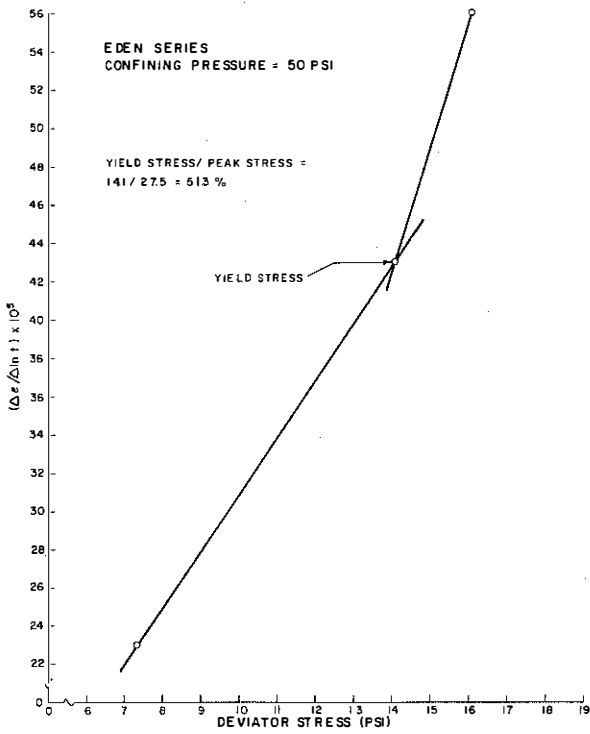
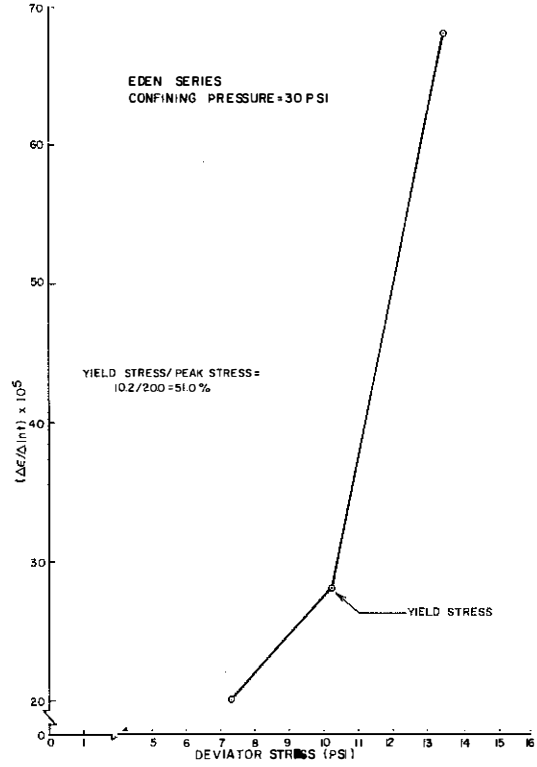
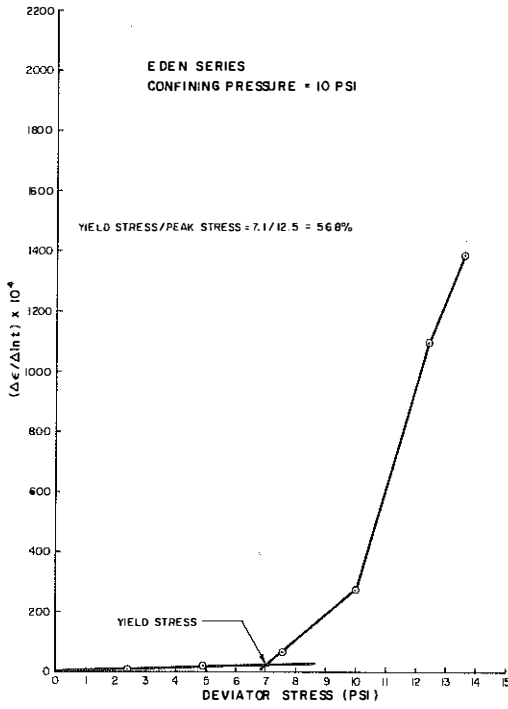


Figure 7. Viscosity Diagrams - Eden Series.

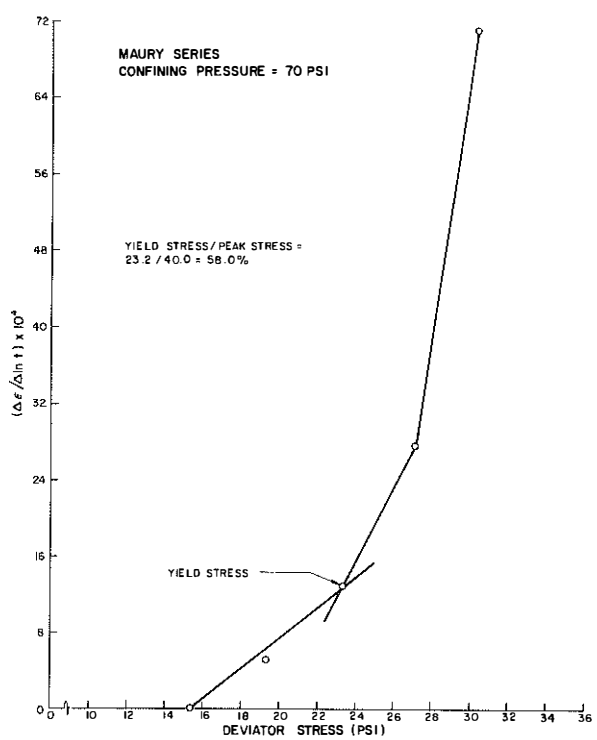
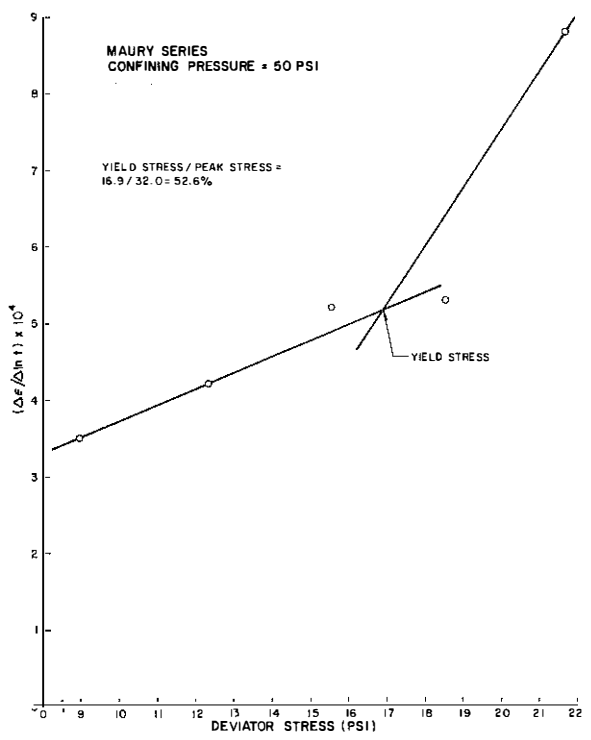
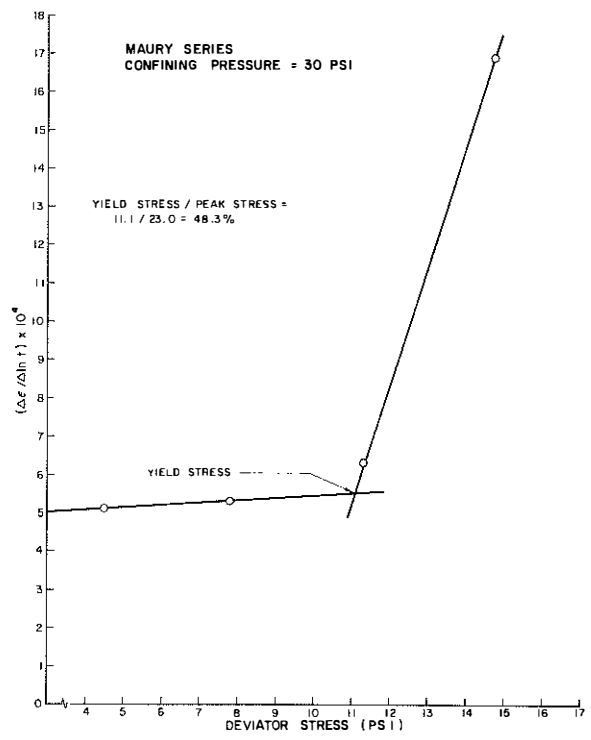
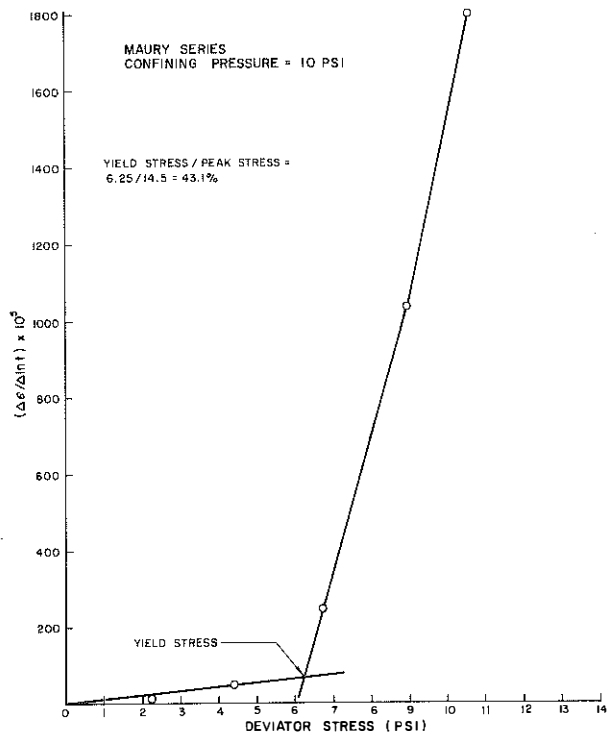


Figure 8. Viscosity Diagrams - Maury Series.

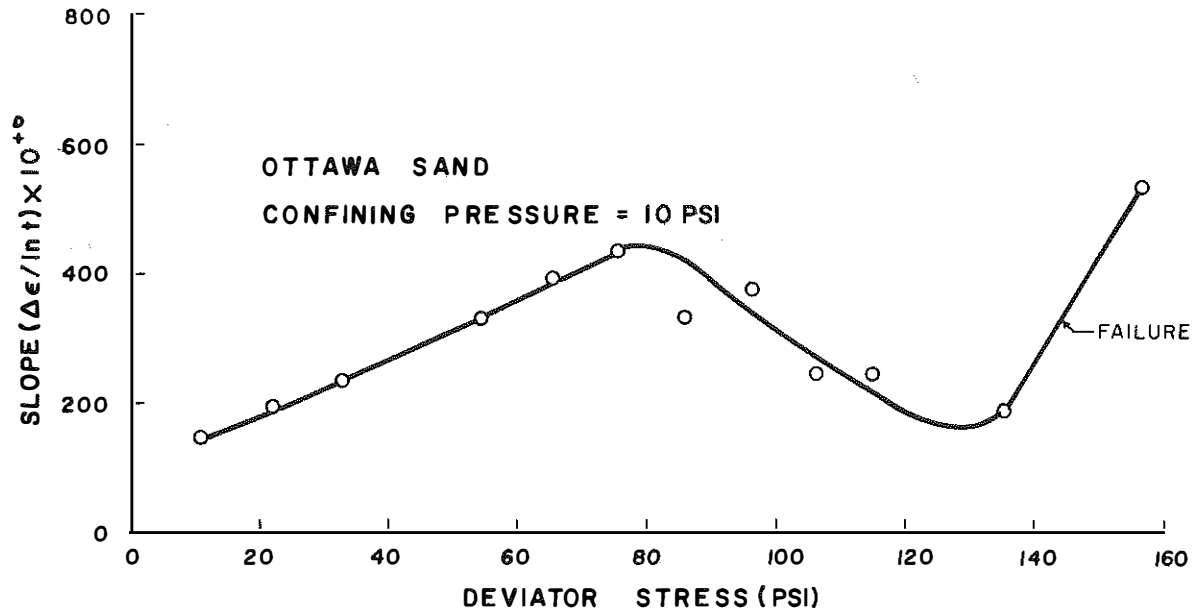


Figure 9. Viscosity Diagram - Ottawa Sand.

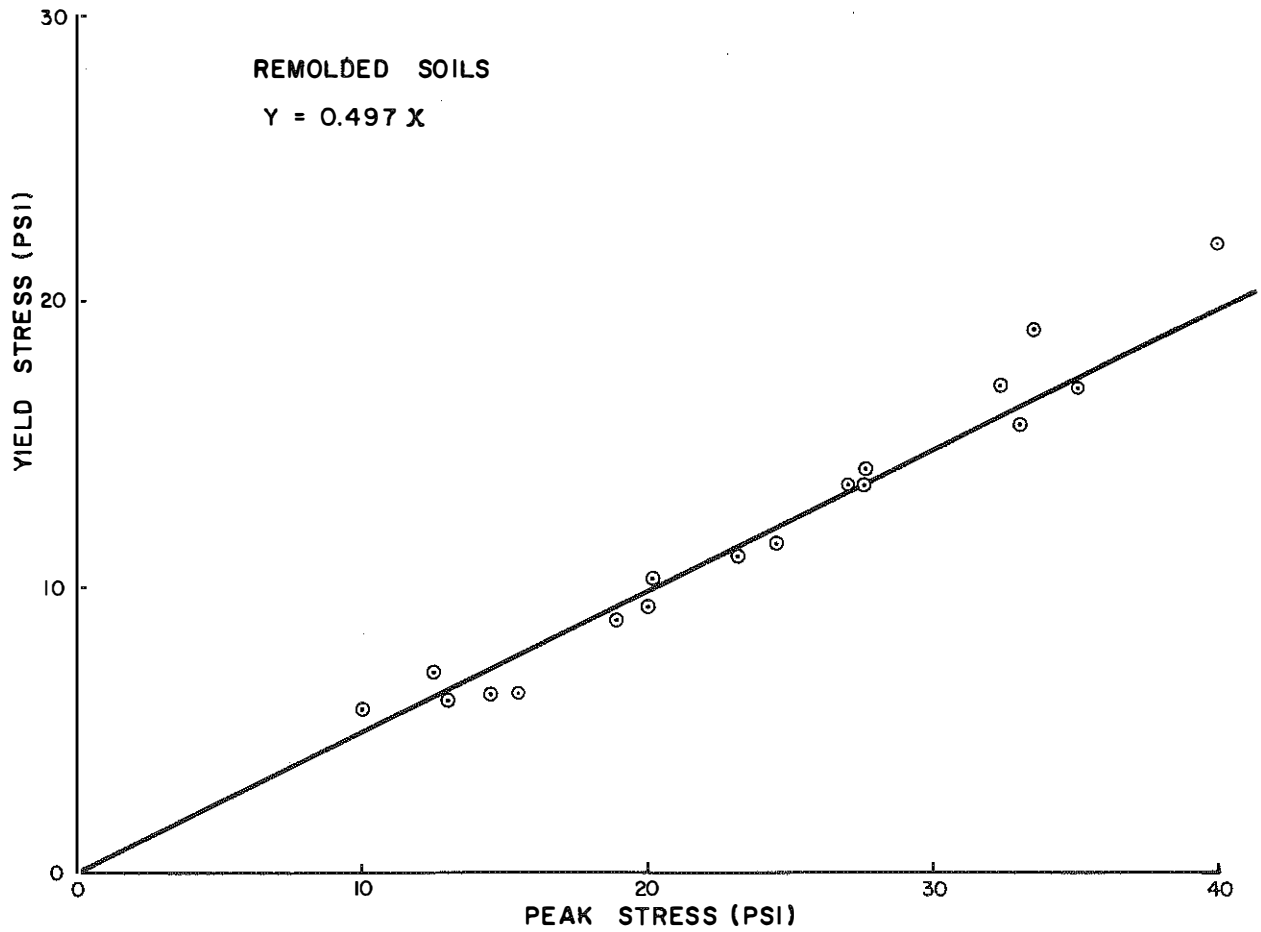


Figure 10. Yield Stress as a Function of Peak Stress - Remolded Soils.



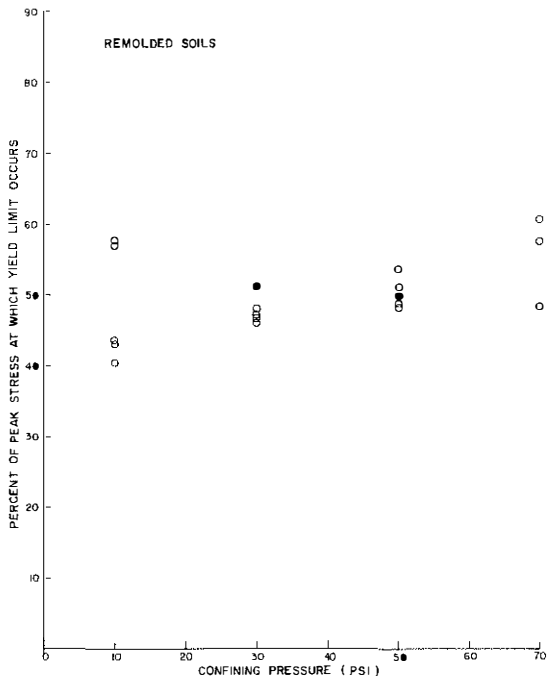
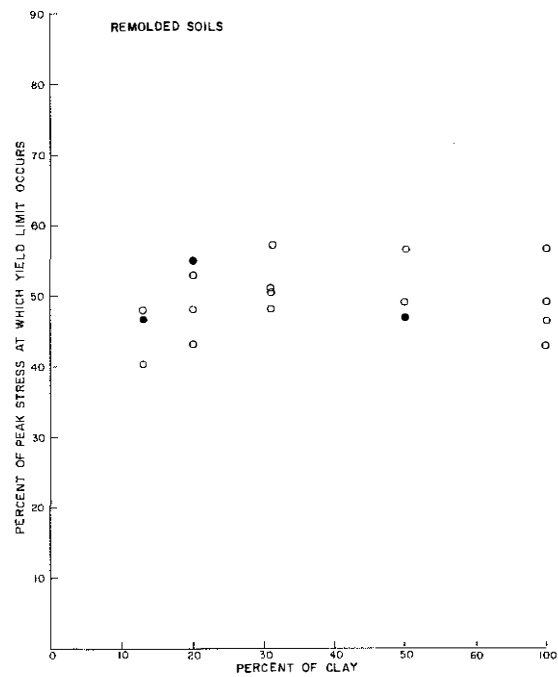
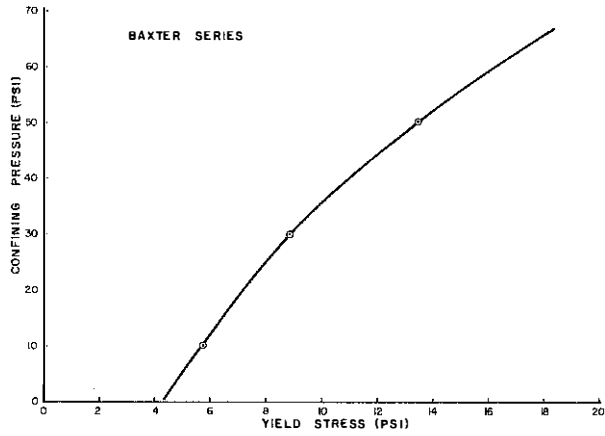


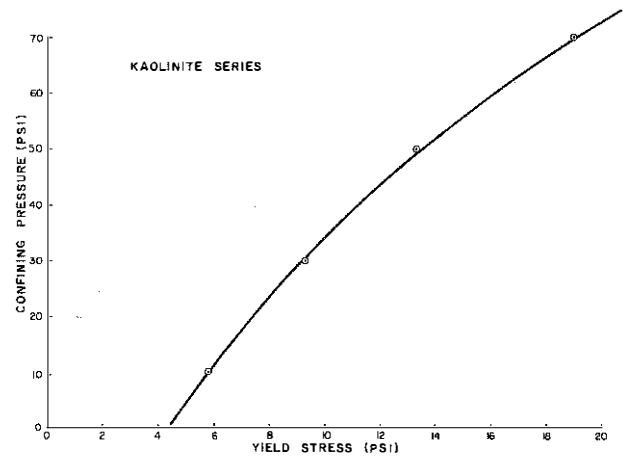
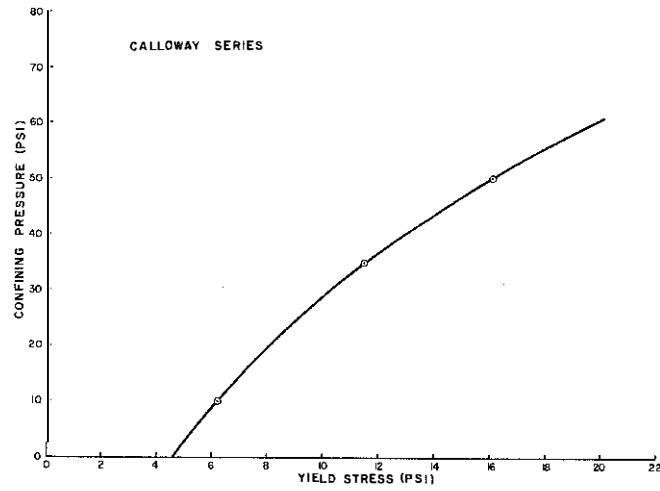
Figure 11. Relationship between Location of Yield Stress and Confining Pressure.

Figure 12. Relationship between Location of Yield Stress and Percent of Clay.





**Figure 13. Relationship between Confining Pressure and Magnitude of Yield Stress.**



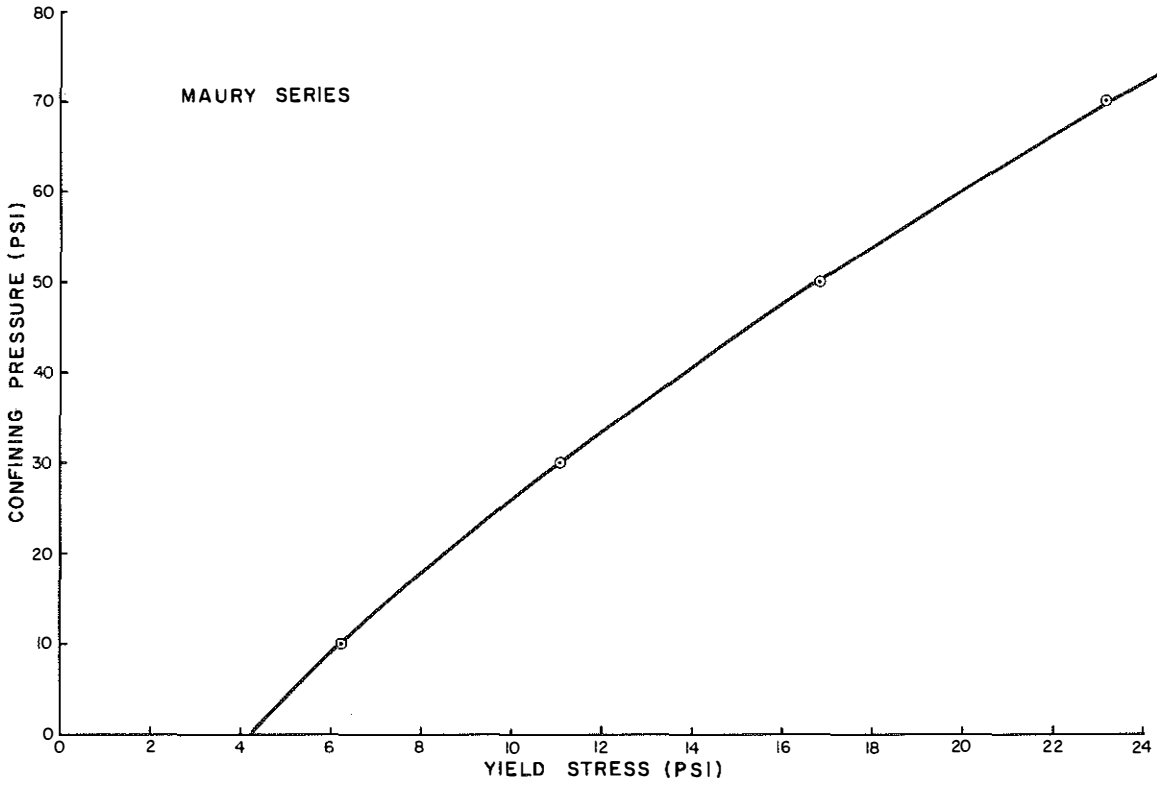
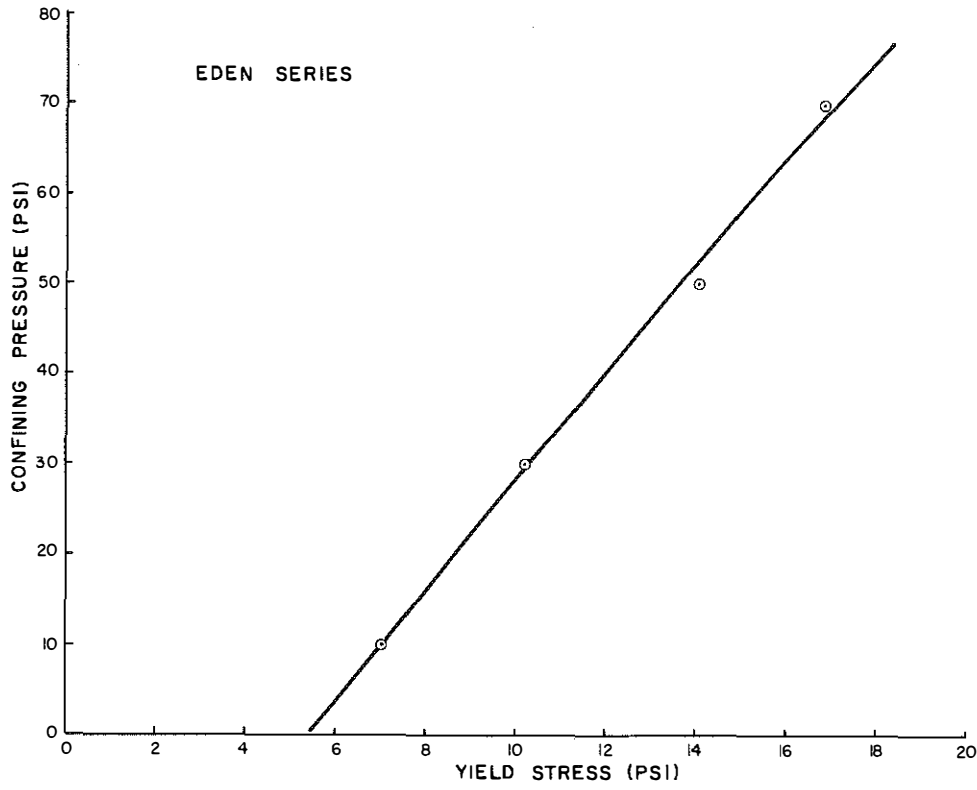


Figure 14. Relationship between Confining Pressure and Magnitude of Yield Stress.

Roscoe and Schofield (10, 19) predicted there should be a constant ratio between pore pressure increment and deviatoric strain increment. Walker (11) and Arulanandan, et al (12) have published data supporting this idea. However, Arulanandan states further this probably holds true for undisturbed soils only. Arulanandan presents data for remolded kaolinite samples that show the pore pressure reaches a peak shortly after loading and then decreases to zero over long periods of time. This difference in behavior between remolded and undisturbed samples in undrained creep tests was attributed to the counterbalancing effects of thixotropic hardening in the remolded soils and the arresting of secondary compression in the undisturbed soils. A more complete discussion of these forces is given in Arulanandan's paper.

Pore pressure did, in fact, decrease to zero over the 24-hour period for the remolded samples in this study (Figure 15). However, it did so in much less time than was indicated in Arulanandan's data.

Mohr's failure envelopes were constructed using the yield stress values and the results are shown in Figures 16 and 17. It was intended that effective strength parameters be used in this analysis. However, the 24-hour pore pressure readings were used (zero psi), making the analysis, in effect, one of total stress. The internal friction angles,  $\phi$ , were very low, ranging from 4.5° to 5.9°. The cohesion values varied from 1.6 to 2.6 psi.

Suklje (3) indicated that any state of stress less than the slopes of the Mohr's envelopes in Figures 16 and 17 will produce creep that is decreasing with the logarithm of time. Any further increase in the slope of stress beyond those presented will produce creep that is constant or accelerating with the logarithm of time. Suklje also stated that cohesion values for creep should be less than those for peak (Table 2).

Relaxation test data from Scott's report (14) were utilized for comparisons of peak relaxation modulus with yield stress. The plots of peak relaxation modulus against peak stress for all remolded soils are shown in the APPENDIX. Following the earlier analysis that yield stress is approximately equal to 50 percent of the peak stress, the plots in the APPENDIX were used to construct Figure 18. A multiple regression was again used to determine the relationship between peak modulus and yield stresses:

$$M_{pr} = 129.3 \sigma_y \quad (4)$$

where  $M_{pr}$  = peak relaxation modulus and  
 $\sigma_y$  = yield stress.

The 95-percent confidence interval for the average,  $y$ , of 131.77 was  $125.51 \leq y \leq 138.04$  (from Equation

3). This analysis has two sources of error: one from scatter evident in the peak relaxation modulus versus peak stress data and the other from peak stress versus yield stress data. Equation 4 would not be as accurate as the regression analysis indicates.

If the peak relaxation modulus is known, an estimate can be made of the peak stress without performing the triaxial test. The yield stress is related to the peak stress by Equation 2:

$$\sigma_y = 0.497 \sigma_u.$$

The yield stress is related to peak relaxation modulus by Equation 4:

$$M_{pr} = 129.3 \sigma_y.$$

Substituting Equation 2 into Equation 4,  $M_{pr} = 129.3 (0.497 \sigma_u)$  or

$$M_{pr} = 64.3 \sigma_u. \quad (5)$$

Figure 19 is a comparison of peak stress versus confining pressure from actual test data with data calculated from Equation 5.

## ANALYSES OF CASE HISTORIES USING RHEOLOGICAL PARAMETERS

### Grayson County, Western Kentucky Parkway, Milepost 96

In June 1968, an investigation was initiated of an unstable embankment (Figure 20) located at Station 6922+50 (Milepost 96) on the Western Kentucky Parkway, approximately one mile west of Leitchfield. This was done under another study KYHPR 68-48, "Investigation of Landslides on Highways".

The unstable area is located in the westbound lanes. Travelling west, the roadway emerges from a cut section to a fill at Station 6924+00. The unstable mass is located in the fill, constructed on a 1°00' curve and a grade of -3.9 percent. Figure 21 is a view of the slide area as it appears from the west.

A complete description of the history, topography, and geology of the slide area will be given in the final report on study KYHPR 68-48.

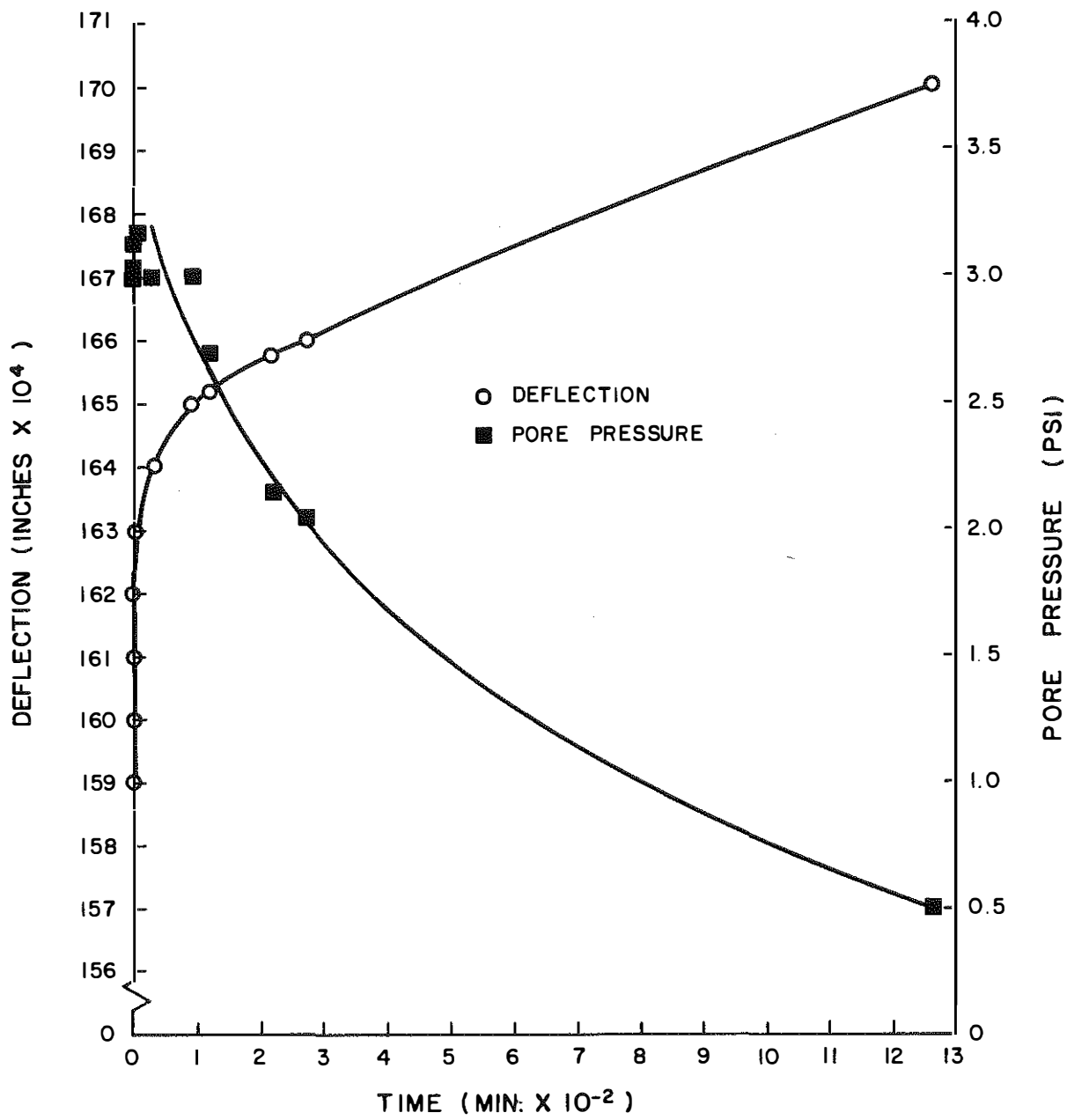


Figure 15. Relationship of Pore Pressure and Deflection to Time.

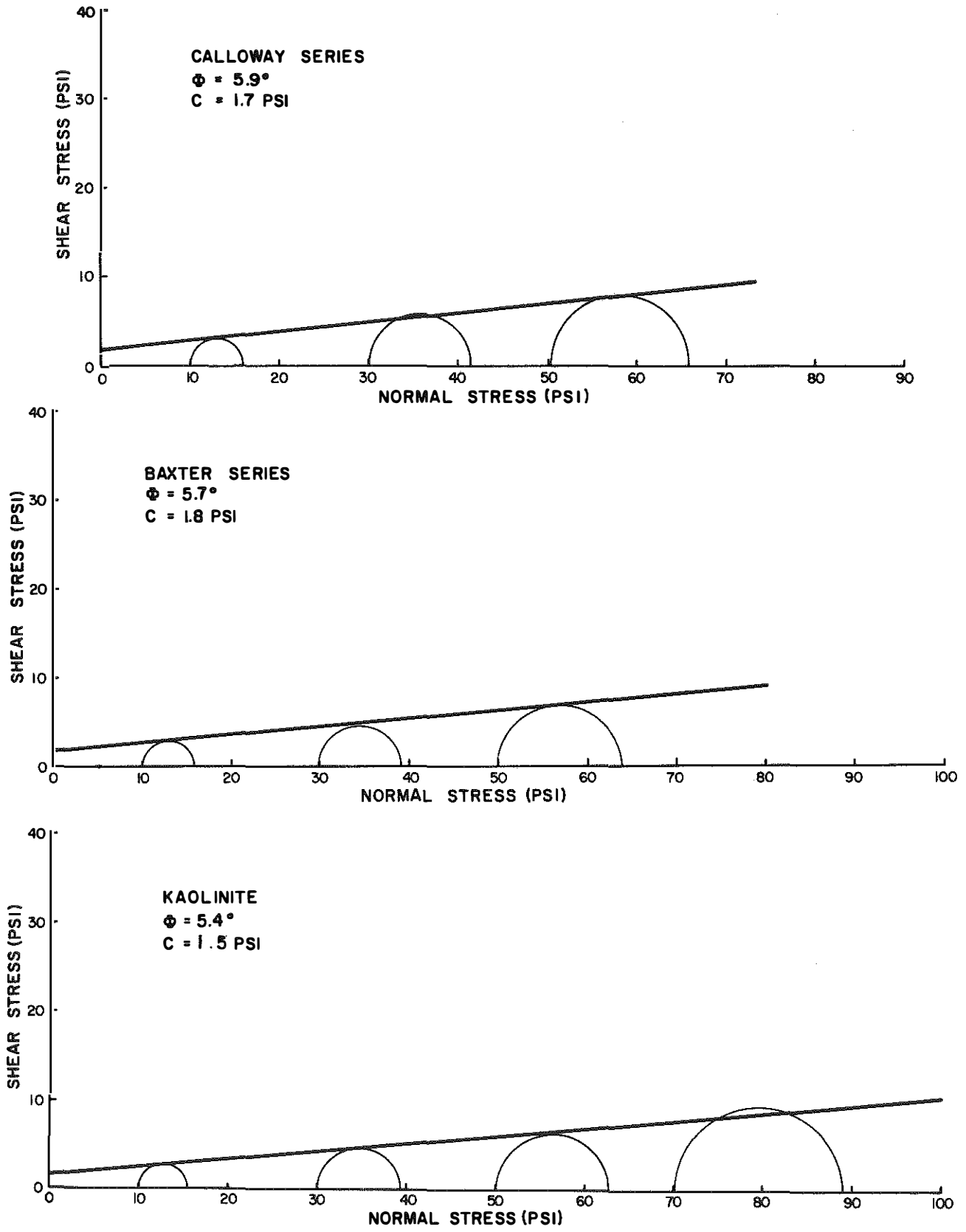


Figure 16. Failure Envelope Using Yield Stress.

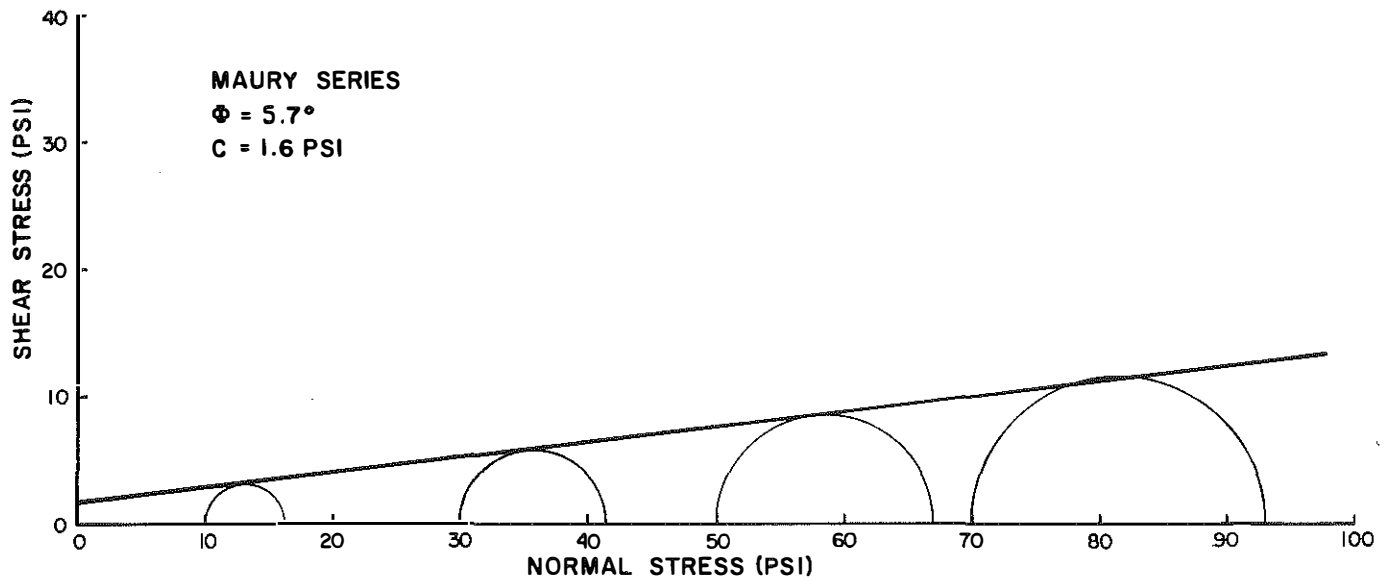
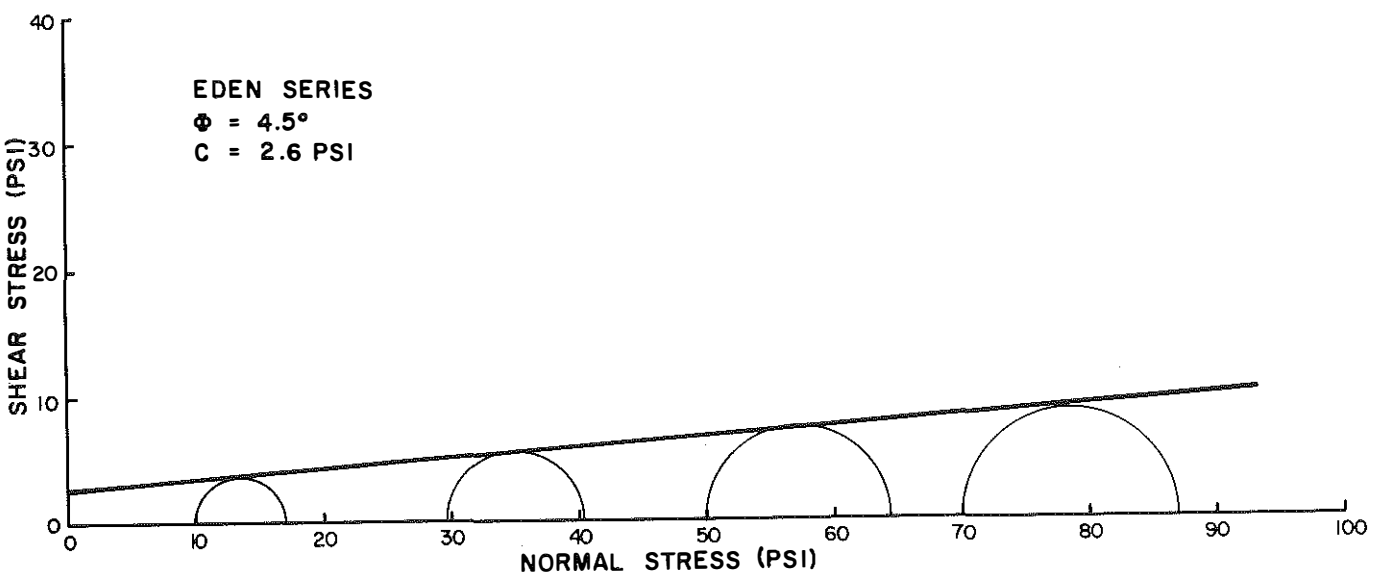
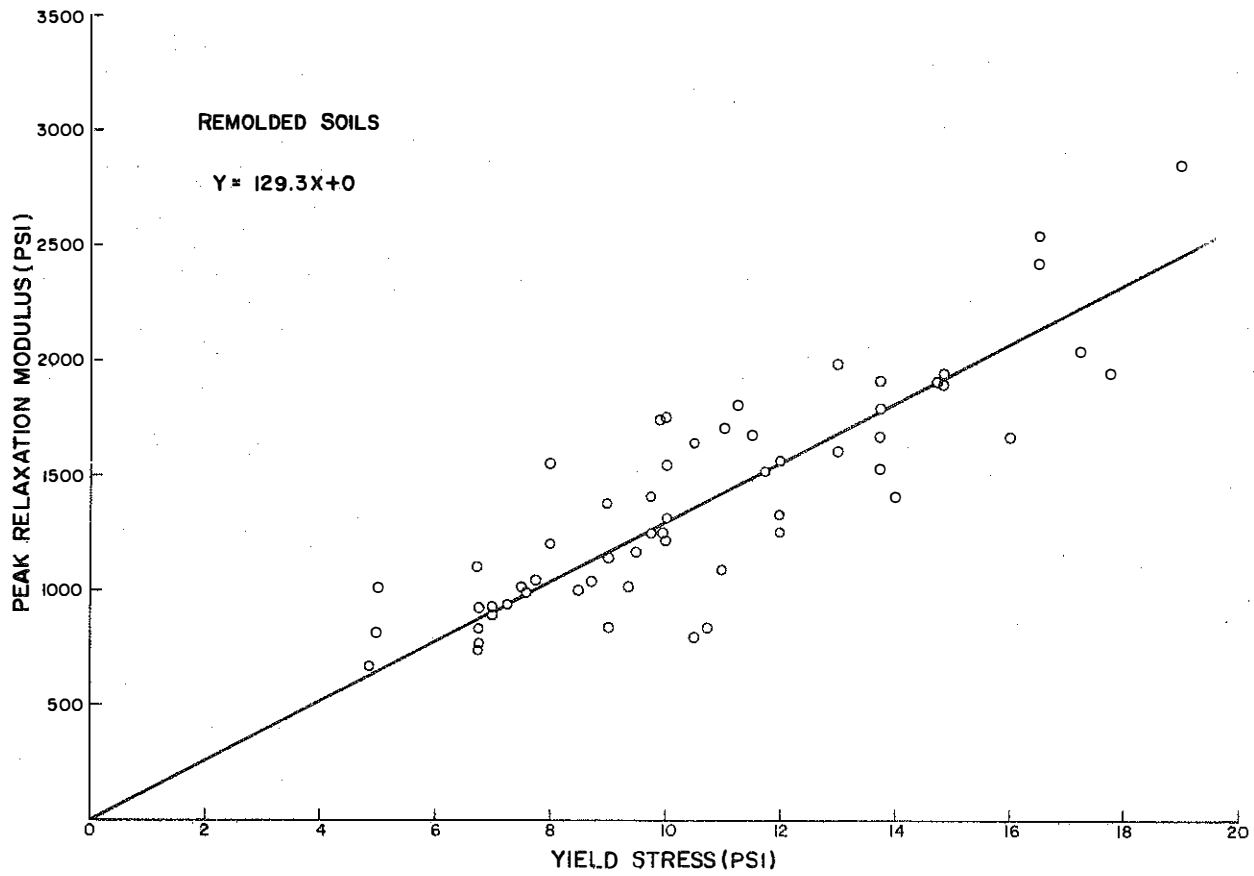


Figure 17. Failure Envelope Using Yield Stress.

**TABLE 2**  
**COMPARISON OF PEAK WITH**  
**CREEP COHESION**

SOIL	COHESION (psi)	
	PEAK	CREEP
Kaolinite	3.3	2.5
Baxter	2.0	1.8
Calloway	0.9	1.7
Eden	2.5	2.6
Maury	3.2	1.6



**Figure 18. Peak Relaxation Modulus as a Function of Yield Stress.**



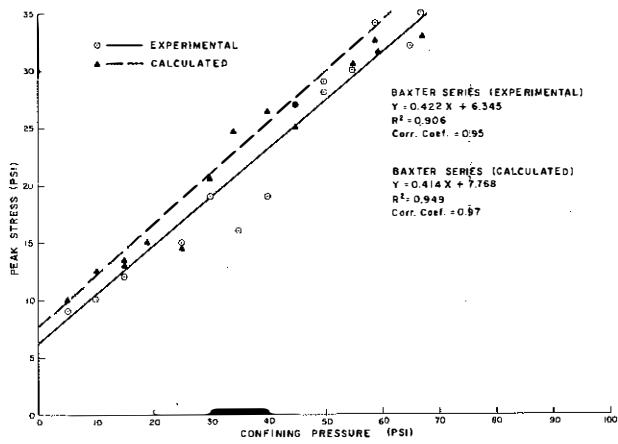
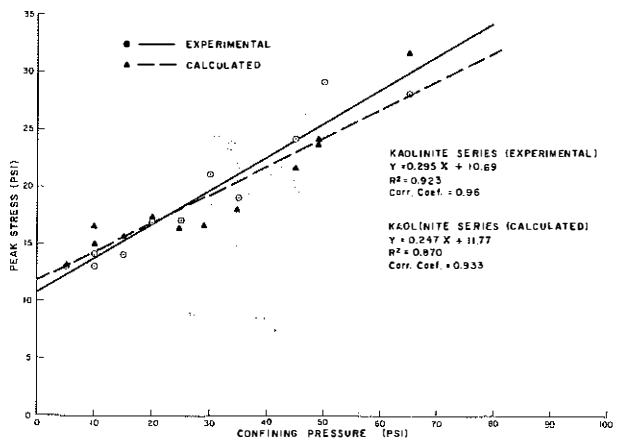
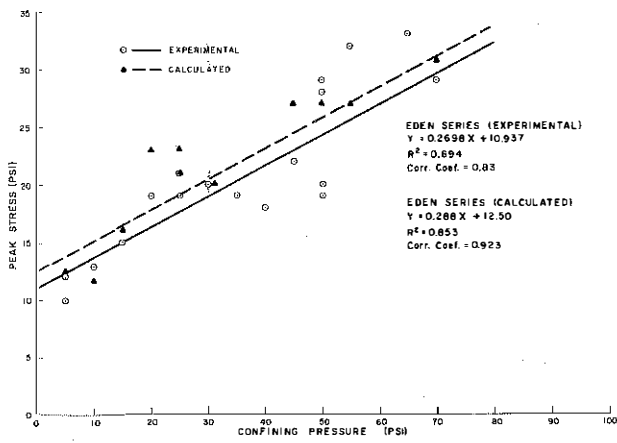
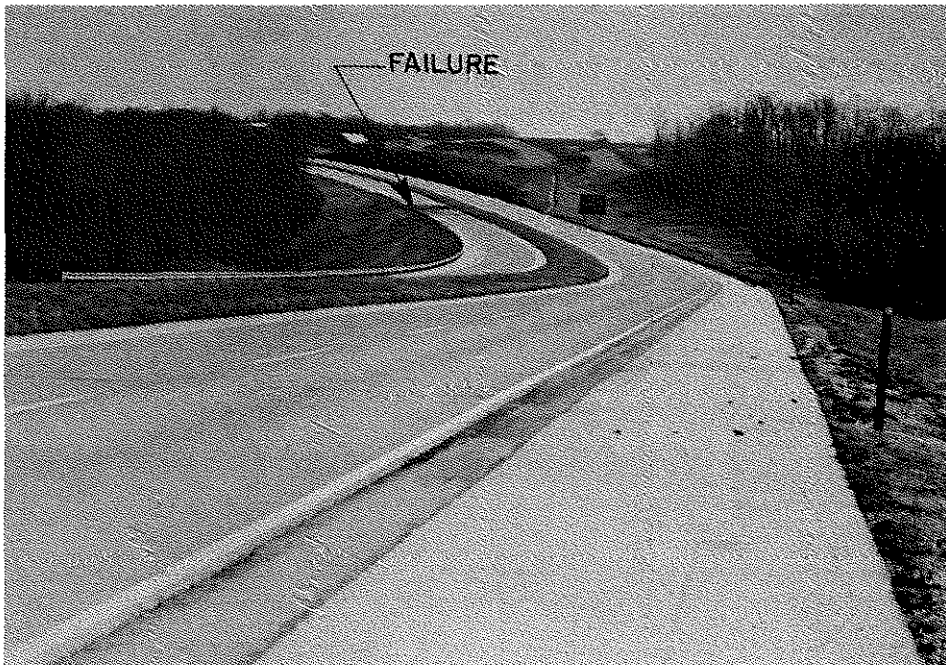


Figure 19. Peak Stress as a Function of Confining Pressure - Calculated versus Experimental.





**Figure 20.** View of Surface Break of Westbound Lanes of Western Kentucky Parkway at Station 6922 + 50.



**Figure 21.** General View of Slide Area on Western Kentucky Parkway near Milepost 96.

### Field and Laboratory Investigations

Nineteen soil borings were made to monitor fluctuations in the water table. Shelby tube samples were obtained from borings 1, 5, 6, 7, 9, 11, 12, and 13 in accordance with the method for thin-walled tube sampling of soils (ASTM Designation: D 1587). These were for strength determination and classification purposes. Figure 22 is a typical cross-section of the slide area showing the soil profile and extreme fluctuations of the watertable.

Two slope inclinometers were installed at Station 6922+50 at the top and at the toe of the embankment. Resultant horizontal movement versus depth curves and resultant horizontal movement versus time curves are shown in Figures 23 and 24.

Shelby tube samples were extruded in the laboratory, cut to the proper length, and covered with wax to insure protection while awaiting testing. Visual descriptions were made using the visual-manual procedure (ASTM Designation: D 2488 T) and moisture content specimens were taken. A complete description of care and preparation of the samples is given in Scott's report (14).

Consolidated-Isotropic-Undrained (CIU) triaxial tests and relaxation tests were performed on the undisturbed specimens and the results analyzed according to procedures outlined by Scott (14). Consolidated-undrained creep tests were also performed using procedures described by Allen (15) and were analyzed by the method given in this report under PROCEDURES.

### Results of Laboratory Tests

Visual inspection indicated Layer 1 (embankment) was a brown-to-gray, slightly organic clay having a very stiff consistency and a moisture content ranging from 13 to 17 percent. These embankment materials had a liquid limit and a plastic index of 26.4 and 12.4, respectively, and classified as an A-6(7) soil (AASHTO). Layer 2 (foundation material) was a brownish-gray clay, firm in consistency, having a moisture content from 14 to 20 percent. The liquid limit was 31.4 and the plastic index was 11.5. The foundation classified as an A-6(7) soil. A summary of the classification data is given in Table 3.

Results of the CIU triaxial tests for Layers 1 and 2 are plotted on a "P-Q diagram" in Figures 25 and 26. Figures 25a and 26a are the same as Figures 25b and 26b except only the peak deviatoric stress points are plotted. The method of least squares was used to construct the failure curve ( $K_f$  line) through the peak deviatoric stress points. The effective internal friction angle,  $\phi'$ , and the effective cohesion,  $c'$ , for Layer 1 were  $26.7^\circ$  and zero, respectively.  $\phi'$  and  $c'$  for Layer

2 were  $25.1^\circ$  and 3.3 psi.

Scott (14) proposed a number of methods for constructing Mohr's failure envelopes solely from information gained from two or three relaxation tests and one triaxial test performed on a single sample. One of these was used in this case history. In this method a sample was set in the triaxial chamber and consolidated overnight under 10-psi confining pressure. A relaxation test was performed the next morning and the confining pressure was then increased to 50 psi. After again consolidating overnight, a second relaxation test was performed. A regular triaxial test was then performed at the end of the second relaxation test. The peak relaxation modulus at 50-psi confining pressure was plotted against peak stress from the triaxial test and a line was drawn through the point (0, 0). The peak stress at 10-psi confining pressure was found by extrapolating horizontally the value of the peak relaxation modulus at 10 psi until it intersected the straight line already constructed. From that intersection point, a line was constructed vertically, intersecting the horizontal axis at the value of the peak stress at 10-psi confining pressure. The stress values thus obtained were used to construct the Mohr's stress circles in Figures 27a and 28a.

To obtain effective stress parameters for Figures 27a and 28a, the value of the product of A and B was plotted against confining pressure of 50 psi and, again, a straight line was drawn between that point and the origin. The product of A and B at 10-psi confining pressure was then read graphically (Figures 27c and 28c). The pore pressure was then calculated from

$$\Delta u = AB (\sigma_1 - \sigma_3), \quad (6)$$

where  $\Delta u$  = change in pore pressure and  
 $\sigma_1 - \sigma_3$  = deviator stress.

The pore pressures were subtracted from the peak stresses (Figures 27b and 28b) to give the values for  $\phi'$  and  $c'$  in Figures 27a and 28a.

Scott's data indicated that a linear relationship existed between peak relaxation modulus versus peak stress and between A times B at failure versus confining pressure. His data also indicated that both relationships passed through the origin. This was the basis for constructing Figures 27b,c and 28b,c. Complete descriptions and discussions of this method and others are given in Scott's report (14).

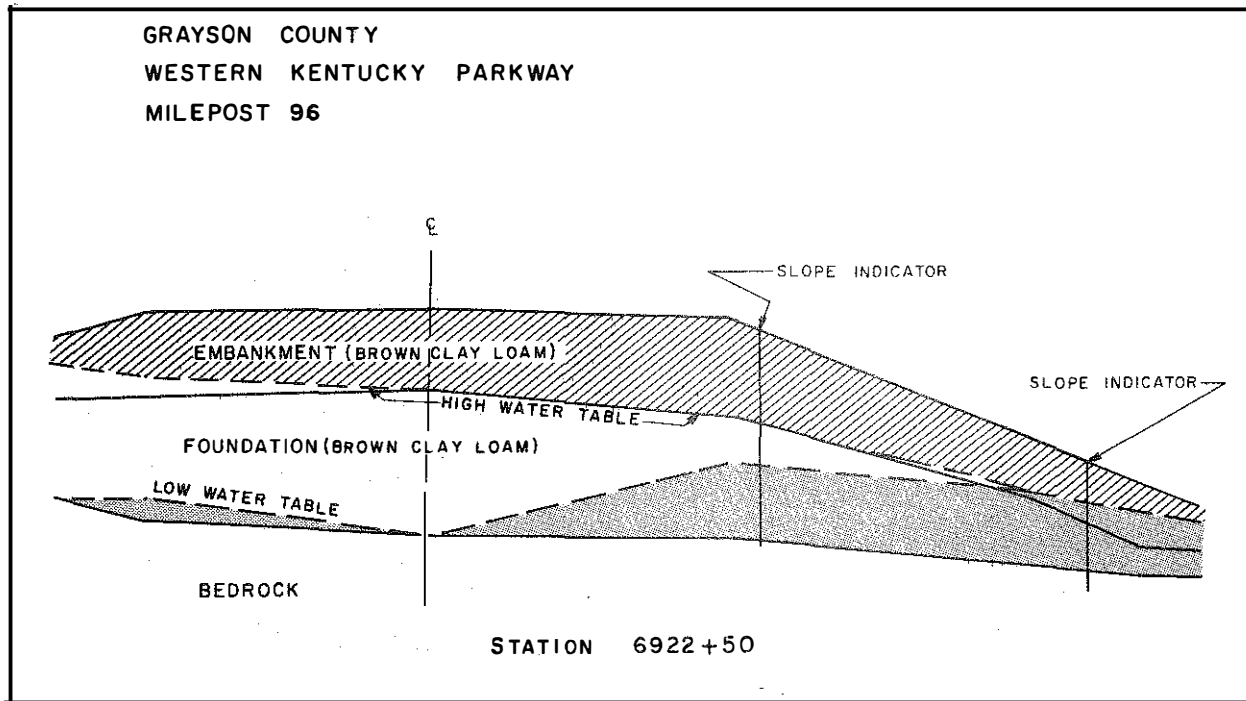


Figure 22. Cross Section of Station 6922 + 50  
 Showing Location of Slope  
 Indicator Casings - Western  
 Kentucky Parkway.

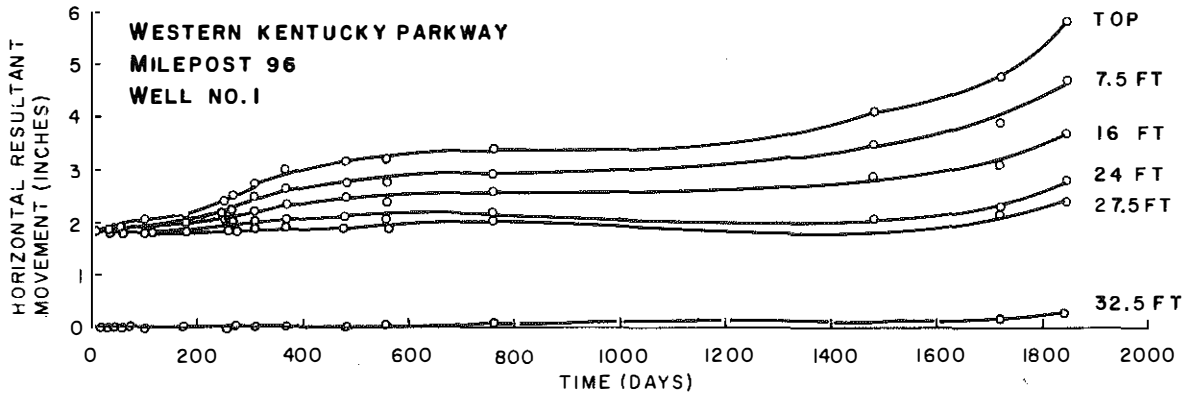
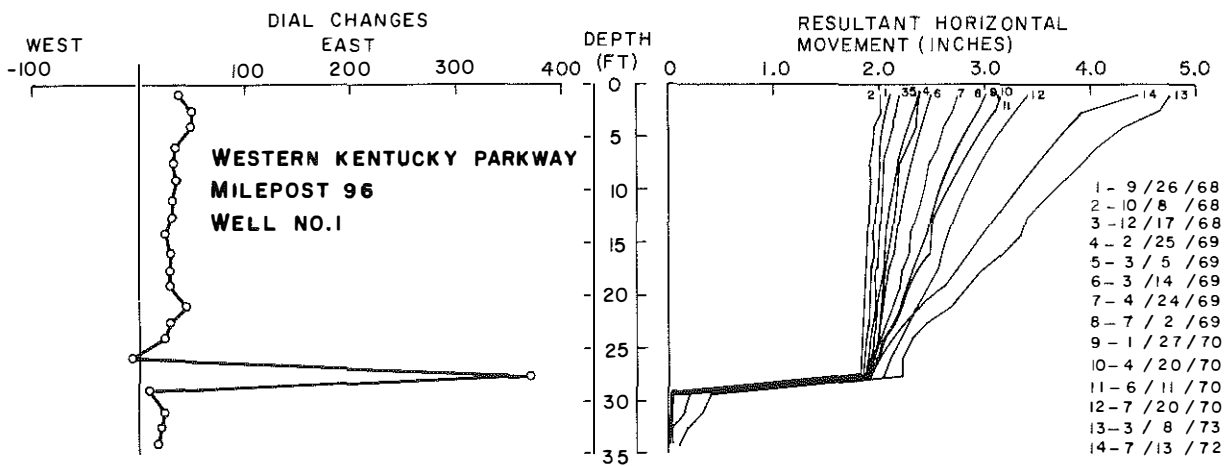


Figure 23. Slope Inclinometer Results, Well No. 1, Western Kentucky Parkway.

**WESTERN KENTUCKY PARKWAY  
MILEPOST 96  
WELL NO. 2**

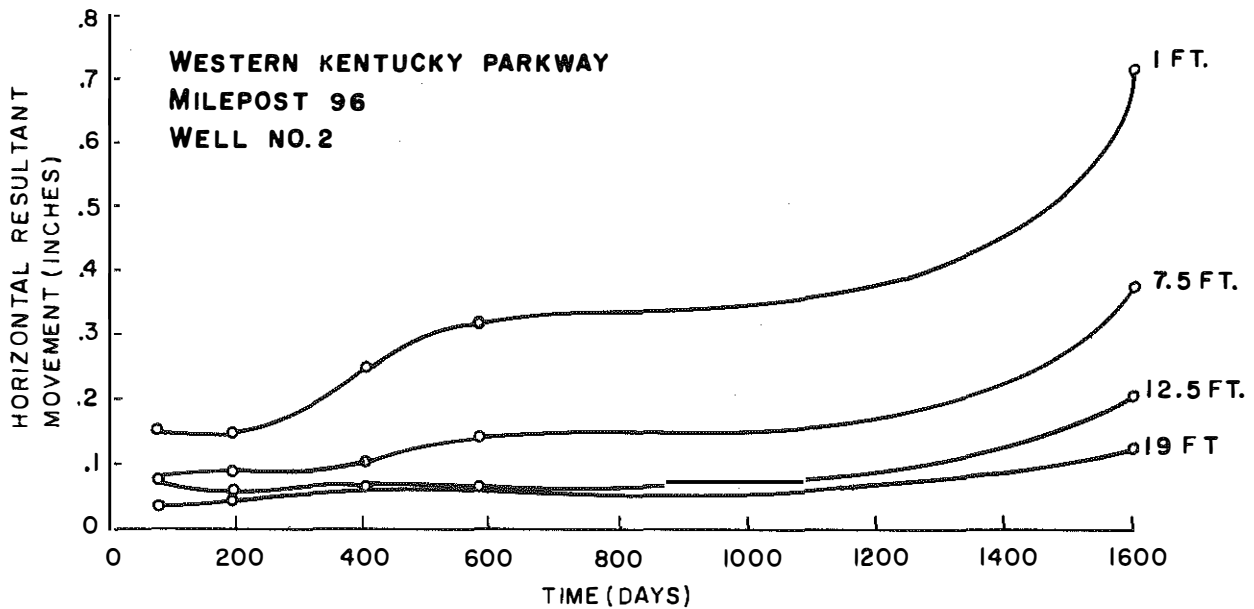
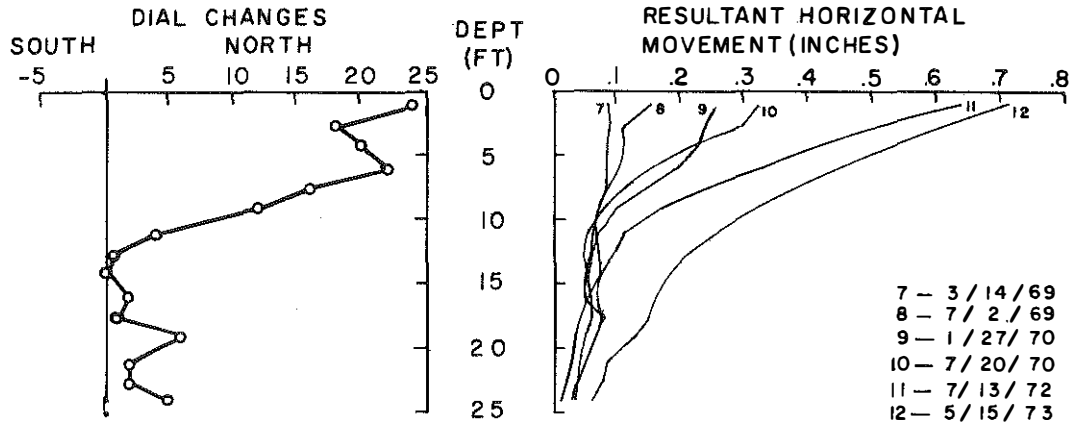
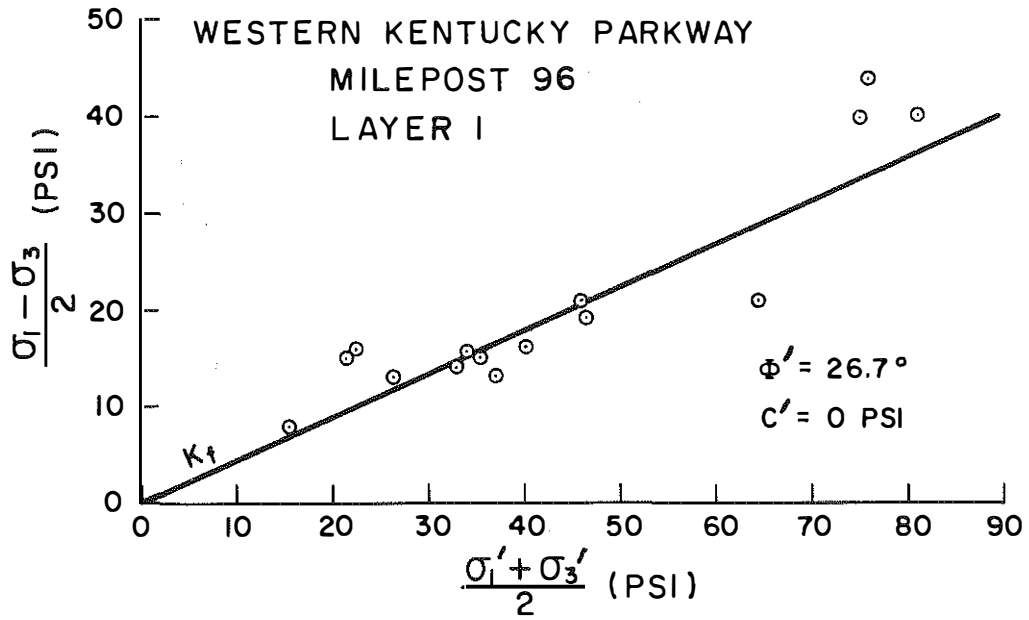


Figure 24. Slope Inclinometer Results, Well No. 2, Western Kentucky Parkway.

a



b

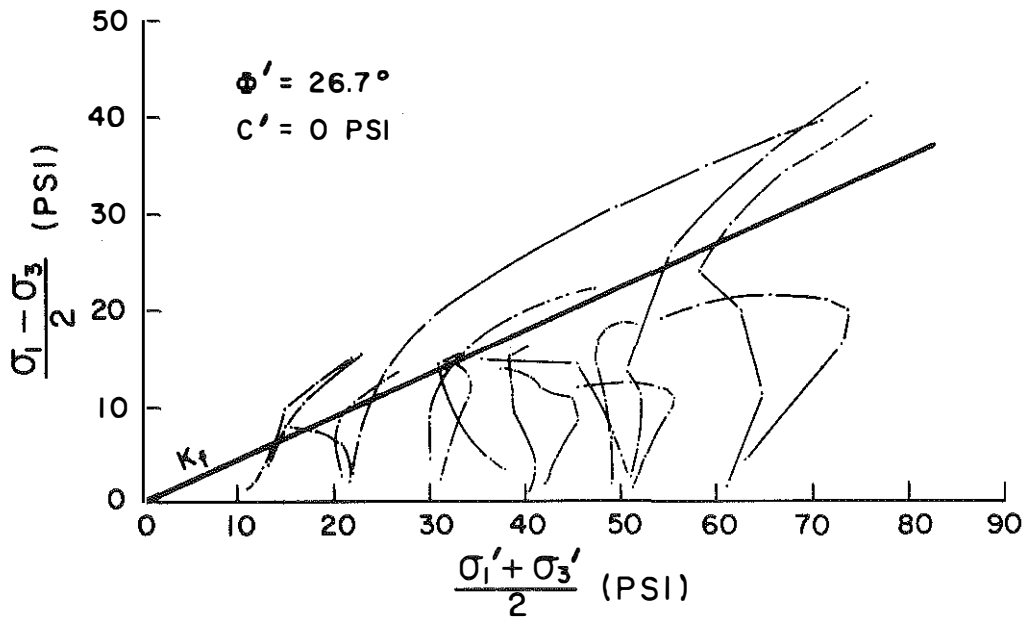
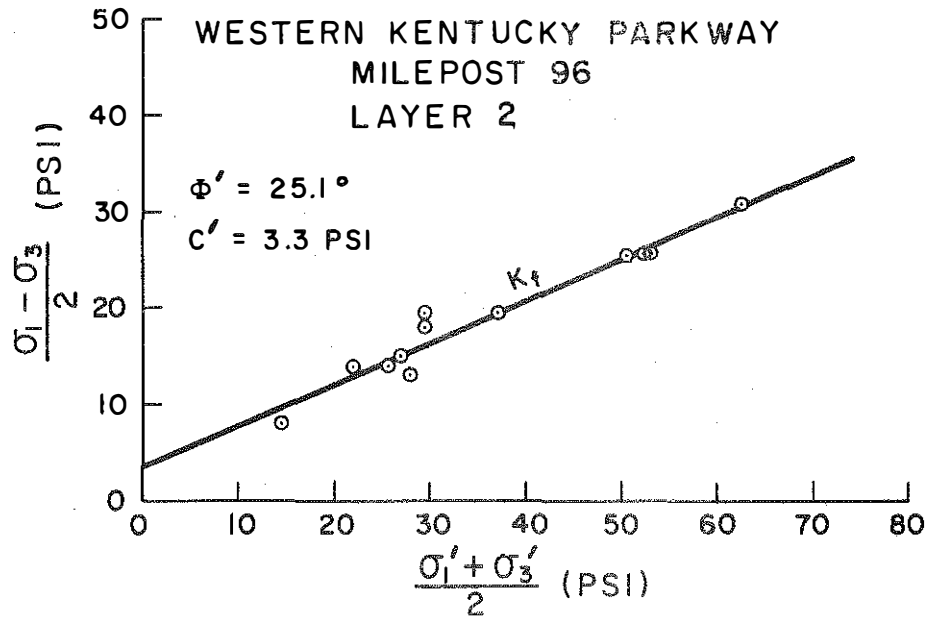


Figure 25. Consolidated, Isotropic, Undrained Triaxial Test Results, Layer 1 (Embankment) - Western Kentucky Parkway.

a



b

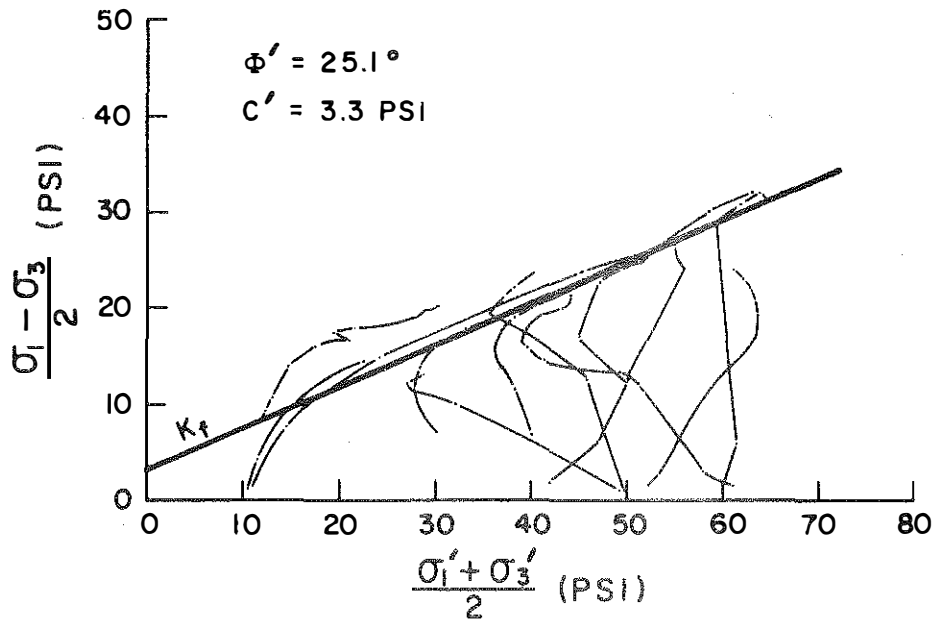
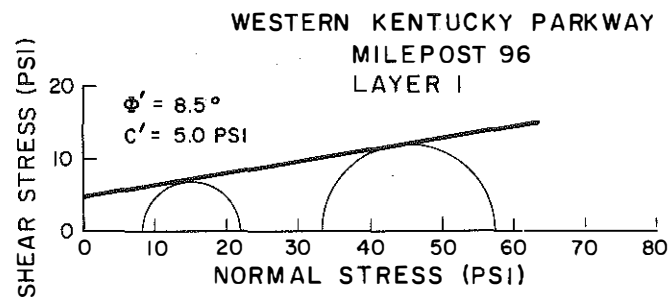


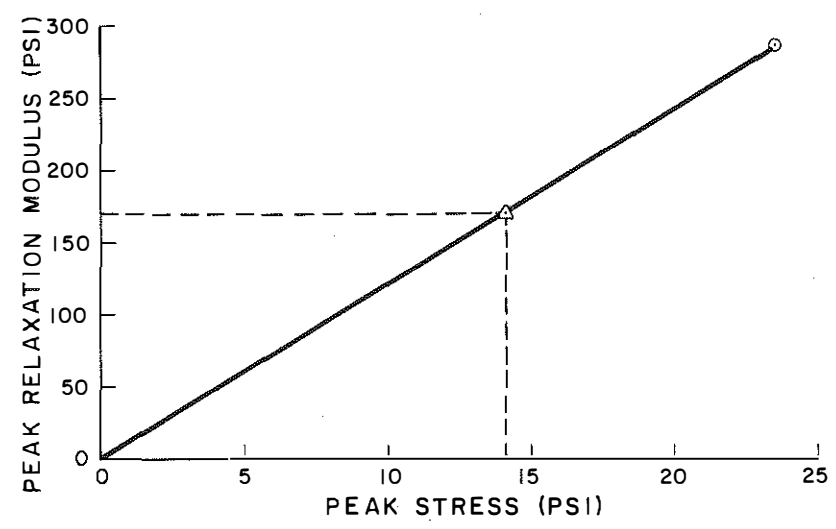
Figure 26. Consolidated, Isotropic, Undrained Triaxial Test Results, Layer 2 (Foundation) - Western Kentucky Parkway.



a



b



c

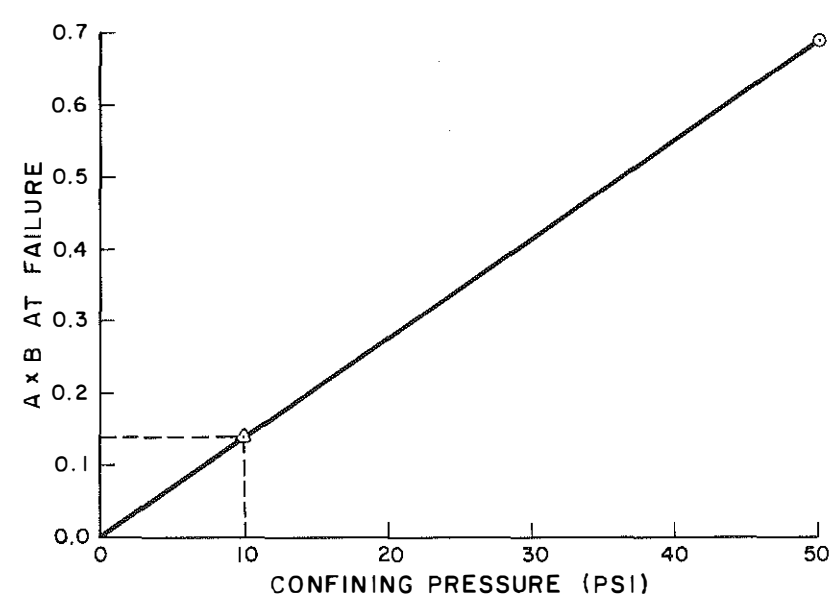
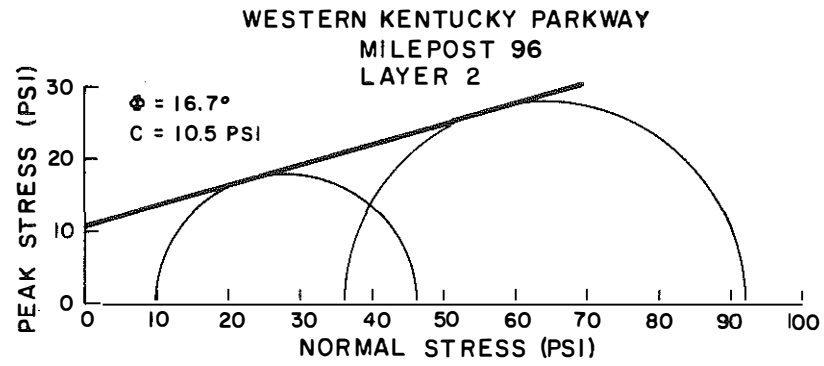
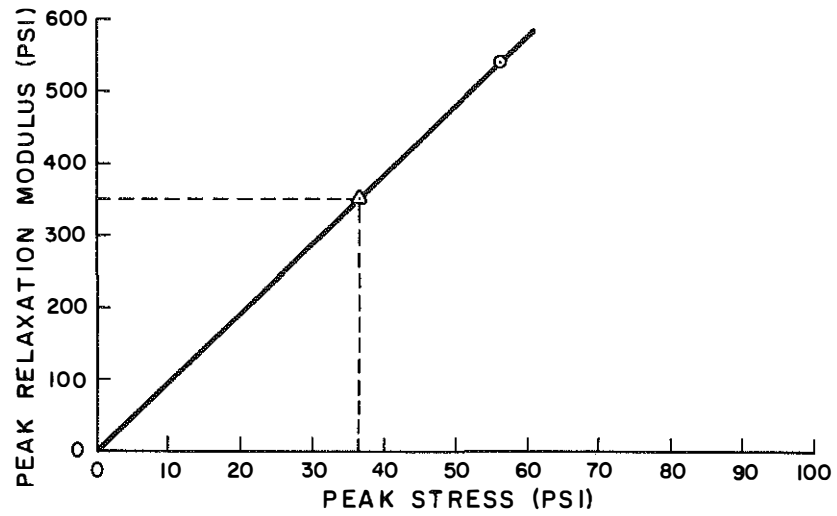


Figure 27. Shear Strength Results from Special Relaxation - Triaxial Test Using One Specimen, Layer 1 (Embankment) - Western Kentucky Parkway.

a



b



c

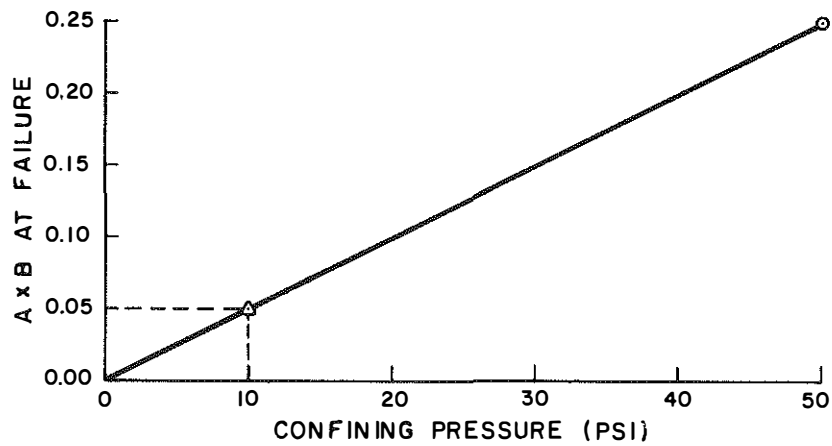


Figure 28. Shear Strength Results from Special Relaxation - Triaxial Test Using One Specimen, Layer 2 (Foundation) - Western Kentucky Parkway.

TABLE 3

SUMMARY OF CLASSIFICATION TEST RESULTS

		WESTERN KENTUCKY PARKWAY STATIONS 6921 - 6924 GRAYSON COUNTY		I 64 STATION 1866 SHELBY COUNTY	
		LAYER 1	LAYER 2	LAYER 1	LAYER 2
Liquid Limit		26.4	31.4	38.1	40.2
Plastic Limit		14.0	19.4	16.8	17.9
Percent Finer Than	1"	100	100	100	100
	3/4"	98	99	98	100
	3/8"	93	95	87	94
	No. 4	92	91	85	91
	No. 10	91	88	84	87
	No. 20	91	86	84	86
	No. 40	90	83	83	85
	No. 60	90	81	83	84
	No. 140	69	71	81	83
	No. 200	63	66	81	82
	.05 mm	58	59	67	75
	.02 mm	57	50	57	59
	.005 mm	27	28	37	41
.002 mm	21	23	30	34	
Classification	Unified	CL	CL	CL	CL
	AASHO	A-6(7)	A-6(7)	A-6(11)	A-7-6(11)
	Textural	Clay Loam	Clay Loam	Clay	Clay

Failure envelopes constructed by this method did not compare well with envelopes obtained from conventional triaxial tests. The effective strength parameters for Layer 1,  $\phi'$  and  $c'$ , were  $8.5^\circ$  and 5.0 psi, respectively. The peak stress for the test run at 50-psi confining pressure and the product A times B appeared low. Both factors would produce small  $\phi'$  angles and high cohesion. Scott's method produced a  $\phi'$  of  $16.7^\circ$  and  $c'$  of 10.5 psi for Layer 2. Again, the product of A times B appeared too low.

Figures 29 and 30 present the viscosity diagrams, obtained from the creep tests, for Layers 1 and 2. As would be expected, there was more scatter in the location of the yield stress in the undisturbed soils than in the remolded soils. Figure 31 shows the relationship between yield stress and peak stress for the undisturbed soils. From a regression analysis, yield stress equalled 52.3 percent of the peak stress compared to 49.7 for the remolded soils.

Mohr's envelopes were constructed for Layers 1 and 2 using the yield stresses (Figures 32 and 33). As in the case of the remolded soils and for the sake of consistency, zero pore pressure was used making the analysis one of total stress. The strength parameters for Layer 1 were  $5.0^\circ$  ( $\phi$ ) and 1.8 psi ( $c'$ ).  $\phi$  equalled  $9.4^\circ$  and  $c$  equalled 0.75 psi for Layer 2.

#### *Stability Analysis (As Built)*

Slope inclinometer data presented in Figures 23 and 24 indicate the well at the top of the embankment (Inclinometer 1) has moved in a northeasterly direction and the top of the casing has moved a total of 5.8 in. Inclinometer 2, at the toe of the embankment is moving northwesterly. The top of the casing has moved approximately 0.7 in. Figure 34 is a plan view of the slide showing the directions of thrust of the moving mass. From visual observations and slope inclinometer data, the failure surface at Station 6922+50 is located in the foundation at 27.5 ft under the shoulder and at 9.0 ft under the toe and intersects the roadway in the middle of the driving lanes. There is no visible break at the toe.

Stability analyses were performed on the cross-section at Station 6922+50 using a computerized solution of Bishop's Simplified Method of Slices, by Yoder and Hopkins (20). Using the peak shear strength parameters obtained from the CIU triaxial tests (Figures 25 and 26) and the highest observed watertable, the "as built" factor of safety was 1.849 (Analysis 10, Table 4). The theoretical failure surface agrees fairly well with the observed (Figure 35). The theoretical factor of safety indicates the embankment should not have failed and the design, therefore, was adequate when using peak strength parameters. However, if one assumes the available cohesion in the foundation is a decreasing

function with time and that it eventually becomes zero, then the long term factor of safety would be 1.044 (Analysis 9, Table 4). This analysis (labeled "Residual" in Table 4) was made assuming high watertable and excess pore pressures due to seepage (Figure 36). It would appear, therefore, that a decrease in cohesion was indeed the case and, consequently, contributed to failure.

Analysis was made using shear strength parameters from Scott's method using relaxation data. Using a low watertable, the "as built" factor of safety was 3.220 (Analysis 4, Table 4). This is 63 percent greater than the peak strength analysis using a low watertable (Analysis 1, Table 4).

Analysis 11 in Table 4 was made using creep strength in conjunction with the high watertable. The minimum factor of safety was 0.701. There was excellent agreement between the observed and theoretical failure surfaces (Figure 37). However, the failure surface in the creep analysis was deeper at the toe than the observed failure surface.

#### *Remedial Analysis*

Three different remedial designs were analyzed. The first was a change in the side slope from 2:1 to 3:1. Analysis 7, using peak parameters and a high watertable with seepage, yielded a factor of safety of 2.178 with the slope change. "Residual" strength (Analysis 8), using the same water conditions, gave a factor of safety of 1.372. However, creep strength (Analysis 6) had a factor of safety of only 0.811 for the slope change. Figure 38 shows the theoretical failure surfaces for these three analyses.

In the second design, a berm 40 ft wide and approximately 25 ft high (Berm 1, Figure 39) was used. Again, using a high watertable with seepage conditions, the factors of safety for peak, "residual", and creep strengths were 3.601, 2.527 and 1.056, respectively. This is obviously an overdesign if one considers only peak or "residual" strength; however, this would be strictly a minimal design if creep strength were the governing factor in design.

To insure a better design that would provide a greater margin of safety against soil creep, the width of the berm was increased to 60 ft (Berm 2). In this analysis (Analysis 17), designing with creep strength gave a factor of safety of 1.407, which was considered an adequate design to insure against large strains resulting from soil creep. Peak and "residual" strength analyses yielded factors of safety of 5.065 and 3.596, respectively, for this case, shown in Figure 40.

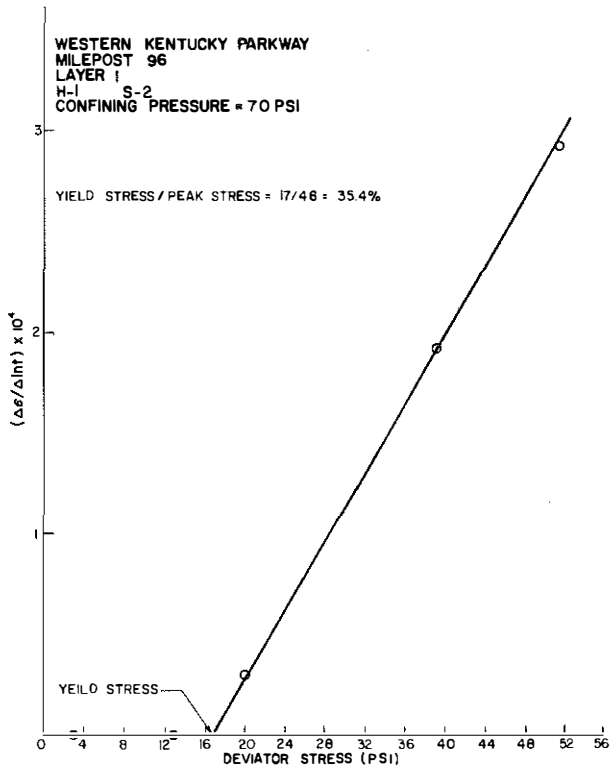
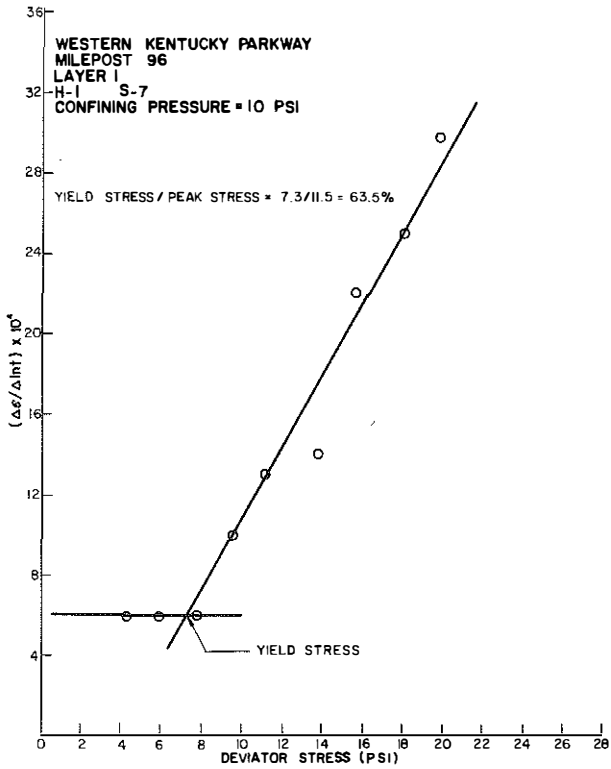
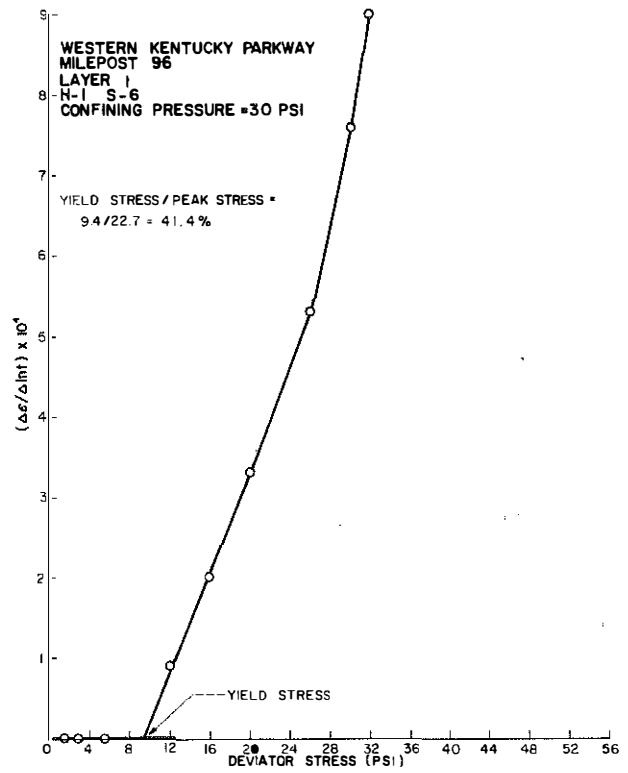


Figure 29. Viscosity Diagrams, Layer 1 (Embankment) - Western Kentucky Parkway.



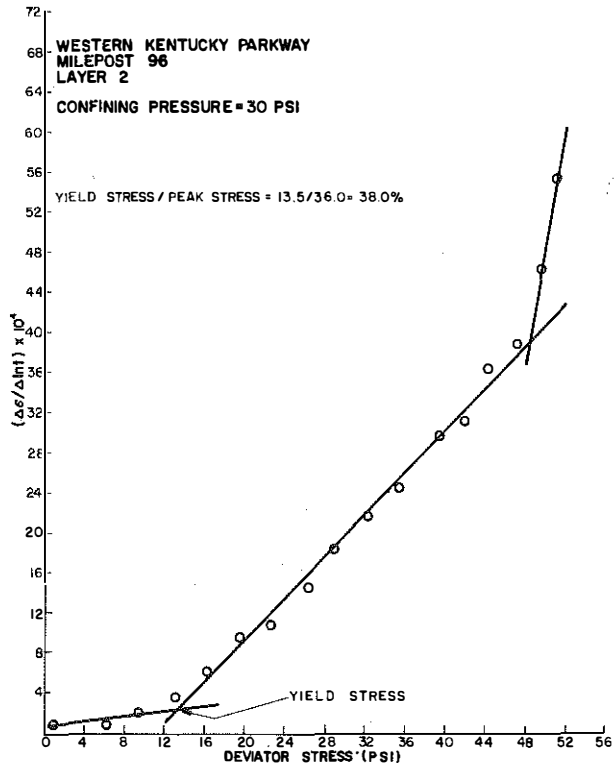
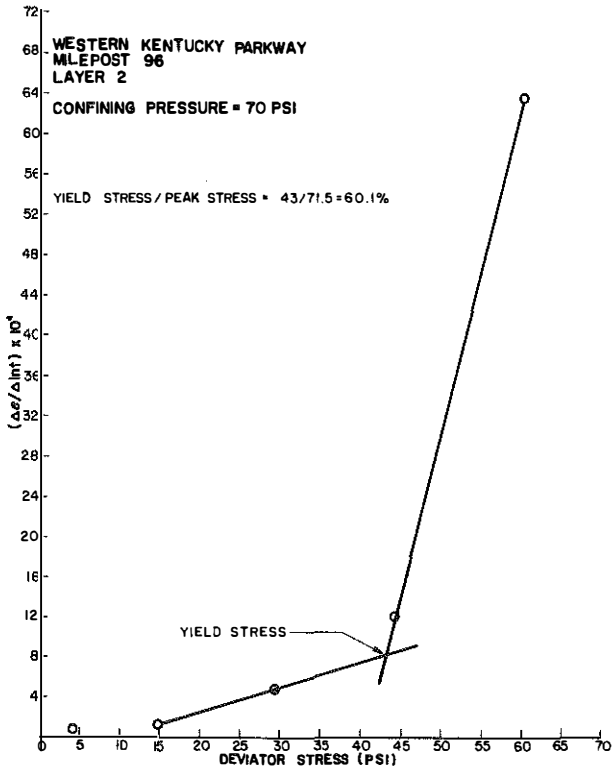
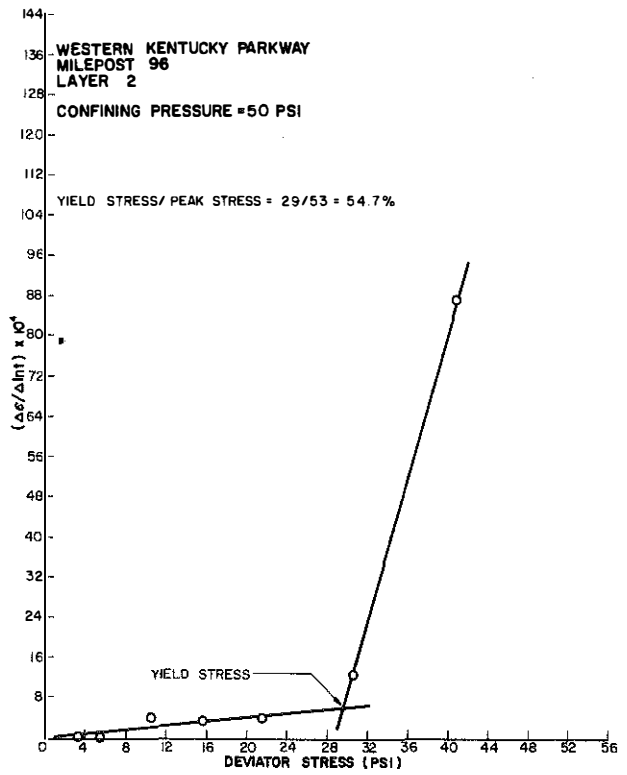


Figure 30. Viscosity Diagrams, Layer 2 (Foundation) - Western Kentucky Parkway.



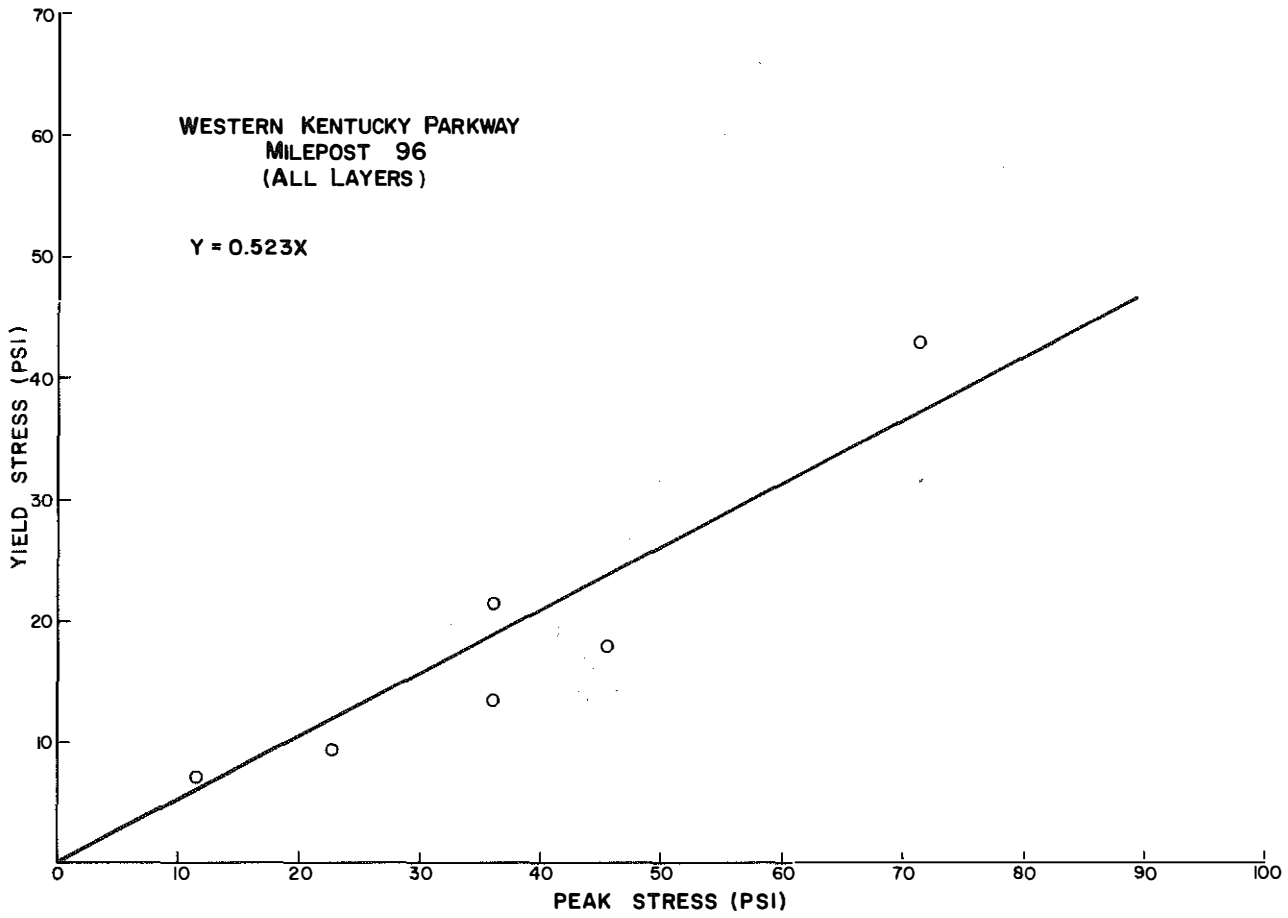


Figure 31. Yield Stress as a Function of Peak Stress, All Layers, Western Kentucky Parkway.

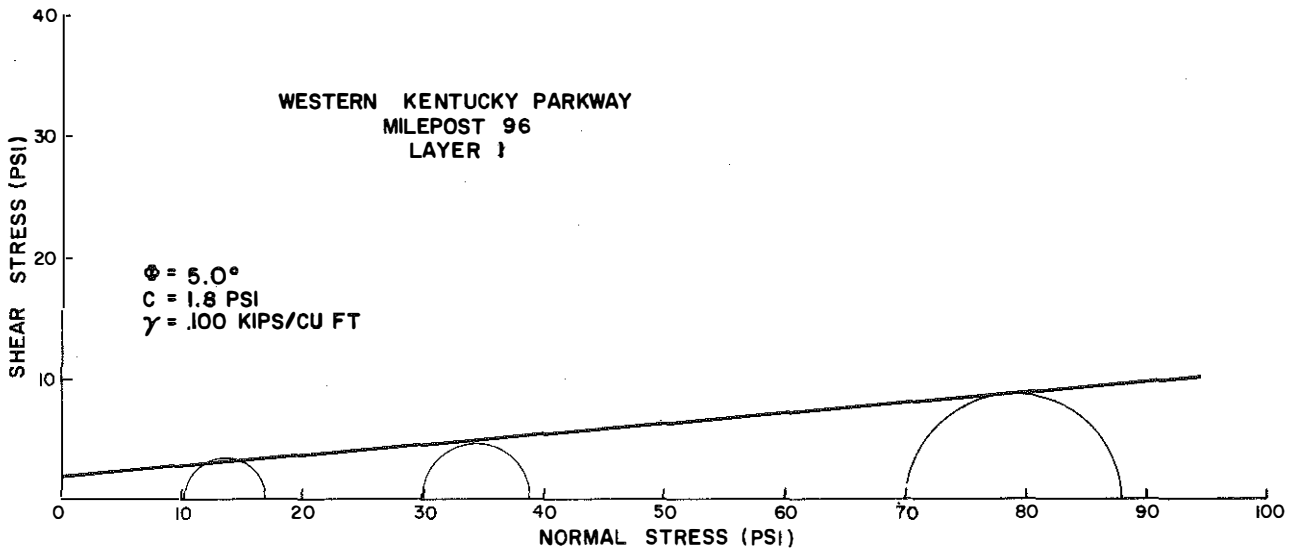


Figure 32. Failure Envelope Using Yield Stress, Layer 1 (Embankment) - Western Kentucky Parkway.

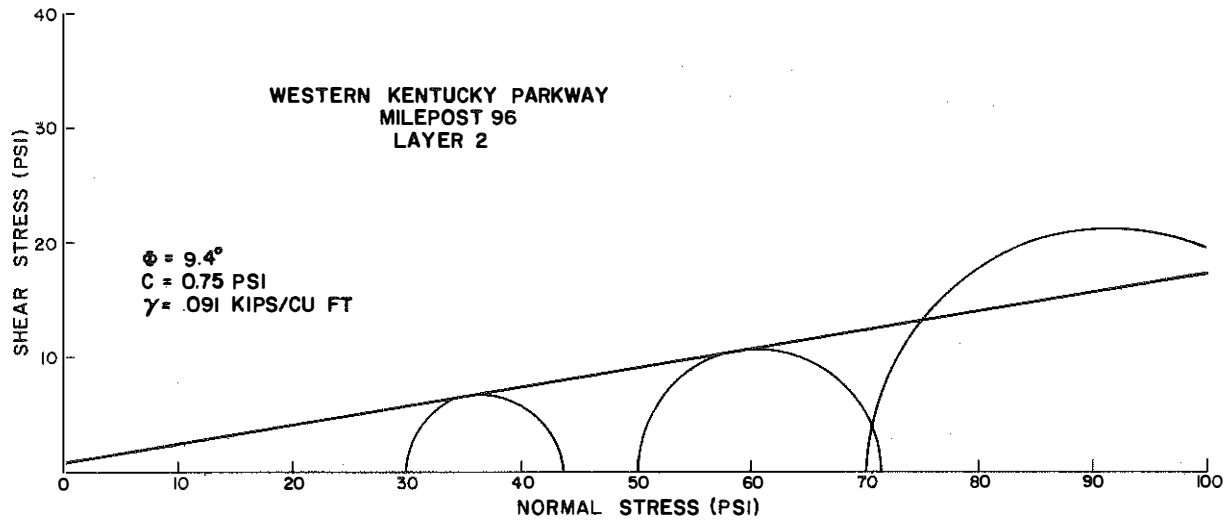


Figure 33. Failure Envelope Using Yield Stress - Layer 2 (Foundation) - Western Kentucky Parkway.

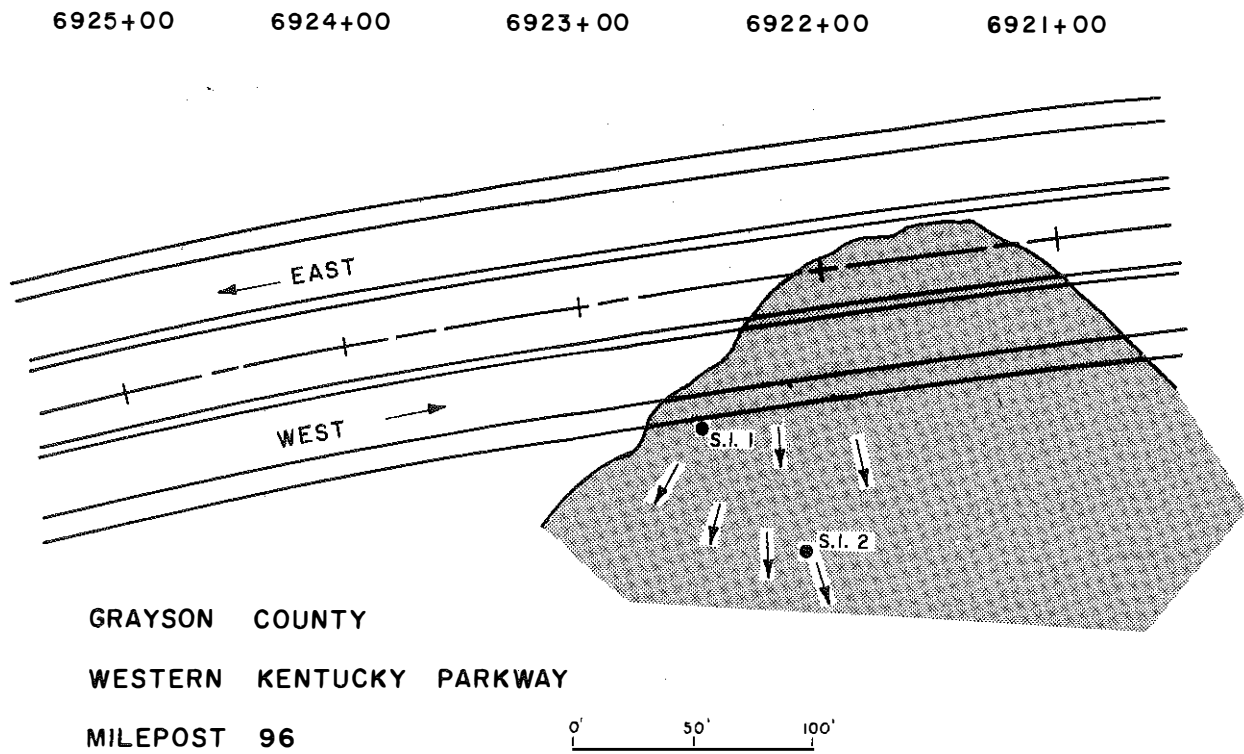


Figure 34. Plan View of Slide Area Showing Directions of Movement of Soil Mass - Western Kentucky Parkway.



TABLE 4

SUMMARY OF STABILITY ANALYSES  
WESTERN KENTUCKY PARKWAY  
MILEPOST 96

ANALYSIS NO.	NUMBER OF LAYERS	STRENGTH PARAMETERS (SEE DEFINITIONS OF STRENGTH) TABLE	WATER TABLE	SIDE SLOPE	FACTOR OF SAFETY	TYPE OF ANALYSIS	DEFINITIONS OF STRENGTH
1	2	Peak Strength (1)	Low	2:1	1.972	Grid Search	(1) PEAK STRENGTH
2	2	Creep Strength (2)	Low	2:1	0.747	Grid Search	Obtained from Conventional Triaxial Tests.
3	2	Residual Strength (3)	Low	2:1	1.185	Grid Search	LAYERS 1 & 3
4	2	Special Strength (4)	Low	2:1	3.220	Grid Search	$\phi = 26.7^\circ$ $c = 0.0 \text{ kips/ft}^2$ $\gamma = .096 \text{ kips/ft}^3$
6	2	Creep Strength (2)	High	3:1	0.811	Grid Search	LAYERS 2 & 4
7	2	Peak Strength (1)	High	3:1	2.178	Grid Search	$\phi = 25.1^\circ$ $c = .475 \text{ kips/ft}^2$ $\gamma = .094 \text{ kips/ft}^3$
8	2	Residual Strength (3)	High	3:1	1.372	Grid Search	(2) "CREEP" STRENGTH
9	2	Residual Strength (3)	High	2:1	1.844	Grid Search	Obtained from Creep Tests.
10	2	Peak Strength (1)	High	2:1	1.849	Grid Search	LAYERS 1 & 3
11	2	Creep Strength (2)	High	2:1	0.701	Grid Search	$\phi = 5.8^\circ$ $c = .259 \text{ kips/ft}^2$ $\gamma = .096 \text{ kips/ft}^3$
12	2	Peak Strength (2)	Low	3:1	2.290	Grid Search	LAYERS 2 & 4
13	2	Creep Strength (2)	Low	3:1	0.850	Grid Search	$\phi = 9.4^\circ$ $c = .106 \text{ kips/ft}^2$ $\gamma = .094 \text{ kips/ft}^3$
14	2	Residual Strength (3)	Low	3:1	1.477	Grid Search	(3) "RESIDUAL" STRENGTH
15	2	Creep Strength (2)	Low	2:1 (Berm 1)	1.087	Grid Search	This is Peak Strength
16	2	Creep Strength (2)	Low	2:1 (Berm 2)	1.422	Grid Search	Obtained from Triaxial Tests with Cohesion Assumed Equal to Zero.
17	2	Creep Strength (2)	High	2:1 (Berm 2)	1.407	Grid Search	LAYERS 1 & 3
18	2	Creep Strength (2)	High	2:1 (Berm 1)	1.056	Grid Search	$\phi = 26.7^\circ$ $c = 0.0 \text{ kips/ft}^2$ $\gamma = .096 \text{ kips/ft}^3$
19	2	Creep Strength (2)	Low	2:1 (Berm 1)	1.477	Detailed Analysis of Failure Circle	LAYERS 2 & 4
20	2	Creep Strength (2)	Low	2:1 (Berm 2)	2.152	Detailed Analysis of Failure Circle	$\phi = 25.1^\circ$ $c = 0.0 \text{ kips/ft}^2$ $\gamma = .094 \text{ kips/ft}^3$
21	2	Creep Strength (2)	High	2:1 (Berm 2)	2.058	Detailed Analysis of Failure Circle	(4) SPECIAL STRENGTH
22	2	Creep Strength (2)	High	2:1 (Berm 1)	1.407	Detailed Analysis of Failure Circle	Obtained in Same Manner as Above.
23	2	Creep Strength (2)	High	3:1	0.904	Detailed Analysis of Failure Circle	LAYERS 1 & 3
24	2	Creep Strength (2)	High	2:1	0.733	Detailed Analysis of Failure Circle	$\phi = 8.5^\circ$ $c = .720 \text{ kips/ft}^2$ $\gamma = .046 \text{ kips/ft}^3$
25	2	Creep Strength (2)	Low	2:1	0.763	Detailed Analysis of Failure Circle	LAYERS 2 & 4
26	2	Peak Strength (1)	Low	2:1 (Berm 1)	3.899	Detailed Analysis of Failure Circle	$\phi = 16.7^\circ$ $c = 1.512 \text{ kips/ft}^2$ $\gamma = .094 \text{ kips/ft}^3$
27	2	Peak Strength (1)	Low	3:1	2.578	Detailed Analysis of Failure Circle	
28	2	Peak Strength (1)	High	2:1 (Berm 1)	3.701	Detailed Analysis of Failure Circle	
29	2	Creep Strength (2)	Low	3:1	0.956	Detailed Analysis of Failure Circle	
30	2	Peak Strength (1)	Low	2:1 (Berm 2)	5.622	Detailed Analysis of Failure Circle	
31	2	Peak Strength (1)	High	2:1	2.083	Detailed Analysis of Failure Circle	
32	2	Peak Strength (1)	High	2:1	1.941	Detailed Analysis of Failure Circle	
33	2	Peak Strength (1)	High	3:1	2.429	Detailed Analysis of Failure Circle	
34	2	Residual Strength (3)	High	2:1 (Berm 1)	2.627	Detailed Analysis of Failure Circle	
35	2	Residual Strength (3)	High	2:1 (Berm 2)	3.952	Detailed Analysis of Failure Circle	
36	2	Residual Strength (3)	Low	2:1 (Berm 2)	4.213	Detailed Analysis of Failure Circle	
37	2	Residual Strength (3)	Low	2:1 (Berm 1)	2.820	Detailed Analysis of Failure Circle	
38	2	Peak Strength (1)	High	2:1 (Berm 2)	5.536	Detailed Analysis of Failure Circle	
39	2	Residual Strength (3)	Low	3:1	1.691	Detailed Analysis of Failure Circle	
40	2	Residual Strength (3)	Low	2:1	1.265	Detailed Analysis of Failure Circle	
41	2	Residual Strength (3)	High	2:1	1.117	Detailed Analysis of Failure Circle	
42	2	Residual Strength (3)	High	3:1	1.545	Detailed Analysis of Failure Circle	
43	2	Residual Strength (3)	High	2:1 (Berm 2)	3.596	Grid Search	

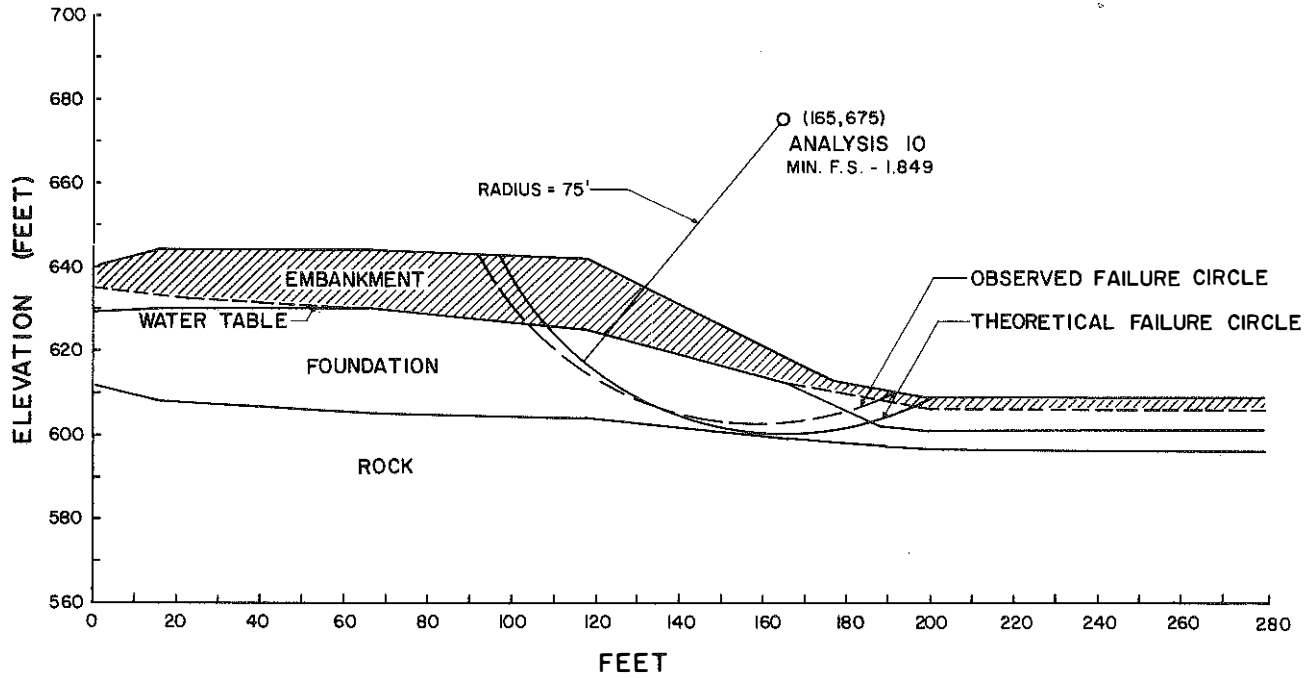


Figure 35. Stability Analysis Results, Analysis 10 - Western Kentucky Parkway.

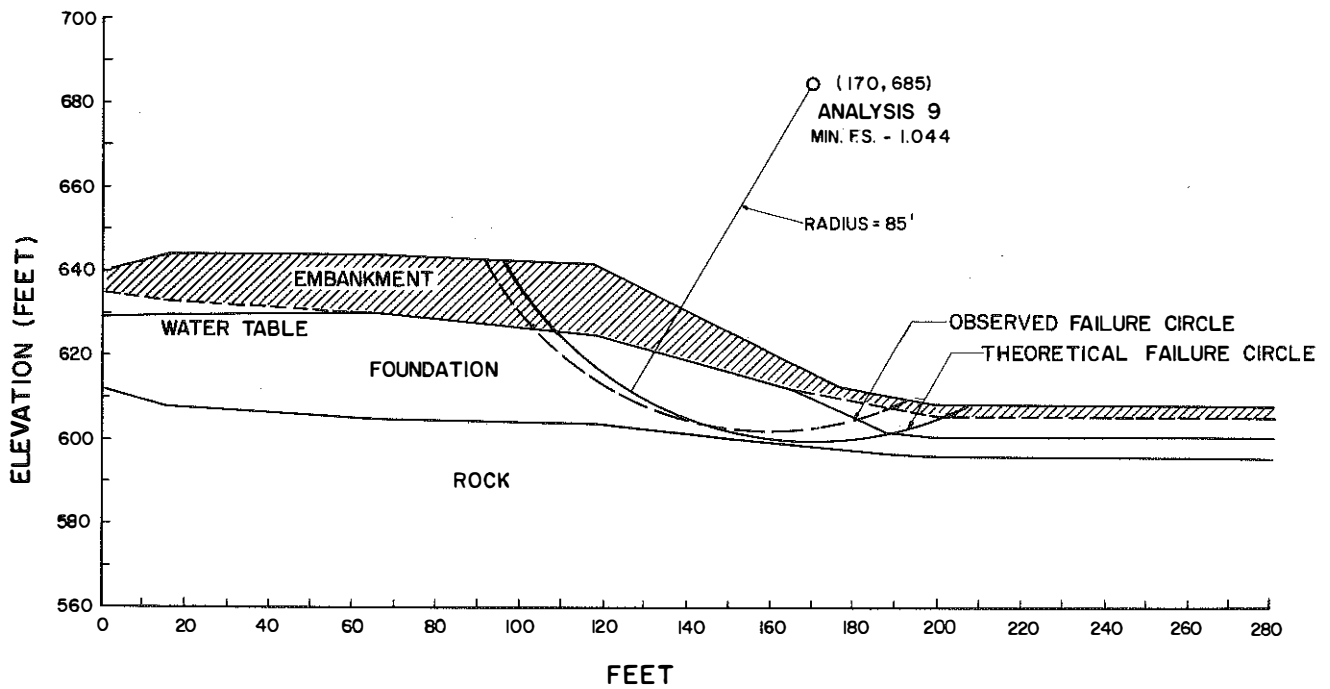


Figure 36. Stability Analysis Results, Analysis 9 - Western Kentucky Parkway.

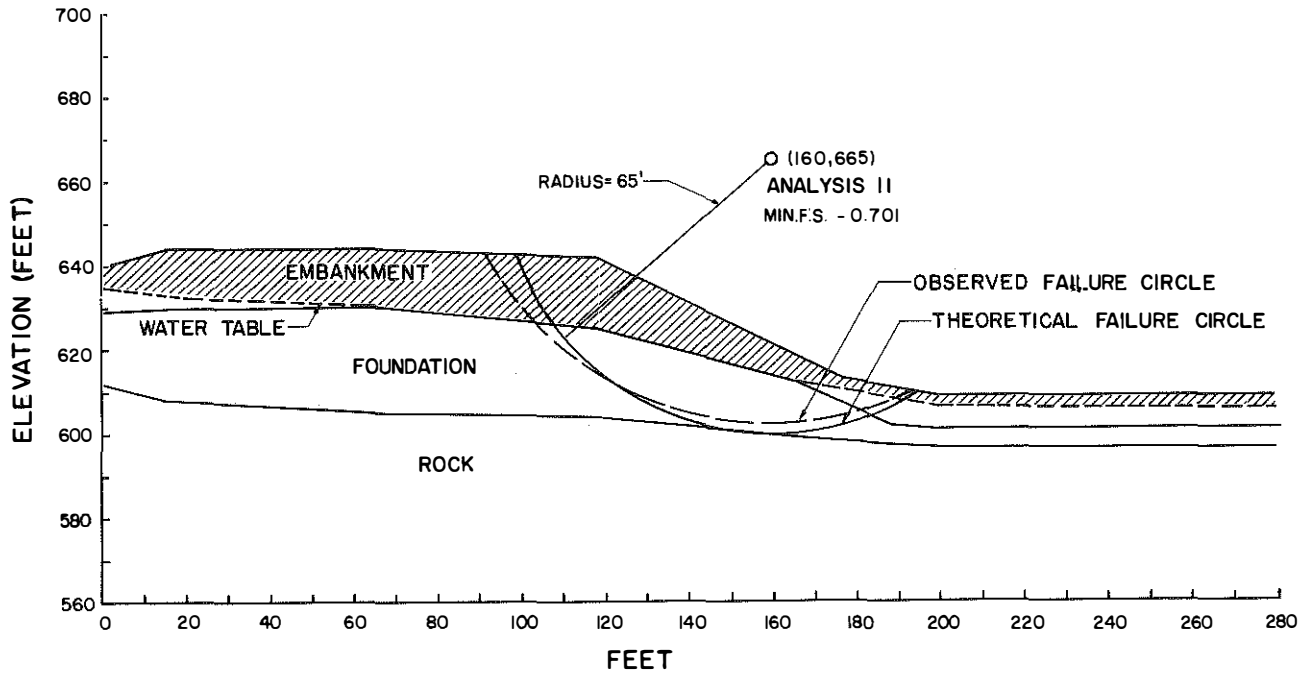


Figure 37. Stability Analysis Results, Analysis 11 - Western Kentucky Parkway.

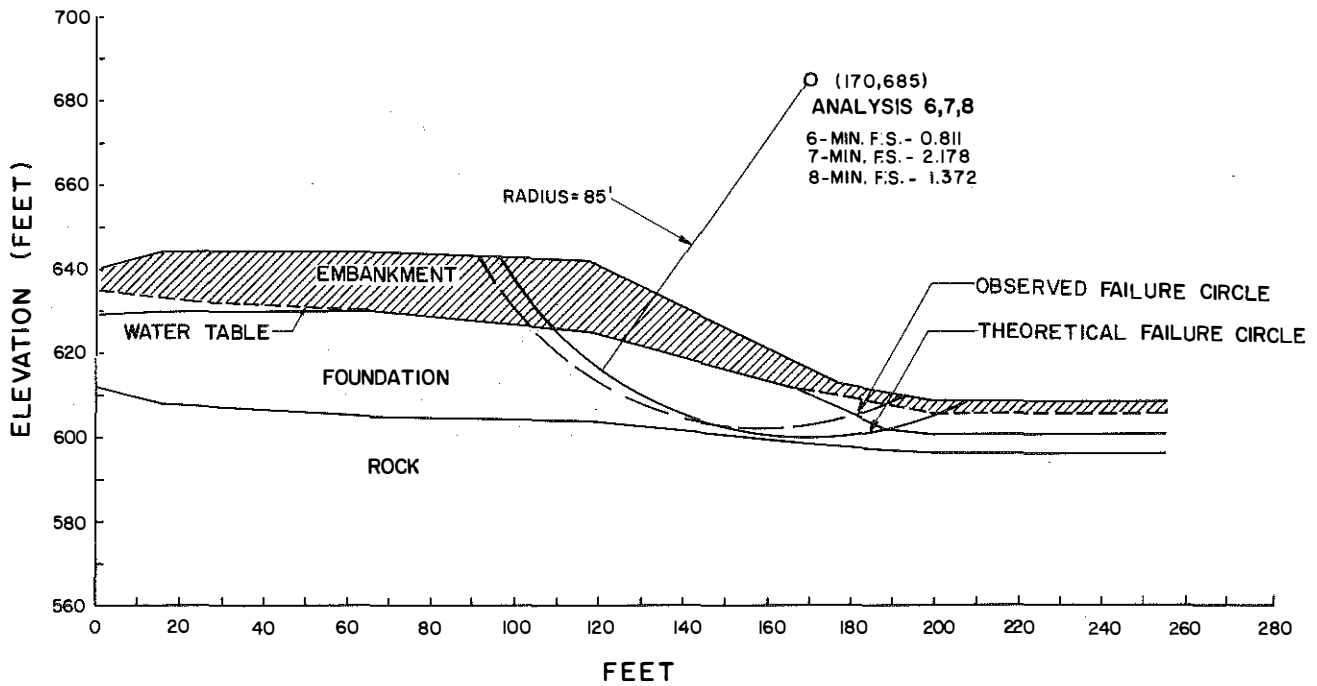


Figure 38. Stability Analysis Results, Analysis 6, 7, and 8 - Western Kentucky Parkway.

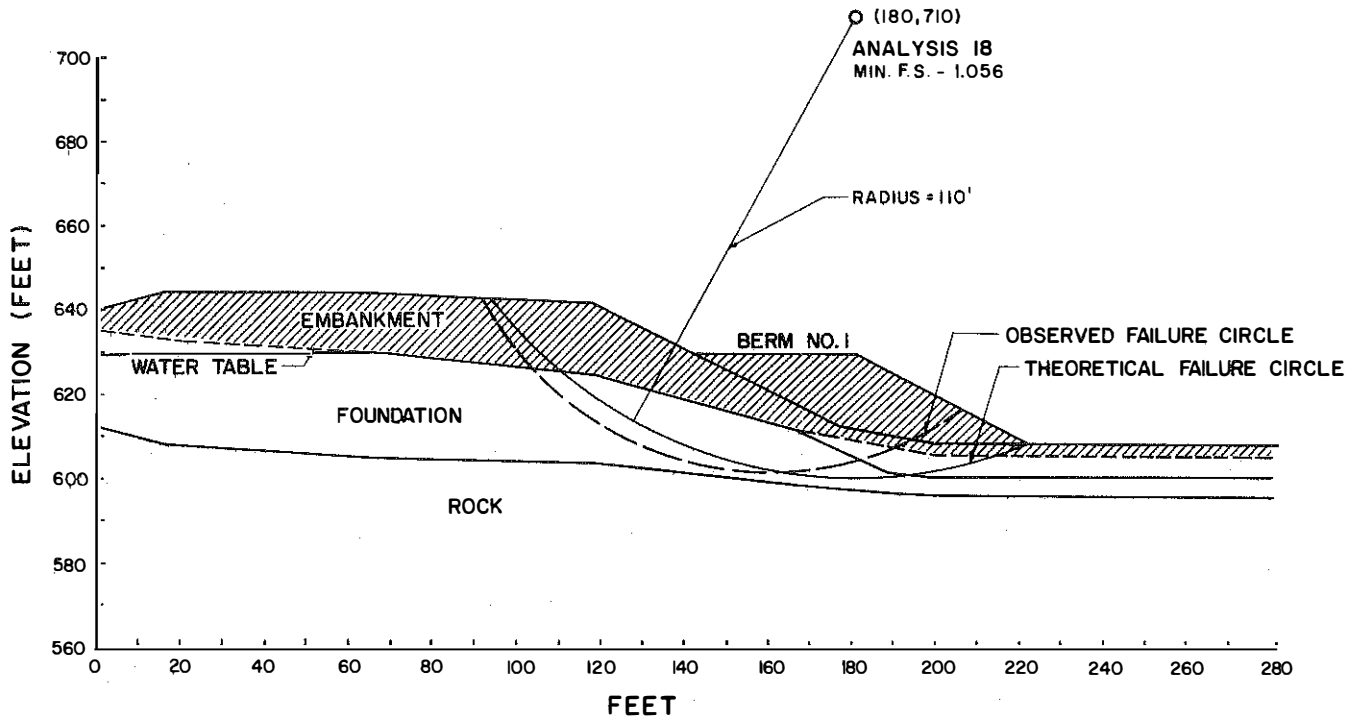


Figure 39. Stability Analysis Results, Analysis 18 - Western Kentucky Parkway.

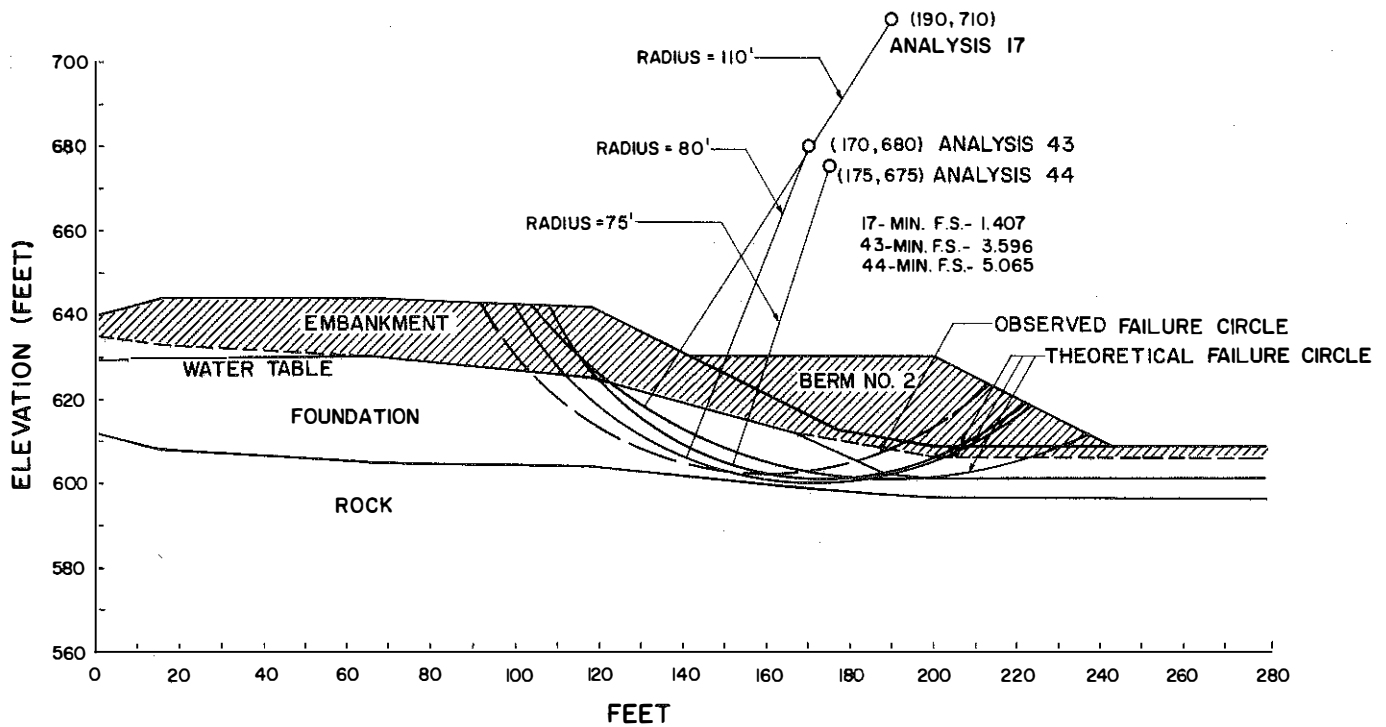


Figure 40. Stability Analysis Results, Analysis 17, 43, and 44 - Western Kentucky Parkway.

In all three remedial designs, material used in the berms and the slope change was assumed to have the same strength parameters as the embankment (Layer 1).

Water did not appear to be a major problem in this slide. The factor of safety decreased only 12 percent (from 1.972 to 1.849 using peak strength) as the watertable was raised from its lowest observed elevation to the highest. The "residual" factors of safety decreased only 14 percent (from 1.185 to 1.044) while the creep factors of safety changed from 0.747 to 0.701, a decrease of five percent.

In summarizing this case history, the analyses indicated the peak strength considerably overestimated the available long-term strength. The "residual" parameters gave a better indication of strength; however, a design based on this definition of strength would appear to have little margin of safety against large strains occurring in the earth structure. To prevent large plastic deformations, it appears creep design would provide the best method because it clearly indicated failure of the embankment of this site. A summary of all computer analyses made on this case history is given in Table 4.

#### **Shelby County, I 64, Milepost 44**

This slide is located on I 64 in Shelby County at Station 1866+00, approximately 1 mile east of the Waddy-Peytona interchange. The highway is divided into two embankments at this location and the unstable mass is located on the slope and inside shoulder of the eastbound lanes. The roadway transitions from a cut to a fill at Station 1865+00 and it is on a -3.0 percent grade. Located at Station 1868+50 is a 6-ft by 6-ft reinforced concrete box culvert, skewed 53 degrees right. Photographs of the slide and its immediate vicinity are shown in Figures 41-43.

Trouble was first noted in 1966; and in 1969, an investigation was undertaken as a part of Research Study KYHPR 68-48. A detailed discussion of the history, geometrics, topography, and geology will be given in the final report on research study KYHPR 68-48.

#### *Field and Laboratory Investigation*

Forty-five borings were made at this site for watertable observations, soil samples, and rock cores. Undisturbed Shelby tube samples were obtained from 11 borings. These samples were obtained and prepared in the same manner as described in the previous case history. Consolidated-Isotropic-Undrained (CIU) relaxation, triaxial, and creep tests were performed along with classification tests on the Shelby tube samples.

Two inclinometer casings were installed at this site. Well No. 1 was located at the top of the embankment,

just behind the guardrail at Station 1865+70. The second (Well No. 2) was installed in the slope halfway between the top and toe of the embankment at Station 1866+00.

#### *Results of Investigation*

From visual identification, the embankment material (Layer 1) was a reddish-brown clay with a stiff to very stiff consistency. The moisture content varied from 18 to 26 percent. The foundation material was a gray-to-brown clay having a stiff consistency and a moisture content varying from 16 to 24 percent.

The embankment material classified as an A-6(11) soil (AASHTO) having a liquid limit of 38.1 percent and a plastic index of 16.8. Hydrometer analysis indicated 43.1 percent was smaller than 5  $\mu$ . The foundation was an A-7-6(11) soil. Its liquid limit was 40.2 percent and the plastic index was 17.9. Forty-eight percent was smaller than 5  $\mu$ . Table 3 summarizes the classification and particle size data.

The "P-Q diagrams" for embankment and foundation are presented in Figures 44 and 45. The shapes of the stress paths indicated that the material in both layers was overconsolidated (16). The effective strength parameters for the embankment were 30° for  $\phi'$  and 42 psf for  $c'$ . The foundation had a smaller  $\phi'$  of 24.2° but a higher  $c'$  of 474 psf.

Employing a second method proposed by Scott (14), an additional failure envelope was constructed for each layer. A plot was made of peak stress versus confining pressure from data obtained from the CIU triaxial tests performed on each layer (Figures 46a and 47a). In Figures 46b and 47b, the product of pore pressure parameters A and B is plotted as a function of confining pressure. To find the effective stress circle for any confining pressure, the peak stress is read from 46a or 47a and the pore pressure at that particular confining pressure is calculated using Equation 6 after reading the value of A times B from 46b or 47b. The failure envelopes in 46c and 47c were calculated for confining pressures of 10, 30, and 50 psi using this procedure. The effective parameters for embankment and foundation were 21.8° ( $\phi'$ ) and zero ( $c'$ ) and 30.0° and zero ( $c'$ ), respectively.

The results of the creep tests are given by the "viscosity diagrams" in Figures 48 through 50. Two creep tests were run on a third layer that was not in the immediate slide area (Figure 50) and was not used in the stability analysis but are presented for record. Analysis of yield stress as a function of peak stress is given in Figure 51. Regression analysis indicated the yield stress was equal to 47.5 percent of the peak stress.



**Figure 41. View of Surface Break at Inside Shoulder of Eastbound Lanes on I 64 at Station 1865 + 50.**

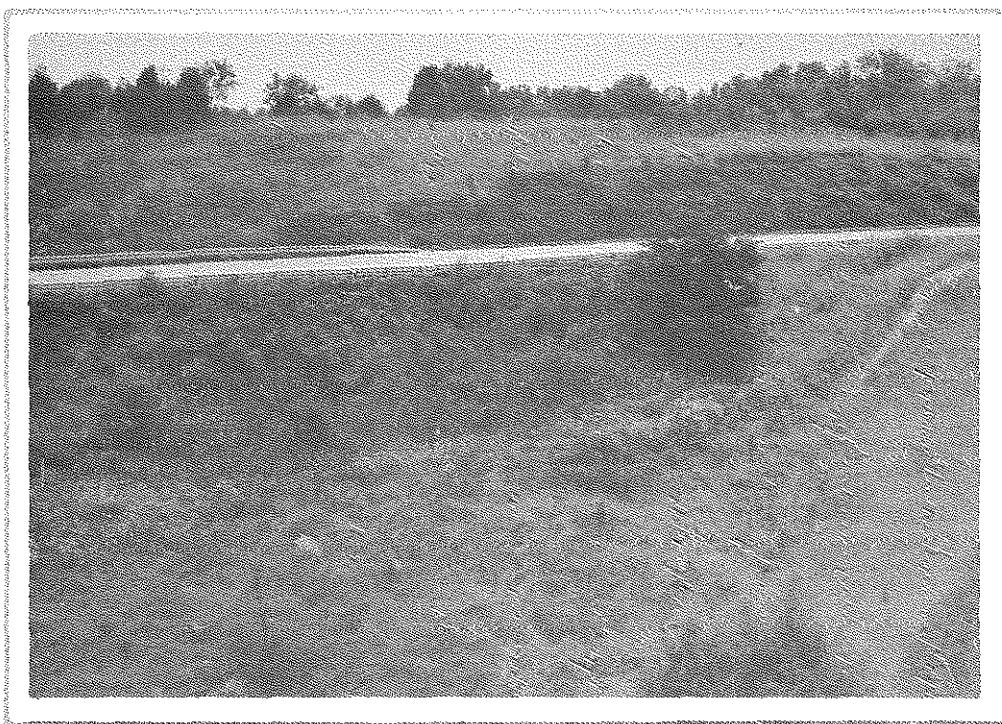


**Figure 42. General View of Slide Area, Looking South, on I 64 Near Milepost 44.**



Figure 43. General View of Slide Area, Looking East, on I 64 Near Milepost 44.

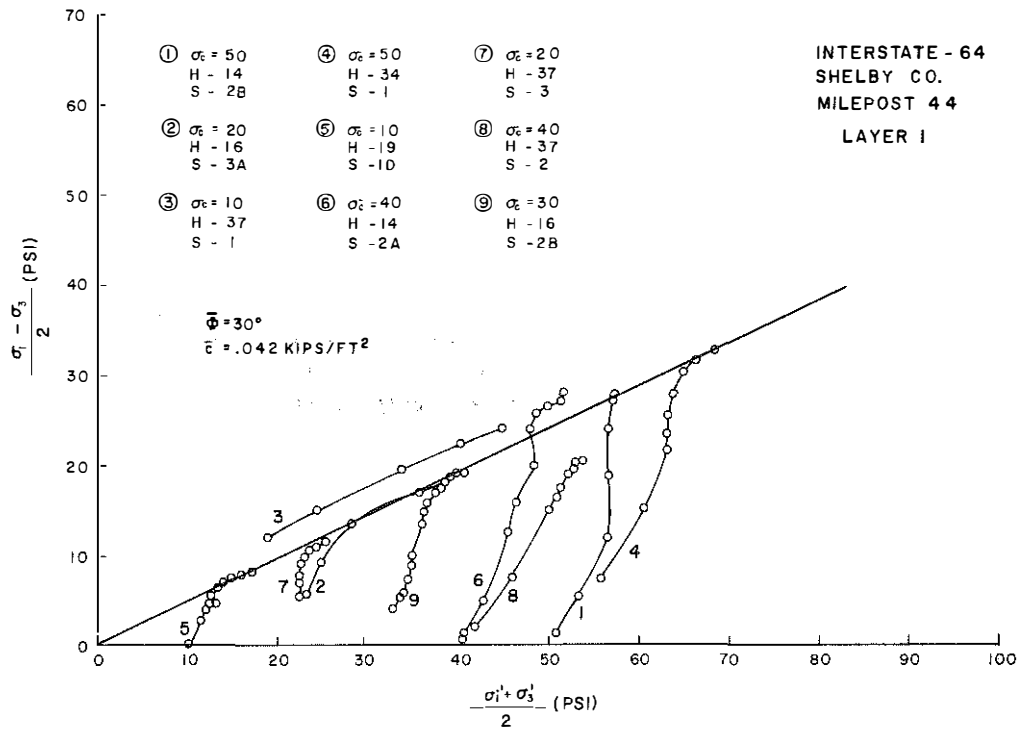


Figure 44. Consolidated, Isotropic, Undrained Triaxial Test Results, Layer 1 (Embankment) - I 64.

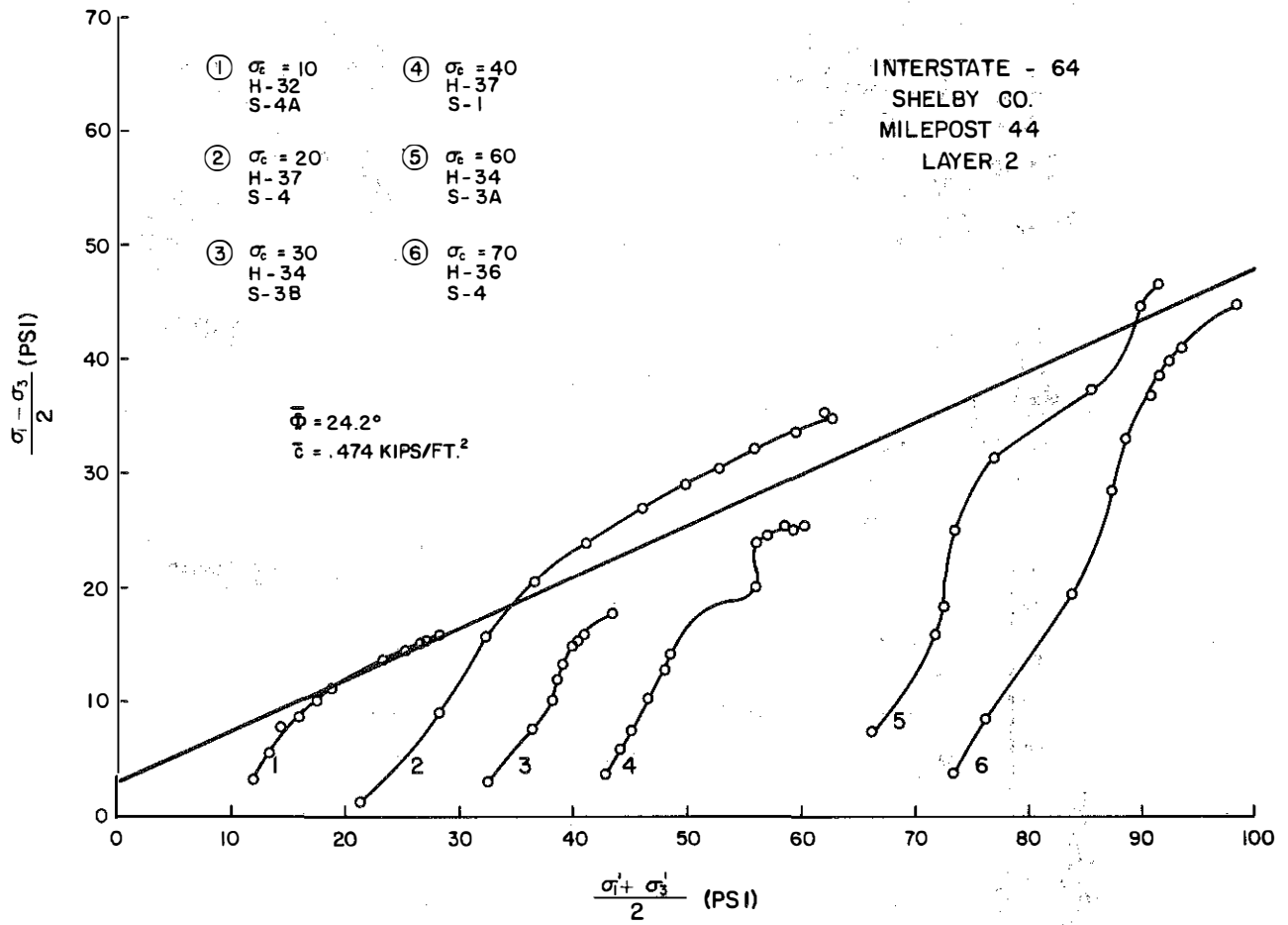
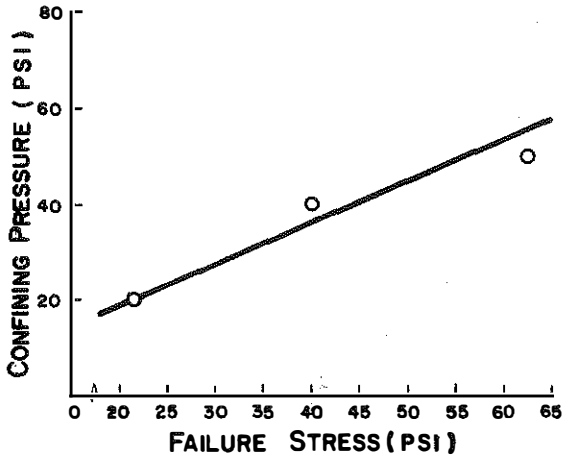


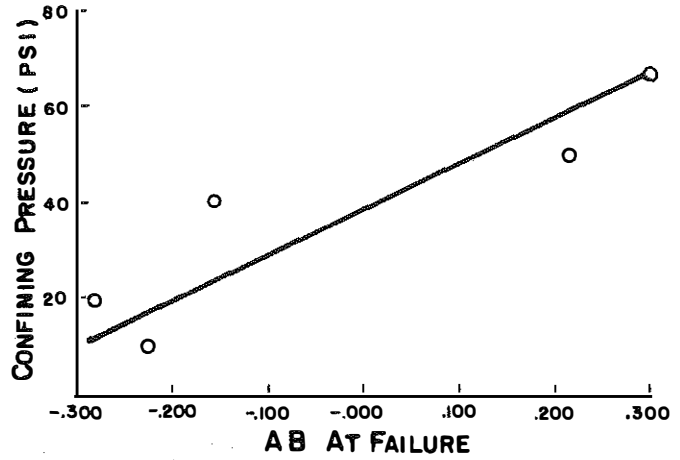
Figure 45. Consolidated, Isotropic, Undrained Triaxial Test Results, Layer 2 (Embankment) - I 64.



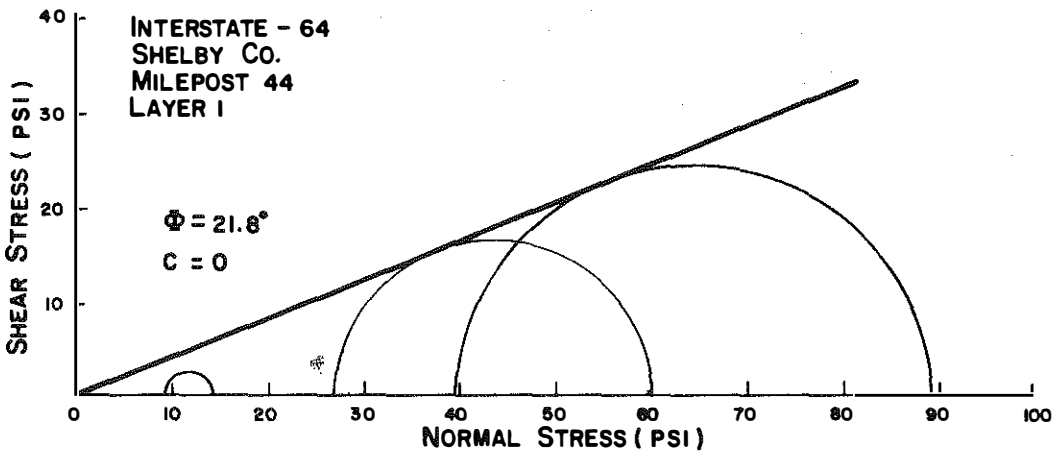
INTERSTATE - 64  
 SHELBY CO.  
 MILEPOST 44  
 LAYER I



a



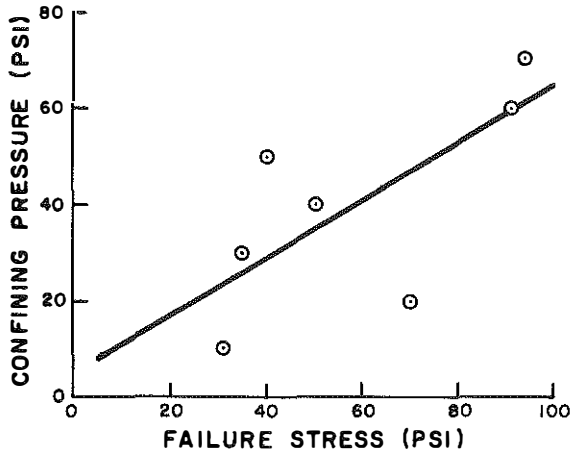
b



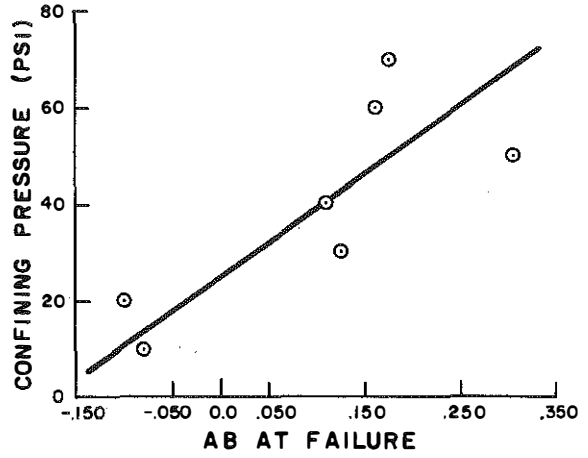
c

Figure 46. Shear Strength Results from Special Relaxation - Triaxial Test Using One Specimen, Layer 1 (Embankment) - I 64.

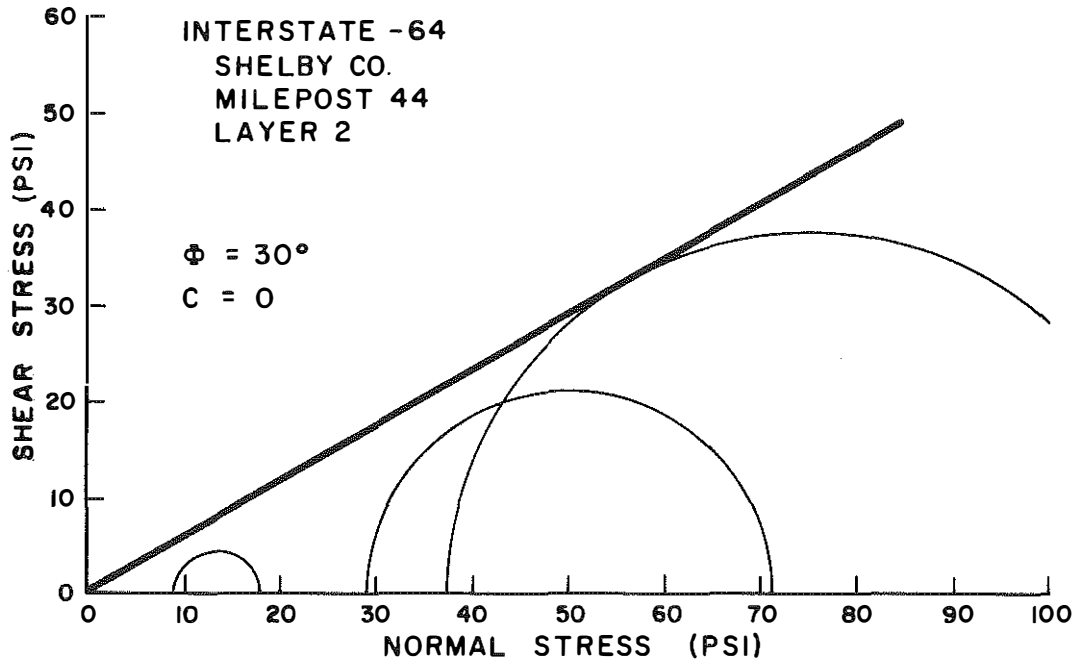
INTERSTATE - 64  
 SHELBY CO.  
 MILEPOST 44  
 LAYER 2



a



b



c

Figure 47. Shear Strength Results from Special Relaxation - Triaxial Test Using One Specimen, Layer 2 (Foundation) - I 64.

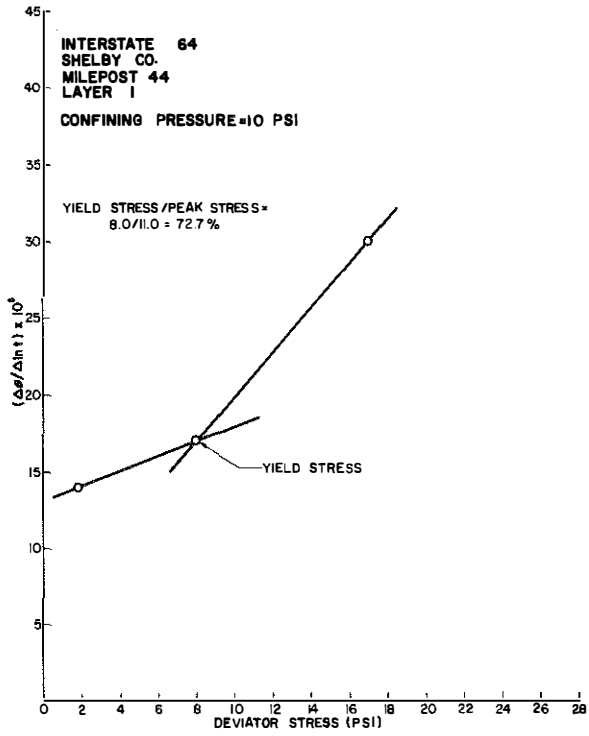
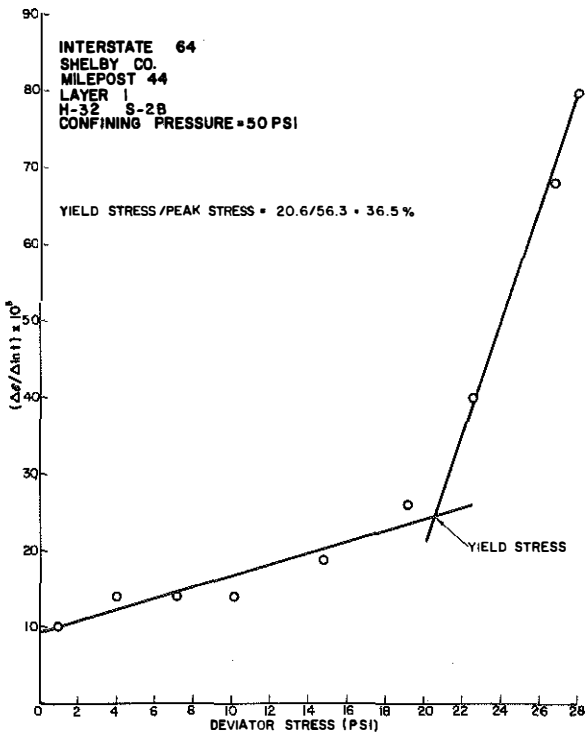
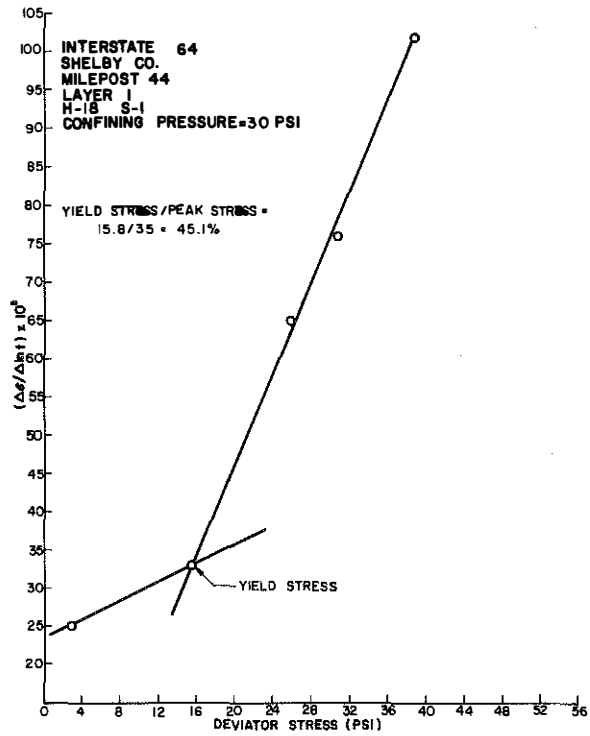


Figure 48. Viscosity Diagrams, Layer 1 (Embankment) - I 64.



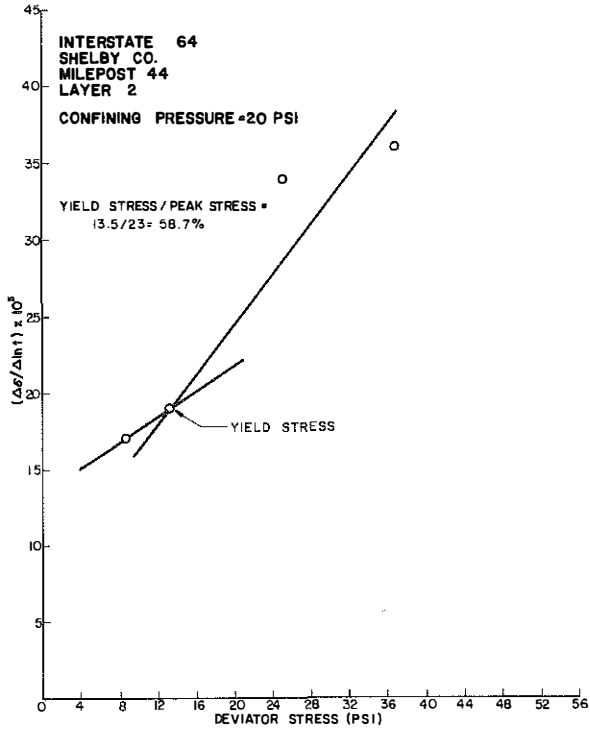
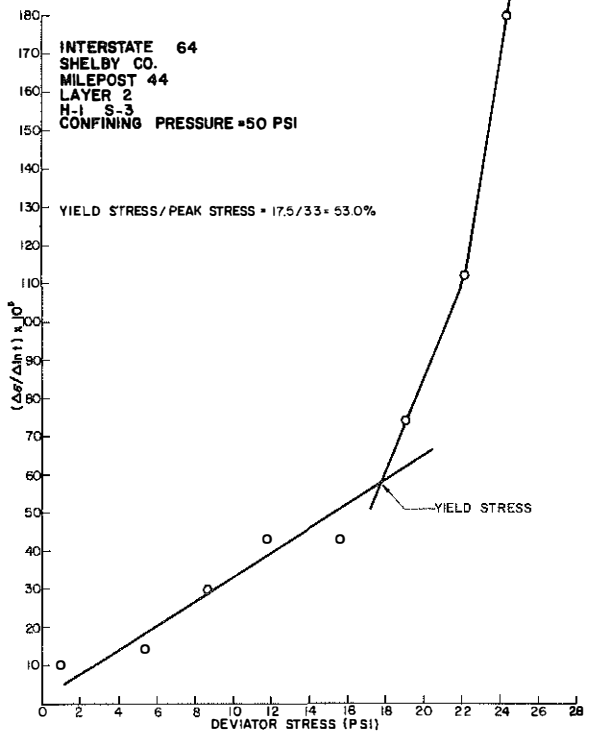
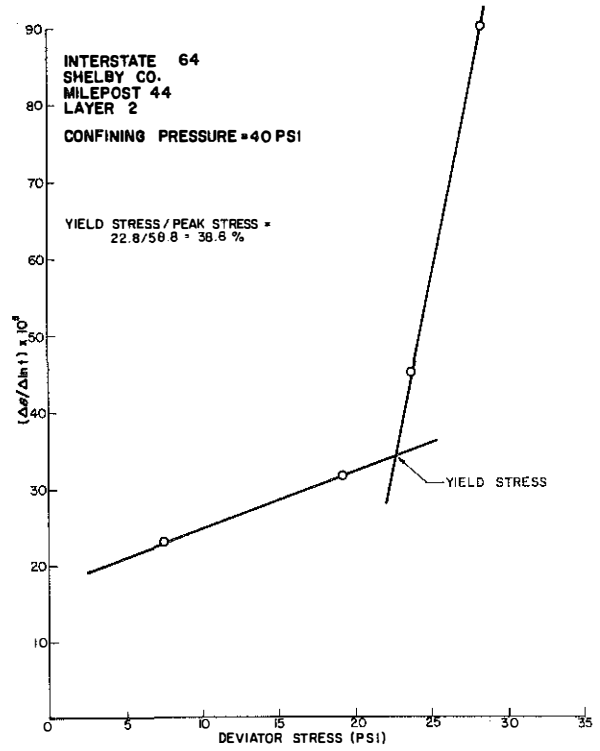


Figure 49. Viscosity Diagrams, Layer 2 (Foundation) - I 64.



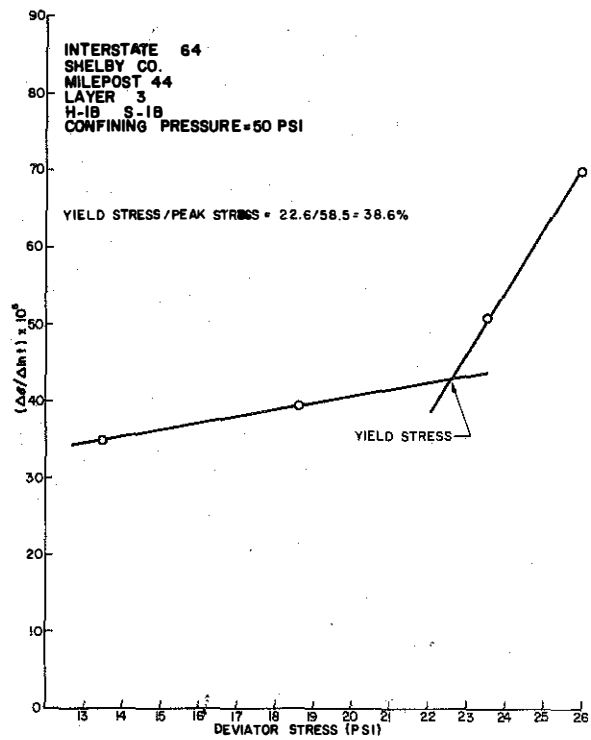
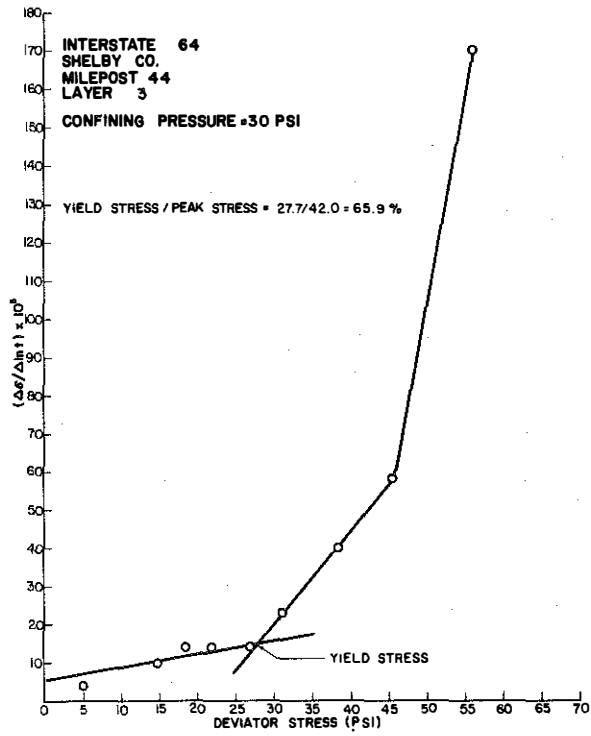


Figure 50. Viscosity Diagrams, Layer 3 - I 64.

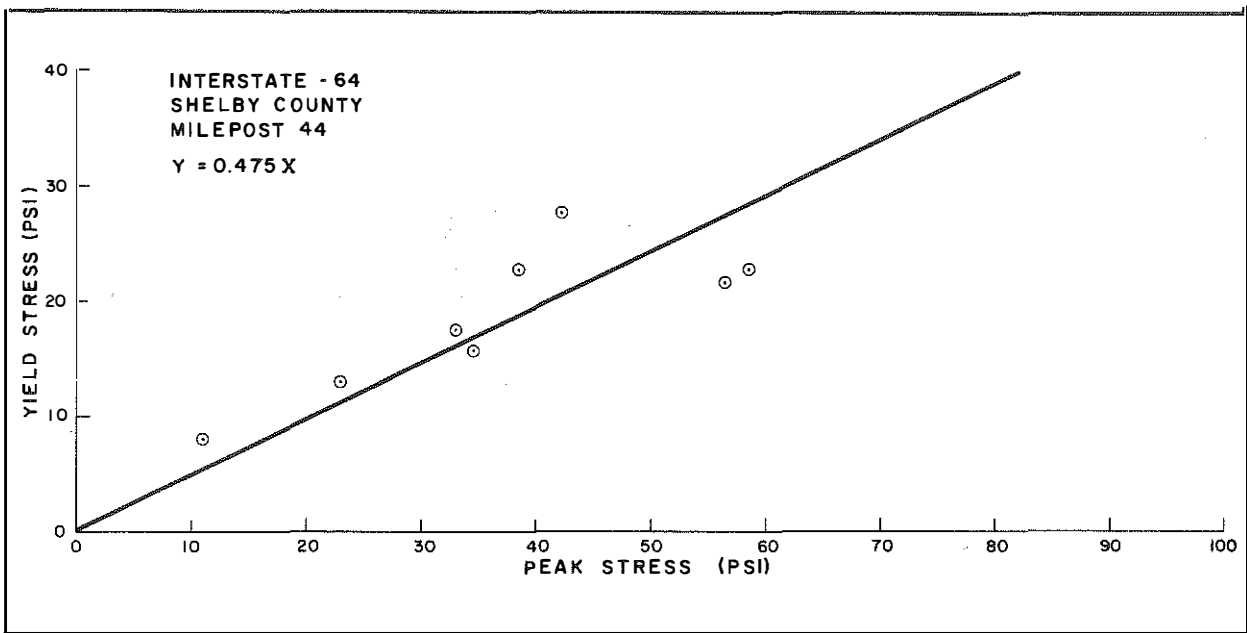


Figure 51. Yield Stress as a Function of Peak Stress, All Layers - I 64.

Strength parameters for the embankment, using yield stress, were  $7.7^\circ$  for  $\phi$  and 2.0 psi for  $c$ . The foundation had a higher  $\phi$  of  $10.2^\circ$ , but cohesion was equal to that of the embankment (Figure 52).

The inclinometers near Station 1866+00 indicate the failure surface is approximately circular and is at a depth of about 15 feet (Figures 53 and 54). Inclinometer No. 2 shows a second shear zone about 5 ft below the surface. This zone was probably initiated as a result of the deeper shear zone. The horizontal movement versus time plot in Figure 53 shows the movement began to accelerate at Well No. 1 between 500 and 700 days. Shortly after 700 days, complete failure occurred closing the well. In spite of repairs at this site, Well No. 2 is open and the reading taken at 1300 days appears to indicate movement has accelerated between 700 and 1300 days (Figure 54). However, it is suspected that most of this movement occurred when the embankment failed, which would probably cause a discontinuity in the curves shortly after 700 days. Sufficient readings were not taken to verify this.

#### *Stability Analysis (As Built)*

Using the effective peak strength parameters from the CIU triaxial tests (Figures 44 and 45), the "as built" factor of safety was 1.010 (Analysis 31, Table 5). This was made using the highest observed water table and also assuming excess pore pressures were present due to seepage. To determine the effect of watertable fluctuations on stability, the line of seepage was dropped to its lowest observed elevation (Analysis 43, Table 5). This increased the factor of safety 40 percent to 1.409, thus indicating water may have been a contributing factor to instability. Figure 55 shows the observed and theoretical failure surfaces for these two cases.

To consider the effect of loss of shear strength on stability because of decreasing cohesion, Analysis 39 was made assuming no cohesion and using  $\phi'$  angles determined from the CIU tests (labeled "residual" strength in Table 5). Using the highest elevation of seepage, this case yielded a factor of safety of 0.719. However, using the lowest observed seepage line (Analysis 45), the "residual" parameters predicted 1.101 (Figure 56).

Using high watertable conditions, the creep strength parameters and the parameters from Scott's proposed method (labeled special strength in Table 5) provided factors of safety of 0.841 and 0.609, respectively (Analyses 50 and 34). In the case of creep analysis, dropping the watertable to its lowest elevation increased the factor of safety only 17 percent to 0.986 (Analysis 47). These cases are shown in Figure 57.

#### *Remedial Analysis*

A number of designs were analyzed. A slope change from 2:1 to 2 1/2:1 was made. Figure 58 shows factors of safety of 1.454, 0.991 and 1.001 for peak (Analysis 32), "residual" (Analysis 44), and creep (Analysis 33), respectively. These were made assuming the highest watertable and that the materials used in making the slope change had the same strength parameters as did the embankment. Although this design yields a theoretical factor of safety slightly greater than one for creep analysis, this could not be considered an adequate design for either creep or "residual" strength.

Changing the slope to 3:1 (Figure 59) increased the factor of safety 87 percent to 1.872 using peak strength (Analysis 27). Analysis 36, using a 3:1 side slope in conjunction with "residual" strength, had a factor of safety of 1.307 -- an increase of 82 percent. An increase of 40 percent was realized (1.181) with the slope change of 3:1 using creep parameters (Analysis 20). The 3:1 slope would appear to be adequate for peak and "residual" strength design. If large amounts of soil creep were to be avoided, this design would be somewhat marginal.

In an effort to increase the factor of safety from a marginal design of 1.181 and to provide better insurance against large creep deformations, a berm 33 ft wide and approximately 25 ft high was analyzed (keeping the slope above the berm at 2:1). This provided adequate security against deep failures; the minimum factor of safety would be approximately 1.30. However, this design would not prevent small failure surfaces from passing through the slope above the berm as there were several circles with factors of safety very close to 1.0. To prevent these shallow failures, the embankment slope was changed to 3:1 and a small 24-ft wide berm was added (Figure 60). Analysis indicated this was a good remedial design inasmuch as shallow failures were not critical and the factors of safety against deep failures using peak, "residual", and creep parameters were 2.112 (Analysis 54), 1.512 (Analysis 56), and 1.306 (Analysis 55), respectively.

The stability analysis program developed by Yoder and Hopkins (20) will provide a detailed printout of all forces on each slice for any given failure circle. An example printout is shown in Figure 61 (Analysis 25). Column eight lists the available shear strength for each slice, and column nine lists the shear stress on each slice. In making remedial designs, special attention was paid to the balance of these two forces for each slice. In each design analyzed, there was a minimum of four or five slices in the upper portion of the slope which was overstressed. In the case of Figure 61, there were eight slices overstressed. In attempting to remedy this, a

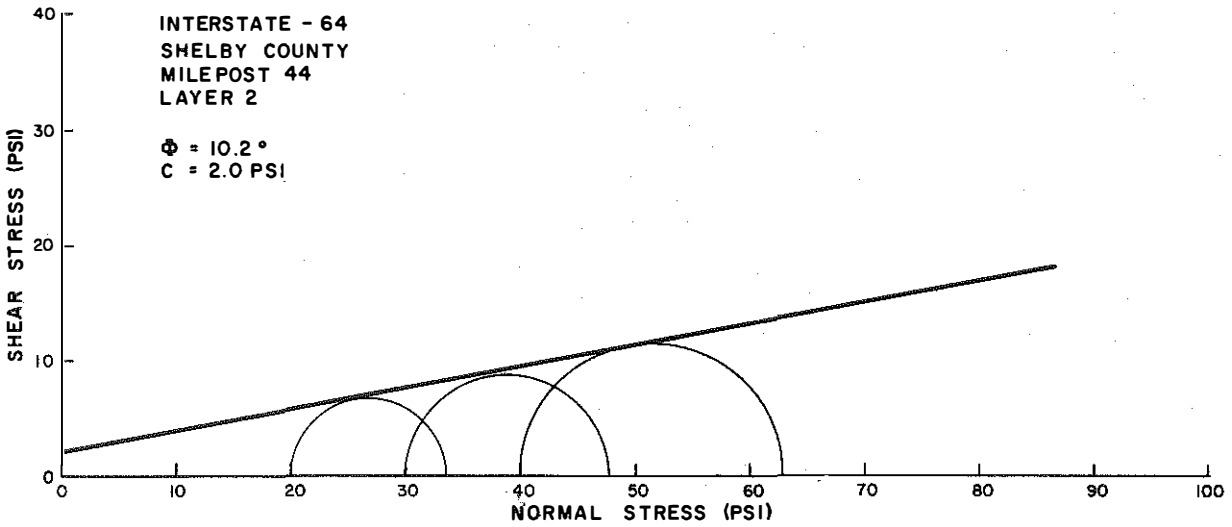
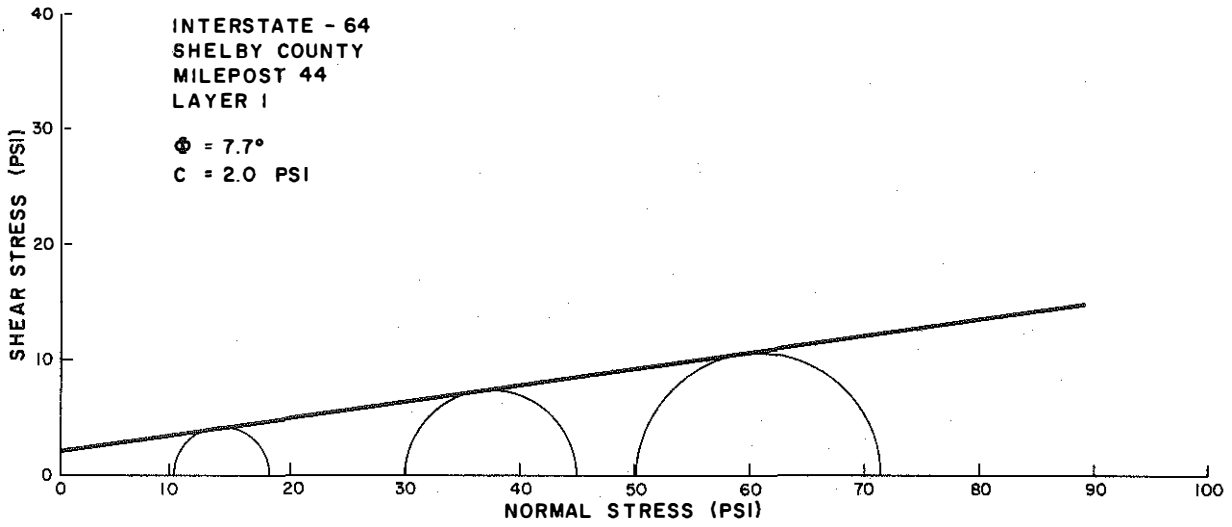


Figure 52. Failure Envelope Using Yield Stress,  
 Layers 1 and 2 - I 64.



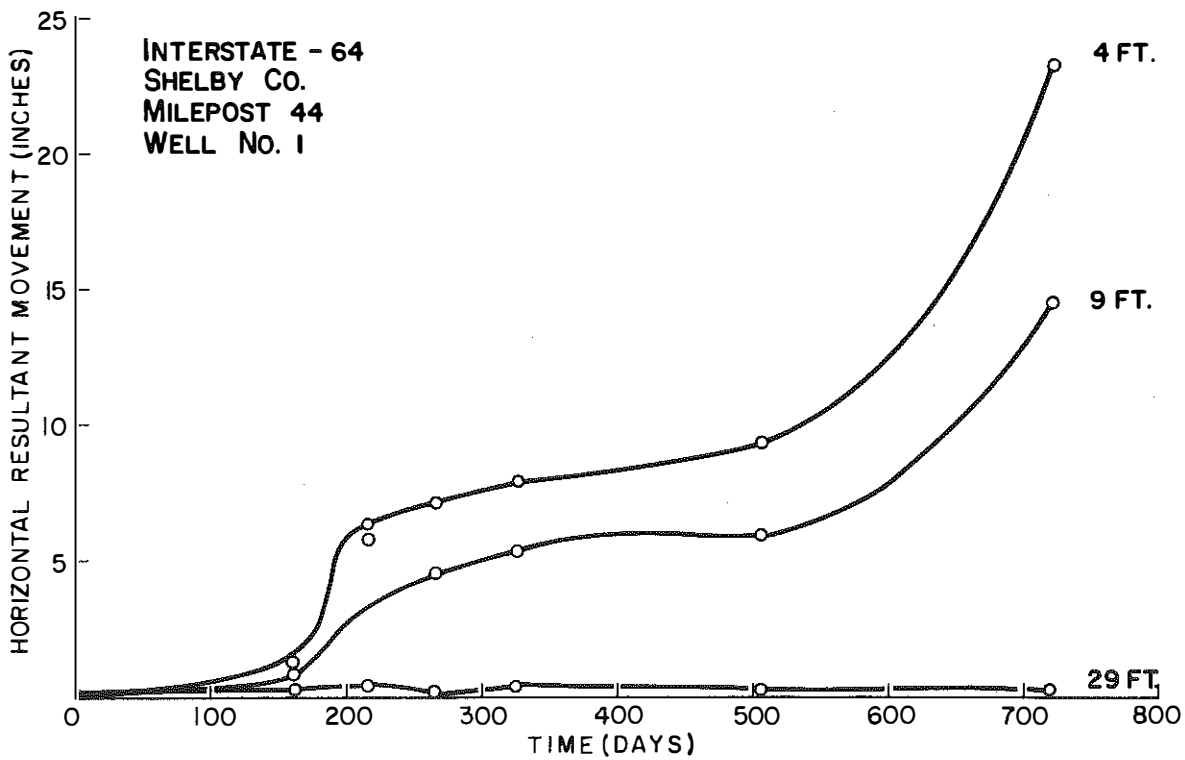
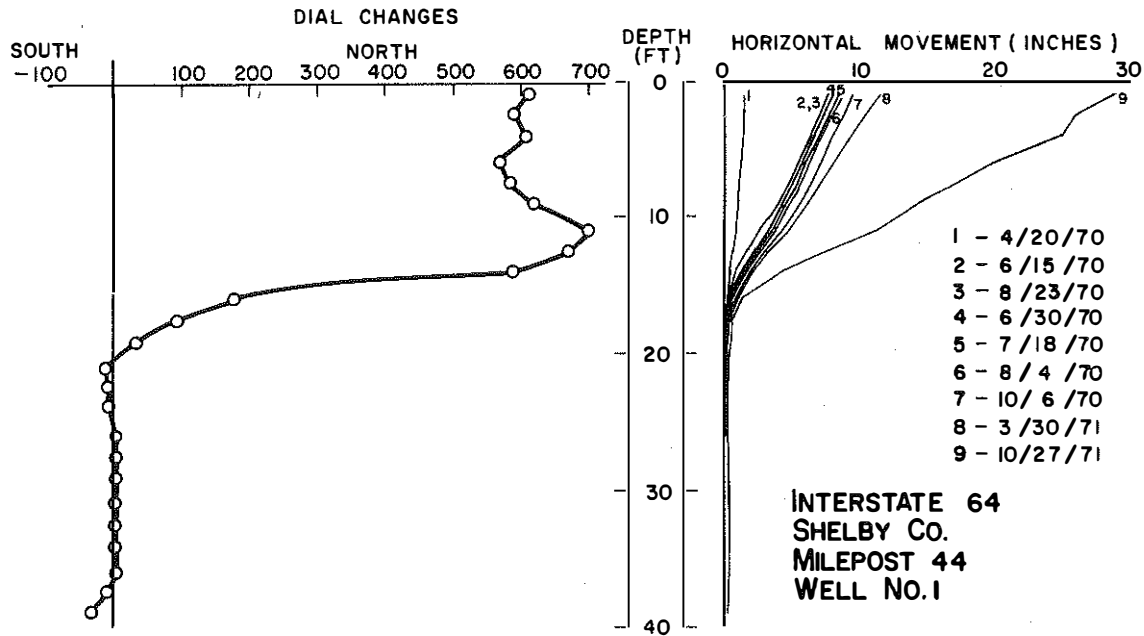


Figure 53. Slope Inclinerometer Results, Well No. 1 - I 64.

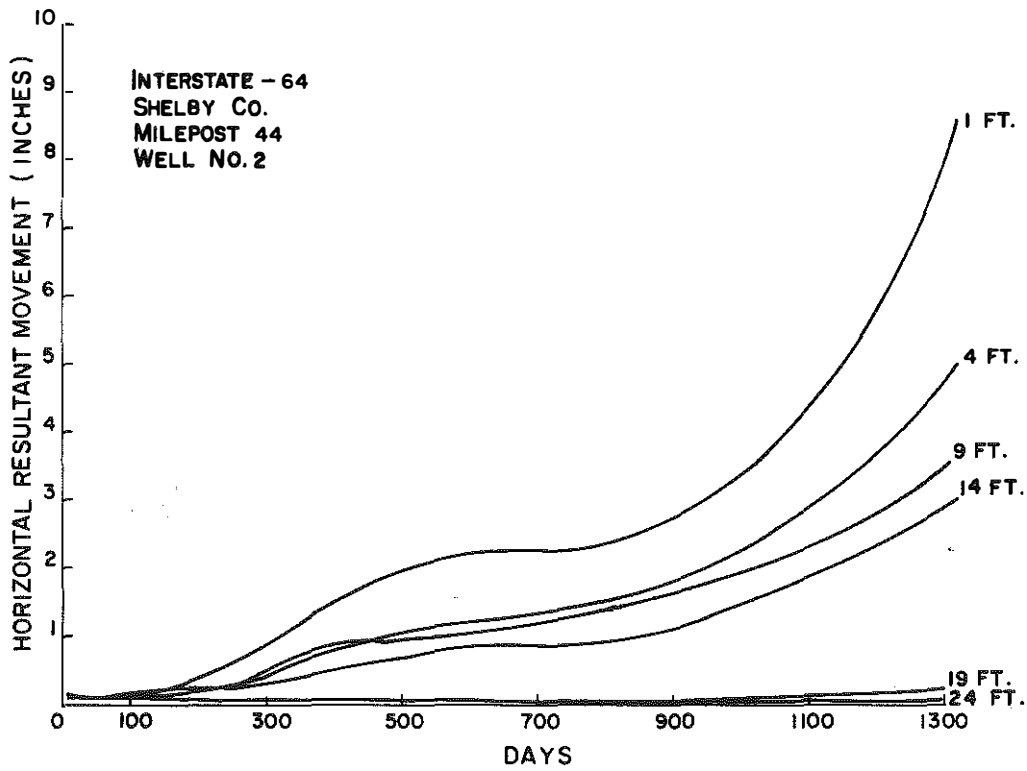
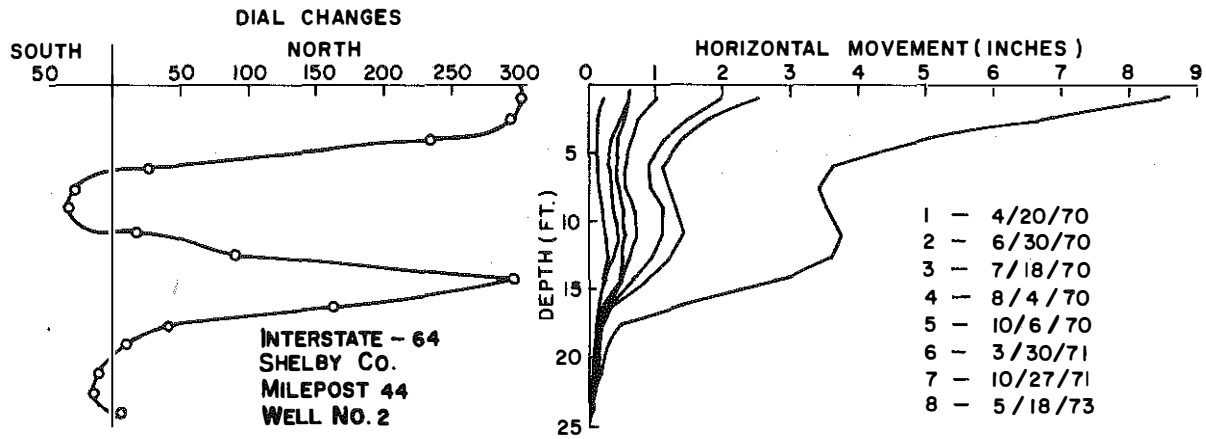


Figure 54. Slope Incliner Results, Well No. 2 - I 64.

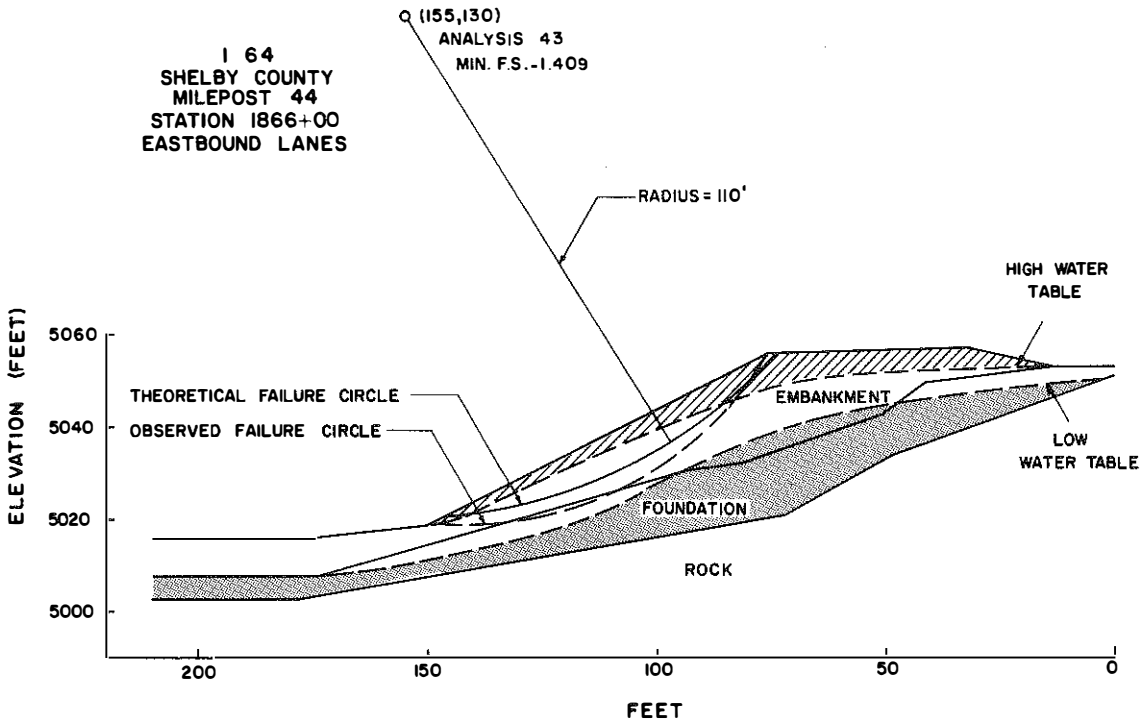


Figure 55. Slope Stability Analysis Results, Analysis 43 - I 64.

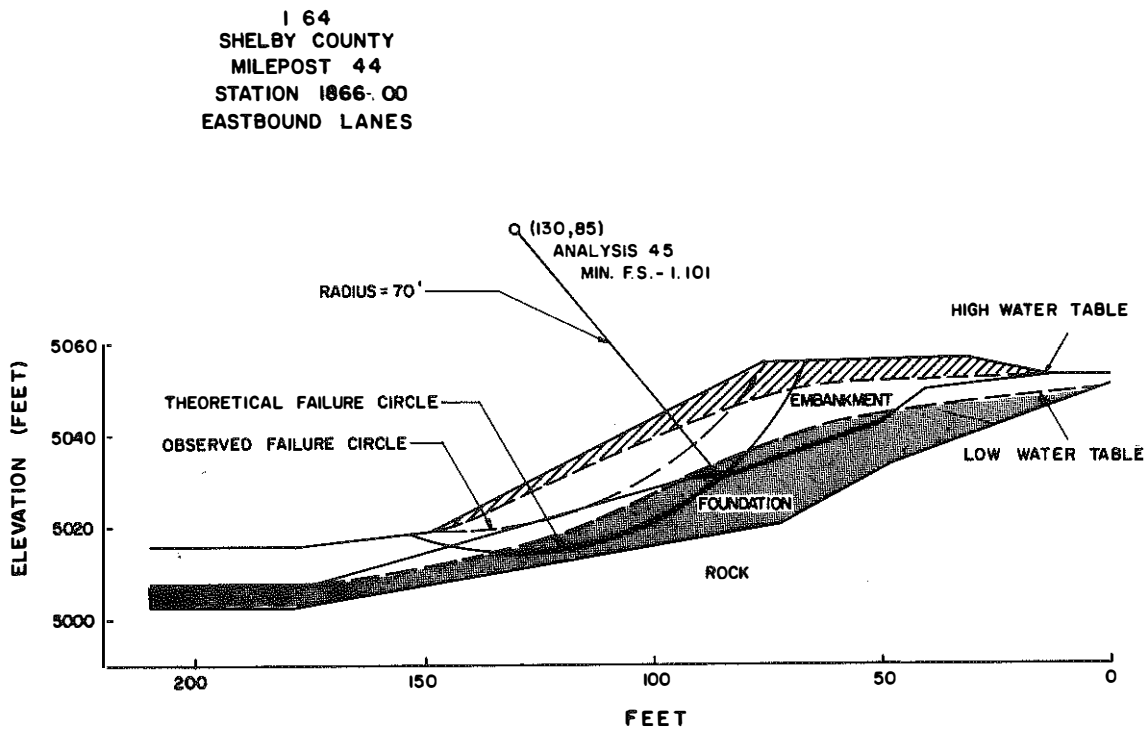


Figure 56. Slope Stability Analysis Results, Analysis 45 - I 64.

I 64  
 SHELBY COUNTY  
 MILEPOST 44  
 STATION 1866+00  
 EASTBOUND LANES

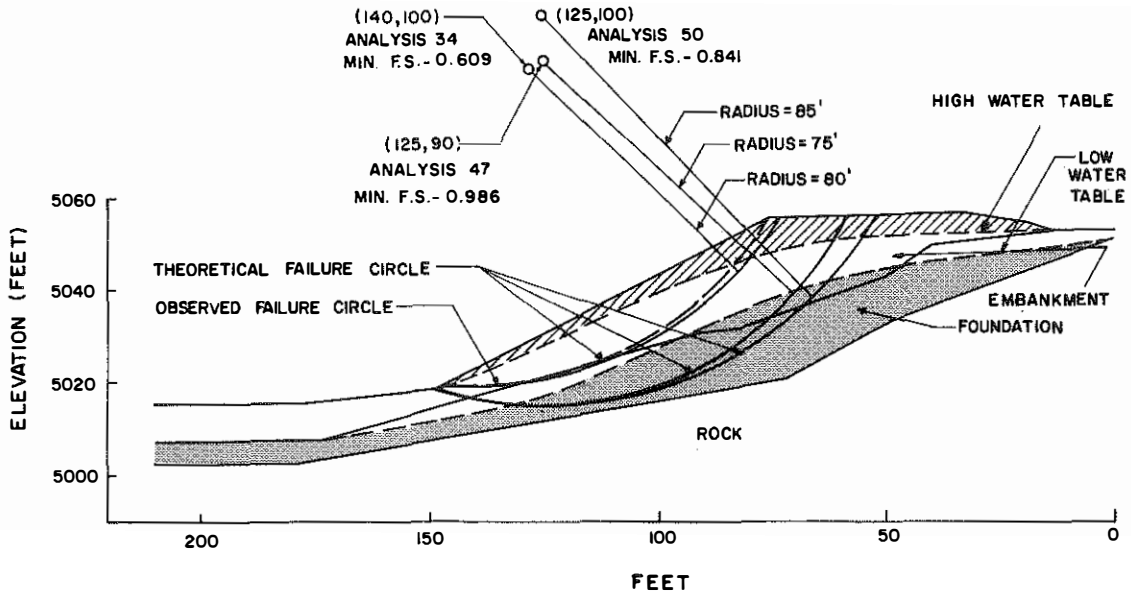


Figure 57. Slope Stability Analysis Results, Analysis 34, 47, and 50 - I 64.

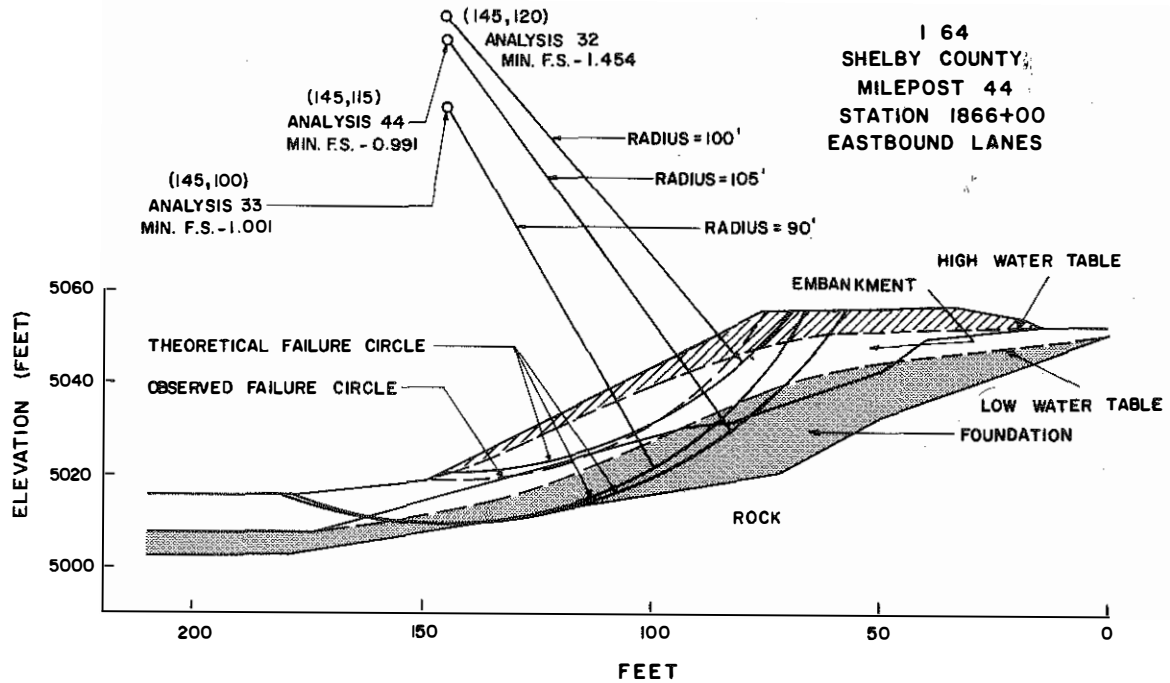
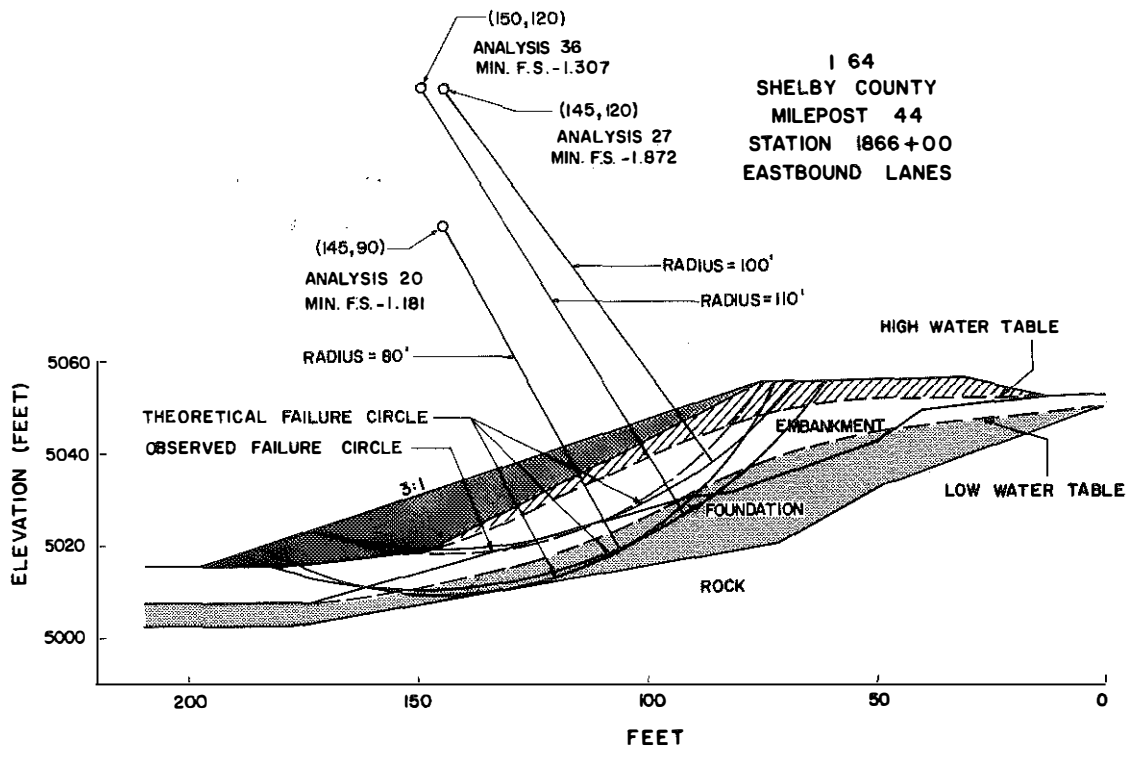


Figure 58. Slope Stability Analysis Results, Analysis 32, 33, and 44 - I 64.



**Figure 59. Slope Stability Analysis Results, Analysis 20, 27, and 36 - I 64.**

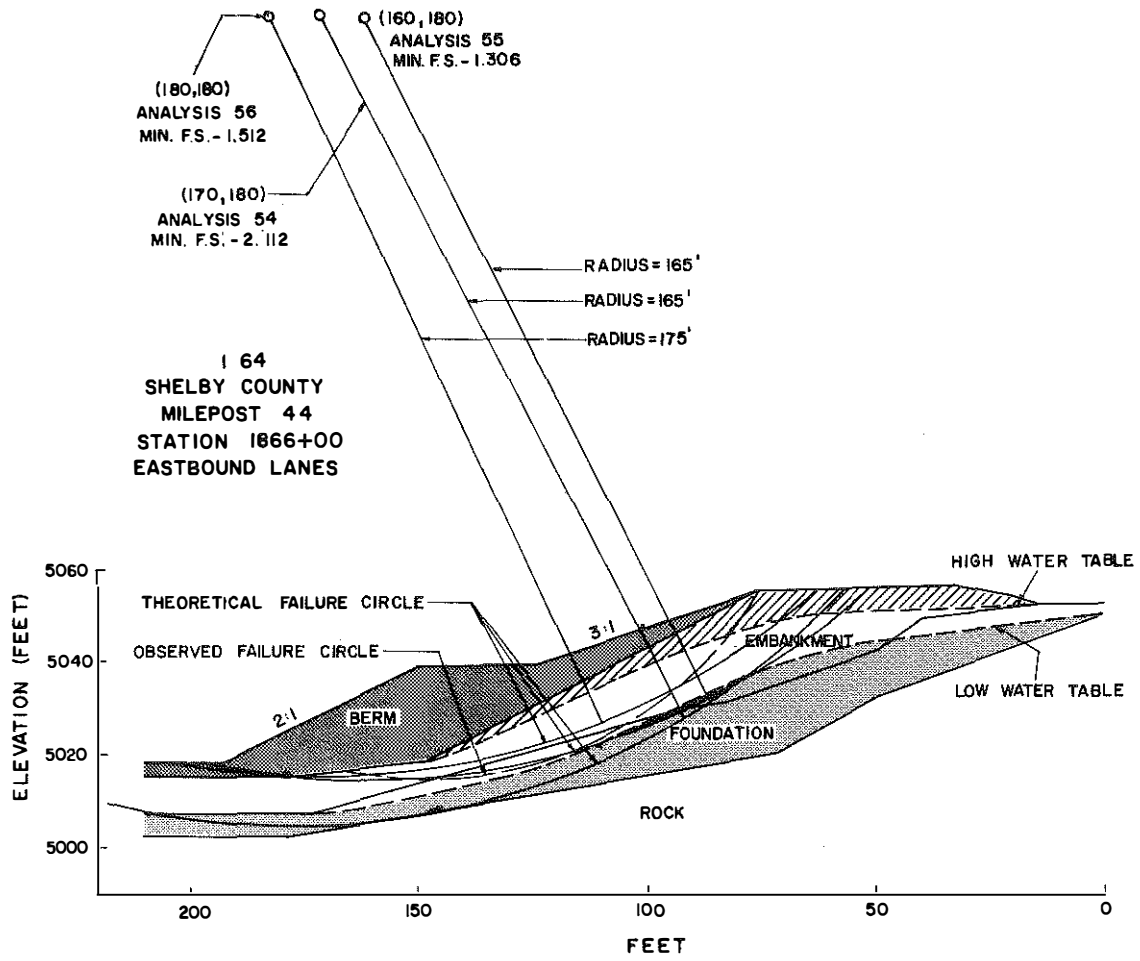


Figure 60. Slope Stability Analysis Results, Analysis 54, 55, and 56 - I 64.

FS = 1.390  
WIDTH OF EACH SLICE = 5.0551

J SLICE	W(J) WEIGHT (KIPS)	WW(J) U (KIPS)	WE(J) (KIPS)	MTHETA	NBAR (KIPS)	CO(M)*BR COHESION (KIPS)	SHEAR STRENGTH (KIPS)	SHEAR STRESS (KIPS)	COSINE THETA	SINE THETA
1	2.262	0.0	2.262	0.5970	0.8513	1.456	2.951	1.941	0.5135	0.8581
2	4.634	0.673	3.962	0.6891	3.786	1.456	2.890	3.664	0.6122	0.7907
3	6.145	1.588	4.557	0.7609	4.647	1.456	2.723	4.444	0.6905	0.7233
4	7.129	2.231	4.898	0.8187	4.871	1.456	2.587	4.676	0.7549	0.6550
5	7.712	2.666	5.046	0.8657	4.948	1.456	2.470	4.539	0.8085	0.5885
6	8.148	2.933	5.215	0.9209	4.961	1.456	2.600	4.246	0.8535	0.5211
7	8.817	3.056	5.761	0.9499	5.504	1.456	2.624	4.000	0.8912	0.4537
8	9.227	3.384	5.842	0.9724	5.557	1.456	2.578	3.564	0.9224	0.3863
9	9.401	3.412	5.989	0.9891	5.699	1.456	2.561	2.998	0.9478	0.3189
10	9.360	3.328	6.032	1.0004	5.757	1.456	2.540	2.354	0.9679	0.2515
11	9.116	3.139	5.477	1.0067	5.742	1.456	2.514	1.678	0.9829	0.1841
12	8.678	2.849	5.829	1.0083	5.659	1.456	2.484	1.013	0.9932	0.1167
13	8.053	2.416	5.637	1.0052	5.557	1.456	2.457	0.397	0.9988	0.0493
14	7.298	1.903	5.394	0.9975	5.427	1.456	2.432	-0.132	0.9991	-0.181
15	6.508	1.297	5.211	0.9853	5.380	1.456	2.429	-0.557	0.9963	-0.855
16	5.605	0.893	4.711	0.9734	5.007	1.456	2.150	-0.857	0.9882	-1.529
17	4.527	0.430	4.097	0.9540	4.543	1.456	2.107	-0.998	0.9754	-2.203
18	3.291	0.0	3.291	0.8128	4.050	0.0	2.836	-0.947	0.9577	-2.877
19	2.088	0.0	2.088	0.7559	2.762	0.0	1.934	-0.741	0.9348	-3.551
20	0.736	0.0	0.736	0.6935	1.061	0.0	0.743	-0.311	0.9063	-4.225
							SUM=	48.610		
							SUM=	34.970		

AVERAGE SHEAR STRESS = 0.296

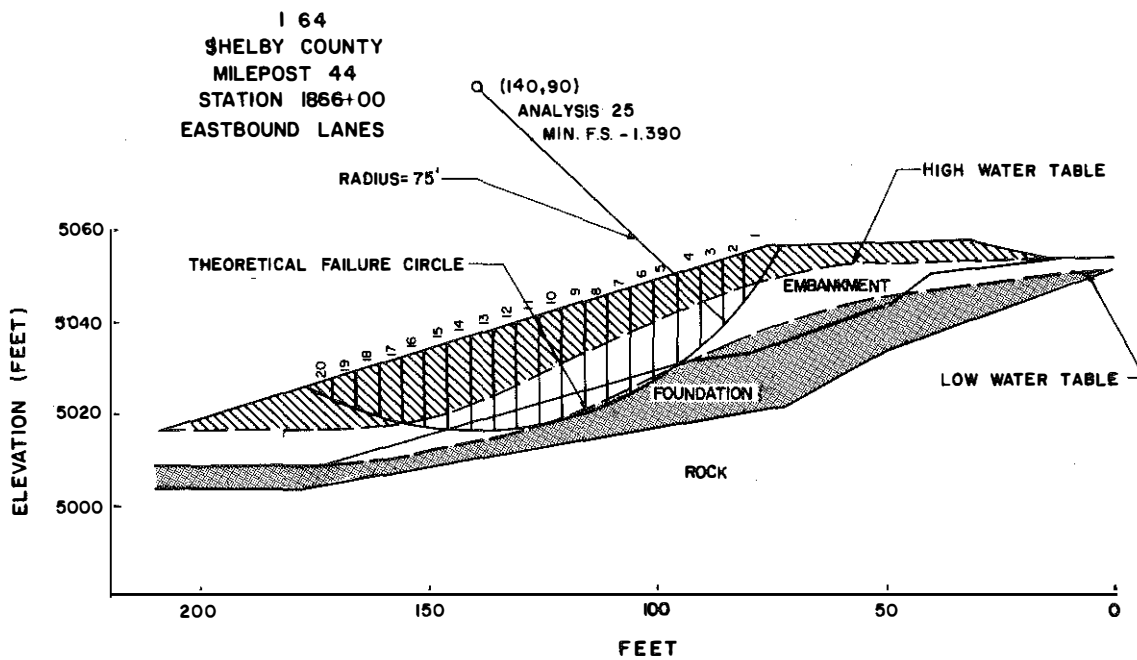




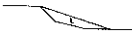




Figure 61. Slope Stability Analysis Results, Analysis 25, Showing Division of Soil Mass into Individual Slices - I 64.

**TABLE 5**  
**SUMMARY OF STABILITY ANALYSES**  
**INTERSTATE 64**  
**MILEPOST 44**

ANALYSIS NO.	NUMBER OF LAYERS	STRENGTH PARAMETERS (SEE DEFINITIONS OF STRENGTH)	WATER TABLE	SIDE SLOPE	CONFIGURATION OF LIGHTWEIGHT MATERIALS	FACTOR OF SAFETY	TYPE OF ANALYSIS	DEFINITIONS OF STRENGTH
31	3	Peak Strength (1)	High	2:1	No Lightweight Materials	1.010	Grid Search	(1) PEAK STRENGTH -- Obtained from Conventional Triaxial Tests.
43	3	Peak Strength (1)	Low	2:1	No Lightweight Materials	1.409	Grid Search	LAYER 1
27	3	Peak Strength (1)	High	3:1	No Lightweight Materials	1.876	Grid Search	$\phi = 30.0^\circ$ $c = .042 \text{ kips/ft}^2$ $\gamma = .099 \text{ kips/ft}^3$
28	3	Peak Strength (1)	High	3:1	No Lightweight Materials	2.182	Detailed Analysis of Failure Circle	LAYERS 2 & 3
40	3	Peak Strength (1)	Low	3:1	No Lightweight Materials	2.095	Grid Search	$\phi = 24.2^\circ$ $c = .474 \text{ kips/ft}^2$ $\gamma = .1066 \text{ kips/ft}^3$
32	3	Peak Strength (1)	High	2 1/2:1	No Lightweight Materials	1.454	Grid Search	(2) CREEP STRENGTH -- Obtained from Creep Tests.
42	3	Peak Strength (1)	Low	2 1/2:1	No Lightweight Materials	1.736	Grid Search	LAYER 1
37	4	Peak Strength (1) (5)	High	2:1		0.845	Grid Search	$\phi = 7.7^\circ$ $c = .288 \text{ kips/ft}^2$ $\gamma = .099 \text{ kips/ft}^3$
38	4	Peak Strength (1) (5)	High	2:1		1.518	Detailed Analysis of Failure Circle	LAYERS 2 & 3
30	4	Peak Strength (1) (5)	High	3:1		1.752	Grid Search	(3) RESIDUAL STRENGTH -- Peak Strength Obtained from Triaxial Tests with Cohesion Assumed Equal to Zero.
50	3	Creep Strength (2)	High	2:1	No Lightweight Materials	0.841	Grid Search	LAYER 1
17	3	Creep Strength (2)	High	2:1	No Lightweight Materials	0.995	Detailed Analysis of Failure Circle	$\phi = 30.0^\circ$ $c = 0$ $\gamma = .099 \text{ kips/ft}^3$
47	3	Creep Strength (2)	Low	2:1	No Lightweight Materials	0.986	Grid Search	LAYERS 2 & 3
20	3	Creep Strength (2)	High	3:1	No Lightweight Materials	1.181	Grid Search	$\phi = 24.2^\circ$ $c = 0$ $\gamma = .1066 \text{ kips/ft}^3$
48	3	Creep Strength (2)	Low	3:1	No Lightweight Materials	1.215	Grid Search	(4) SPECIAL STRENGTH -- Obtained from the Special One-Specimen Test Method Developed in the First Phase of this Research Study.
18	3	Creep Strength (2)	High	4:1	No Lightweight Materials	2.047	Detailed Analysis of Failure Circle	LAYER 1
33	3	Creep Strength (2)	High	2 1/2:1	No Lightweight Materials	1.001	Grid Search	$\phi = 21.8^\circ$ $c = 0$ $\gamma = .099 \text{ kips/ft}^3$
49	3	Creep Strength (2)	Low	2 1/2:1	No Lightweight Materials	1.115	Grid Search	LAYERS 2 & 3
24	3	Creep Strength (2)	High		No Lightweight Materials	1.245	Detailed Analysis of Failure Circle	$\phi = 30.0^\circ$ $c = 0$ $\gamma = .1066 \text{ kips/ft}^3$
26	4	Creep Strength (2) (5)	High	3:1		1.108	Grid Search	(5) In Problems Where a Lightweight Material was used, Properties of said Materials Were Assumed to Be as Follows:
25	4	Creep Strength (2) (5)	High	3:1		1.390	Detailed Analysis of Failure Circle	$\phi = 35.0^\circ$ $c = 0$ $\gamma = .070 \text{ kips/ft}^3$
29	4	Creep Strength (2) (5)	High	3:1		1.377	Detailed Analysis of Failure Circle	
39	3	Residual Strength (3)	High	2:1	No Lightweight Materials	0.719	Grid Search	
45	3	Residual Strength (3)	Low	2:1	No Lightweight Materials	1.101	Grid Search	
36	3	Residual Strength (3)	High	3:1	No Lightweight Materials	1.307	Grid Search	
46	3	Residual Strength (3)	Low	3:1	No Lightweight Materials	1.680	Grid Search	
44	3	Residual Strength (3)	High	2 1/2:1	No Lightweight Materials	0.991	Grid Search	
41	3	Residual Strength (3)	Low	2 1/2:1	No Lightweight Materials	1.002	Grid Search	
34	3	Special Strength (4)	High	2:1	No Lightweight Materials	0.609	Grid Search	
35	3	Special Strength (4)	High	3:1	No Lightweight Materials	1.307	Grid Search	
54	3	Peak Strength (1)	High	3:1 (Berm 2)	No Lightweight Materials	2.112	Grid Search	
55	3	Creep Strength (2)	High	3:1 (Berm 2)	No Lightweight Materials	1.306	Grid Search	
56	3	Residual Strength (3)	High	3:1 (Berm 2)	No Lightweight Materials	1.512	Grid Search	



## DISCUSSION

number of cases were analyzed using a lightweight material in various configurations on the side slope (listed in Table 5). Properties of this material were assumed to be as follows:  $\phi' = 35^\circ$ ,  $c' = 0$ , and unit weight = 70 pcf. This effectively reduced the number of overstressed slices along the observed failure surface but did not eliminate overstressing completely. The lightweight material also allowed shallow failures in the upper portions of the slope.

Bishop (21), Skempton (22), and others (23, 24) have shown this mechanism of local overstressing to be a major factor in the initial stages of formation of a failure surface. Overstressing causes a redistribution of stress along the critical circle and possibly overstresses other slices which originally were not overstressed. This may cause a concentration of shear stresses (13, 22) and consequent failure.

In summarizing this case history, it appears the embankment, as constructed, had little margin of safety inasmuch as the peak strength yielded a factor of safety just over one under high watertable conditions. There was a very definite loss of shear strength with time -- probably caused by large shear strains due to soil creep and(or) consolidation in the foundation. Additionally, the presence of a high watertable and excess pore pressures were major contributors to the apparent loss of shear strength indicated by the various analyses in Table 5.

It is noted that the "as built" factor of safety using "residual" strength was lower than the creep strength factor of safety. However, in the analysis of remedial designs, a very small increase in the cross sectional area sharply increased the factor of safety when using "residual" strength. Small increases in cross sectional area did not increase the factor of safety to as large a degree when using creep strength. This, in effect, made the creep strength the governing factor because it took a much larger cross sectional area to bring the factor of safety up to an acceptable value. Figure 62 is a graphic illustration of this relationship.

Analysis 56 appears to be the best design as all three strength definitions (peak, "residual", creep) appear to have adequate factors of safety. These safety factors could be increased even more if a method were provided to drain the embankment and lower the watertable. This could probably be accomplished best by trenching to a depth of about 15 ft in the ditch on the right shoulder and backfilling with a granular material. A granular blanket under the berm and slope change would keep the newly constructed portion of the embankment from becoming saturated but would provide little drainage for the existing embankment.

If the assumption is made that excess pore pressures exist in the soil and cause or are caused by undrained creep, then peak pore pressures recorded in the laboratory during the creep tests should be accounted for in making stability analyses. Figures 63 and 64 compare the failure envelopes constructed using effective yield stress with those of total yield stress for the embankment materials of both case histories. The  $\phi'$  angle for the Western Kentucky Parkway (Milepost 96) increased from  $5.0^\circ$  to  $5.7^\circ$  while the cohesion increased from 1.8 to 2.1 psi. At Milepost 44 on I 64, the  $\phi'$  angle increased from  $7.7^\circ$  to  $11.4^\circ$  and the cohesion decreased from 2.0 to 1.5 psi. In soils having a high clay content, it would be reasonable to assume that excess pore pressures arise from undrained creep; therefore, an effective stress analysis would be the best indication of stability.

Figure 65 is a comparison of the total stress  $\phi$  angle, the effective stress  $\phi'$  angle and residual stress  $\phi'$  angle for kaolinite. The residual angle was obtained from tests on a modified Karol-Warner Company shear box apparatus. It appears that the  $\phi'$  angle using residual strength from the shear test, is always larger than the effective  $\phi'$  angle obtained from the yield strength. Comparisons between the "residual" and yield strengths were not made for the other soils, but more comparisons should and will be made in the future.

The methods of obtaining a failure envelope from one triaxial sample, using the peak relaxation moduli from three relaxation tests, should be used with caution, especially with undisturbed soils. The pore pressure parameters A and B, being largely affected by the overconsolidation ratio, may not necessarily be linear with confining pressure and could lead to erroneous results when extrapolating from the confining pressure at which the triaxial test was run to a smaller confining pressure.

The peak relaxation modulus at 50-psi confining pressure did not appear to yield a linear relationship with the peak relaxation moduli obtained at 10- and 30-psi confining pressure when the three were plotted against confining pressure. It was suspected that strain hardening caused this as the sample was deformed 0.01 in. three times. Data reported by Konder(25), Krizek (26), and Allen (15) appear to support this. This non-linearity would produce extrapolation errors when trying to determine the peak stress knowing only the peak relaxation modulus. It must be concluded that this method should only be used when the availability of samples is severely limited.

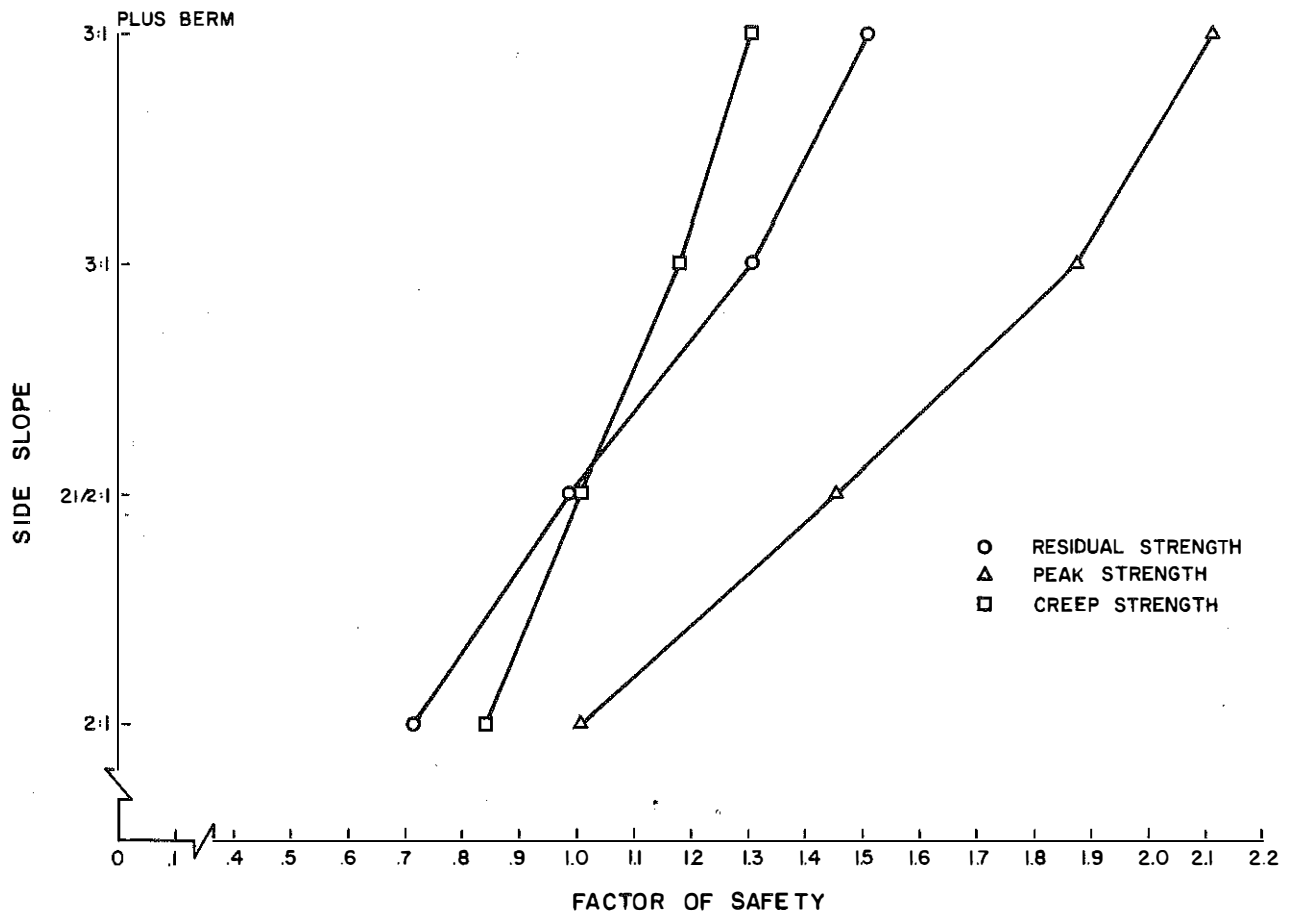


**Figure 62. Factor of Safety as a Function of Side Slope Configuration - I 64.**

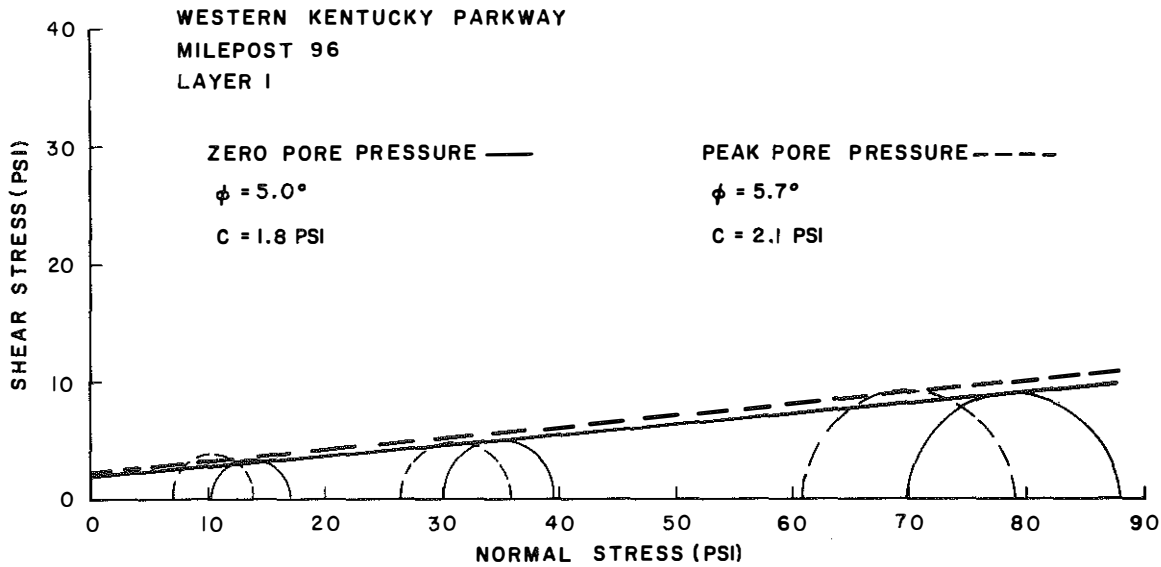


Figure 63. Relationship between Failure Envelopes Using Total Stress Analysis and Effective Stress Analysis, Layer I (Embankment), Milepost 96 - Western Kentucky Parkway.

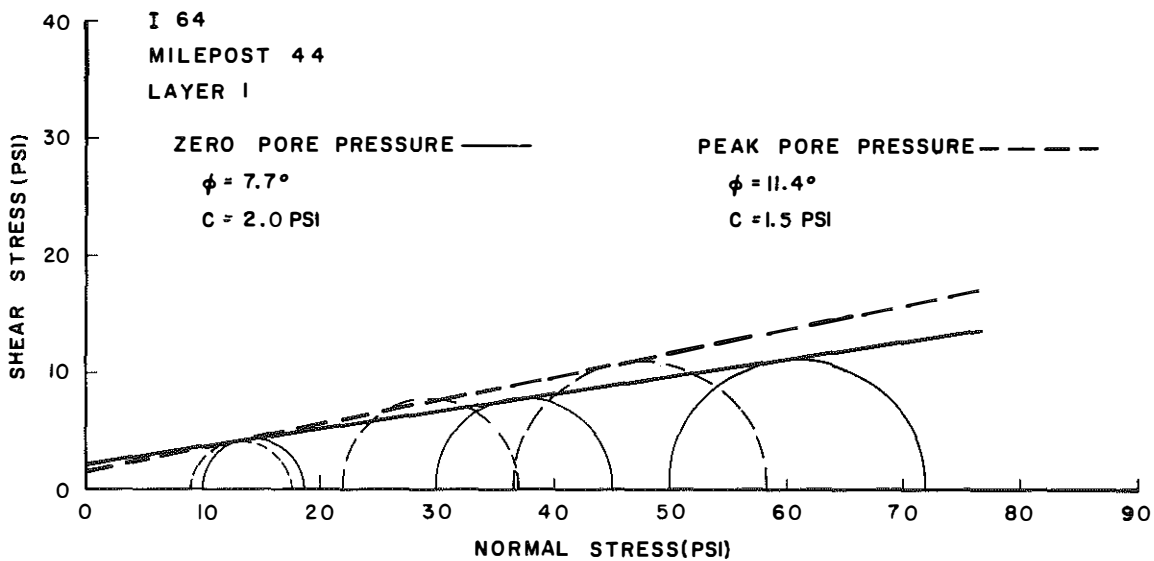


Figure 64. Relationship between Failure Envelopes Using Total Stress Analysis and Effective Stress Analysis, Layer I (Embankment), Milepost 44 - I 64.

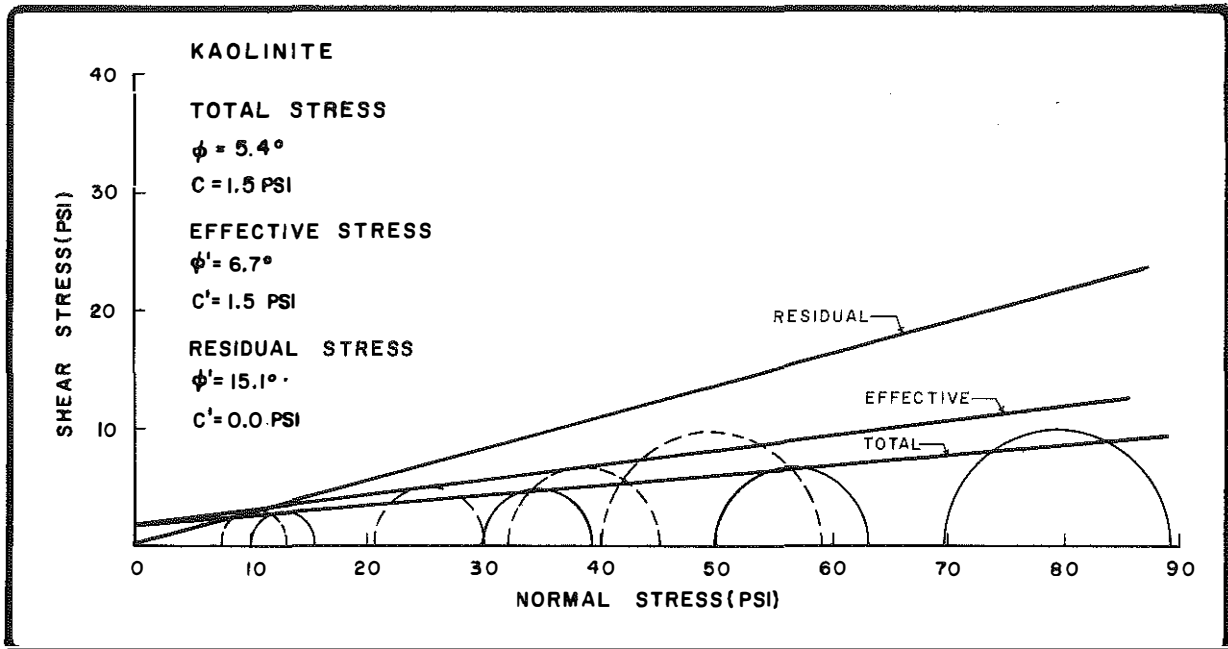


Figure 65. Comparison of Shear Strength Parameters Using Residual, Effective, and Total Stresses Kaolinite Series.

The effect of consolidation on the creep behavior of soils was not studied. It is known that consolidation can increase the effective stress on a soil mass and thereby initiate or accelerate creep. However, it is also known that consolidation increases the magnitude of the yield stress. Murayama and Shibata (1) indicate that if a clay is consolidated by  $\sigma_m$  exceeding  $\sigma_{mc}$ ,  $\sigma_{uc}$  increases to  $\sigma_u$  and are related in the following way:

$$\sigma_u/\sigma_{uc} = \sigma_m/\sigma_{mc}$$

where  $\sigma_{mc}$  = preconsolidation pressure,  
 $\sigma_{uc}$  = yield stress at the preconsolidation pressure,  
 $\sigma_m$  = the new consolidation pressure (always larger than  $\sigma_{mc}$ ), and  
 $\sigma_u$  = yield stress at the new consolidation pressure.

Therefore, it would appear that consolidation has a somewhat compensating effect, with the total effect being equal to the difference between the two.

It was originally intended to perform hysteresis tests on soils, however, considerable problems with the equipment prevented accurate results from being obtained. Therefore, the data on the few tests performed were neither reported nor analyzed.

## IMPLEMENTATION

It is anticipated that further creep and relaxation testing will continue in analyzing other landslides and bridge approaches. Further testing will be performed to obtain better correlations between yield strength data and residual strength data. The technical skills and knowledge gained from this study are being applied to asphalt and subgrade materials in studying the rutting behavior of flexible pavements. For the past several months, several bridge approaches and landslide corrections have been designed in this state to higher apparent factors of safety than are usually considered adequate by less detailed analyses.

## REFERENCES

- Schultze, E. and Krause, J., *Pore-Water Pressure and Creep in One-Dimensional Compression of Silts, Rheology and Soil Mechanics*, Symp., Grenoble, April, 1964, Springer-Verlag, N.Y., Kravtchenko, J. and Sirieys, P., Editors.
- Murayama, S. and Shibata, T., *Rheological Properties of Clays, Proceedings, Fifth International Conference on Soil Mechanics and Foundation Engineering*, Paris, Vol I, 1961.
- Suklje, L., *Common Methods of Stability Analysis, Rheological Aspects of Soil Mechanics*, Wiley, New York, 1969.
- Bishop, A. W. and Lovenbury, H. T., *Creep Characteristics of Two Undisturbed Clays, Proceedings, Seventh International Conference on Soil Mechanics and Foundation Engineering*, Mexico, Vol I, pp 29-37, 1969.
- Singh, A. and Mitchell, J. K., *General Stress-Strain-Time Function for Soils, Journal of the Soil Mechanics and Foundations Division, ASCE*, Vol 94, No. SM1, Proc. Paper 5728, pp 21-45, January 1968.
- Mitchell, J., Campanella, R. and Singh, A., *Soil Creep as a Rate Process, Journal of Soil Mechanics and Foundations Division, ASCE*, Vol 94, No SM1, Proc. Paper 5751, pp 231-253, January 1968.
- Mitchell, J. K. and Campanella, R. G., *Creep Studies on Saturated Clays, STP No. 361*, American Society for Testing and Materials, 1963.
- Casagrande, A. and Wilson, S., *Effect of Rate of Loading on Shear Strength of Clays and Shales at Constant Water Content, Geotechnique*, 2, No. 3, pp 251-263, 1951.
- Vislov, S. and Skibitsky, A., *Problems of the Rheology of Soils, Proceedings, Fifth International Conference on Soil Mechanics and Foundation Engineering*, Paris, Vol I, 1961.
- Roscoe, K. and Schofield, A., *Yielding of Clays in States Wetter than Critical, Geotechnique*, 13, No. 3, pp 211-240, 1963.
- Walker, L. K., *Undrained Creep in a Sensitive Clay, Geotechnique*, 19, No. 4, pp 515-529, December 1969.
- Arulanandan, K., Shen, C. and Young, R., *Undrained Creep Behavior of a Coastal Organic Silty Clay, Geotechnique*, 21 No. 4, pp 359-375, 1971.

13. Murayama, S. and Shibata, T., *Flow and Stress Relaxation of Clays, Rheology and Soils Mechanics*, Symp. Grenoble, April 1964, Springer-Verlag, N.Y., Kravtchenko, J. and Sirieys, P., Editors.
14. Scott, G. D., *Rheological and Ultimate Strength Properties of Cohesive Soils*, Division of Research, Kentucky Department of Highways, February 1970.
15. Allen, D. L., *A Rheological Study of Cohesive Soils*, Division of Research, Kentucky Department of Highways, September 1972.
16. Murayama, S. and Shibata, T., *On the Rheological Characteristics of Clay*, Part I, Disaster Prevention Research Inst., Kyoto University, Bulletin No. 26, 1958.
17. Kawakami, F. and Ogawa, S., *Yield Stress and Modulus of Elasticity of Soils, Rheology and Soil Mechanics*, Symp., Grenoble, April 1964, Springer-Verlag, N.Y., Kravtchenko, J. and Sirieys, P., Editors.
18. Hunter, J., **Introduction to Statistics**, Vol 1, Westinghouse Learning Corporation, 1968.
19. Roscoe, K. and Schofield, A., *Mechanical Behavior of an Idealized Wet Clay*, **Proceedings**, European Conference on Soil Mechanics, Wiesbaden 1, 1963, pp 47-54.
20. Yoder, S. and Hopkins, T. C., *Slope Stability Analysis: A Computerized Solution of Bishop's Simplified Method of Slices*, Division of Research, Kentucky Department of Highways, February 1973.
21. Bishop, A. W. and Bjerrum, L., *The Relevance of the Triaxial Test to the Solution of Stability Problems*, **Proceedings, Research Conference on Shear Strength of Cohesive Soils**, ASCE, 1960.
22. Skempton, A. W., *Long Term Stability of Clay Slopes, 4th Rankine Lecture*, **Geotechnique**, 14, No. 2, pp 77-102, 1964.
23. Bjerrum, L., *The Third Terzaghi Lecture: Progressive Failure in Slopes of Overconsolidated Plastic Clay and Clay Shales*, **Journal of Soil Mechanics and Foundations Division**, ASCE, Vol 93, Part I, No. SM5, Proc. Paper 5456, pp 3-49, September 1967.
24. Yen, B. C., *Stability of Slopes Undergoing Creep Deformation*, **Journal of Soil Mechanics and Foundations Division**, ASCE, Vol 95, SM5, Proc. Paper 6675, pp 1075-1096, July 1969.
25. Konder, R. L., *Energy Dissipation Response of a Cohesive Soil*, U.S. Army Engineer Waterways Experiment Station, Vicksburg, Miss., AD 613071, 1964.
26. Krizek, R. J., *Constitutive Behavior of Clay Soils*, **Proceedings, Fifth International Congress on Rheology**, Shiegeharu Onogi, Editor, Vol 2, p 469, 1970.

# APPENDIX

